Characterization of Diacylglycerol Metabolizing Enzyme Functional Specificity in Native Biological Systems

Timothy Brandon Ware

Ashburn, Virginia

B.S. Chemistry with Specialization in Chemical Biology, University of Virginia, 2016

A Dissertation presented to the Graduate Faculty of the University of Virginia in Candidacy for the Degree of Doctor of Philosophy

Department of Chemistry

University of Virginia

May 2021

Abstract

The production and breakdown of fats (i.e., lipid metabolism) is a vital biological process for sustaining life. Lipids shape biological membranes, serve as fuel for cells in times of need, and function as potent cellular signals to dictate when and where cognate receptor proteins carry out biochemical activity. A critical gap in the field of lipid biology is a fundamental understanding of how cells decide which lipids, among the sea of thousands of chemical variants, carry out specific biological tasks required for survival. The agents in promoting lipid metabolism are enzymes that perform explicit actions to change the state of lipids. Enzymes that vary in expression, localization, and function, suggesting a tight regulation of loosely processed lipids, especially in the case of signaling lipids that act as secondary messengers.

Diacylglycerols (DAGs), in particular, are one such poorly understood signaling lipid system where specificity is expected to serve a pivotal role in its functionality, yet few examples have been reported in literature. Many DAG metabolizing enzymes regulate distinct biological processes throughout human biology however, what remains unclear are the underlying mechanisms which impart unique functionality while exhibiting minimal structural diversity. Lipid specificity offers an explanation why certain lipids of the same class are used more over others in biological processes. The work presented in this dissertation leverages the implementation of advanced bioanalytical approaches to elucidate lipid-protein interplay in living cell systems to provide critical insight into how DAG metabolizing enzymes regulate fundamental biological processes.

The goal of this dissertation is to apply recently advanced analytical methodology towards discovering novel specificity and functionality of DAG metabolizing enzymes and their associated signaling networks. In Chapter 2, we utilize high-resolution liquid chromatography mass spectrometry (LC-MS/MS) and engineering of recombinant proteins to elucidate the structure-function relationship of diacylglycerol lipid kinases (DGK) regulatory domains which impart

substrate specificity to in a cellular context. Chapter 3 discusses the approaches used to characterize the novel substrate specificity of diacylglycerol lipase beta (DAGLβ), expanding our understanding of how these enzymes may regulate immune responses and energy catabolism. Chapter 4 examines a proposed convergence of inflammatory signaling networks attenuated by DAGLβ expression and activity involving both inflammatory lipid production and protein kinase signaling cascades. Lastly, Chapter 5 examines the body of work presented in this dissertation and discusses limitations of implemented approaches along with future directions for deeper exploration of DAG metabolizing enzyme signaling pathways.

Acknowledgments

I would like to first thank my PI and mentor Dr. Ku-Lung (i.e., Ken) Hsu for his guidance and support these past five years. He took a chance on a first-year graduate student with zero research experience when few other would and I like to believe that the gamble paid off. I will always be grateful for the experiences and instruction I have received, even if at the moment I was resenting the ever-growing workload. However, I believe that those challenges helped mold me into a more competent and capable researcher.

Next, I would like to thank University/Department of Chemistry faculty and staff, past and present. To Michael Birckhead, Debbie Scott, and Danny Via, thank you for always being of incredible assistance in sending out and acquiring orders needed for my experiments. To Drs. Thurl Harris, Timothy Bullock, and Aron Lichtman thank you for always being supportive of my research and career through collaborations and compositions of recommendation letters on short notice. To Dr. Cameron Mura, thank you for taking the time six years ago to talk to a random undergraduate student in your office about graduate research at length and even going so far as to write me a letter of recommendation to enter the program. To Dr. Carol Price, thank you for always having your door open to talk and catch up whenever the urge came. To Dr. Bob Nakamoto, thank you and the Biophysics Department for supporting me since my second year with the NIH training grants. I always looked forward to those Friday journal clubs at Synder because it was an excuse to take a scenic walk, be out the lab for two hours and eat lunch. Thank you to Cecelia Cropley for always being on top of grant submission requirements and deadlines, without your assistance it is unlikely the F31 would have been awarded at all.

To the many colleagues I have the pleasure of calling friends, thank you for bringing joy and conversation to the monotonous life that is research. In particular I would like to thank my fellow Biochem lab TAs; Reilly, Catherine, and Arlie for remaining stalwart friends over the years and being supportive without purposefully meaning to. The memories we have acquired along the

way will stay with me all through my life as some of the best I have ever had in Charlottesville and at UVA.

To my fellow lab members, thank you for being supportive and helpful throughout the years. Even though at times it felt as though I was your parent, it was rewarding to watch you succeed. I wish you all the best in your future endeavors and hope your future salaries accurately reflect your capabilities and expertise.

Lastly, I would like to thank my family, who to this day, still believe I work for the CIA and therefore can not divulge what I actually do in lab. Thank you to my parents for always saying how proud you are of me even if you do not completely understand what it is I do because your support has made these last five years bearable and enriching. To my brothers, thank you for always evolving because whenever I come home to visit, you have changed in some way that makes catching up exciting. Finally thank you to my grandmother for her unconditional love and support. I am thankful and grateful to everyone who has supported me along the way, in every respect, large and small, and I will cherish the memories and lessons learned during these years throughout the rest of my life.

Table of Contents

Chapter 1. Introduction

1.1 *Overview of Diacylglycerol Functional and Structural Properties*

Diacylglycerols (DAGs) are produced through a variety of metabolic processes and perform distinct roles in signaling mechanisms based on cell/tissue-specific and spatiotemporal properties[1,2]. DAGs are neutral glycerolipids that possess two fatty acid chain esters of numerous carbon chain lengths and saturation (**Figure 1.1**). The variety in these fatty acyl chain combinations offer the potential for thousands of natural DAG variants to exist at any given moment. Furthermore, fatty acyl chain compositions confer much of its variation with respect to hydrophobic capabilities. These effects subsequently influence interactions with specific lipid membranes or protein fold environments, dictating much in the way this lipid class functions throughout cellular biology. Despite growing interest in understanding DAG-mediated biology, a critical gap in our knowledge remains uncertainty in the specific DAG signals that enact much of the interesting signaling effects observed. One reason for this limitation is due to the diversity not only in fatty acyl chain composition, but also its isomeric properties.

Isomers can exhibit differentially linked functional groups, serving as constitutional (structural) isomers or they can differ in how they are geometrically arranged in space, acting as spatial (stereo) isomers. In fact, DAG represents an intriguing case of stereoisomers as they can exist as non-superimposable enantiomers due to the presence of a chiral center carbon in the *sn*-2 or central carbon position (**Figure 1.1**). This means that theoretically, apart from molecular differences between DAG species, those of similar molecular composition may also differ based on small, yet significant stereochemical changes. In the onset of scientific investigations into specific DAG interactions, these considerations confounded much of the observations being made due to the inability of researchers to distinguish DAG structural isomers based on the limitations of implemented analytical approaches. It remains an analytical challenge to this day,

in many situations, to accurately assign isomeric properties to particular DAG species. While chiral resins can be used in many instances to separate enantiomers through chromatographic processes these approaches often limit the breadth of total analytical coverage. As such, inferences into assigning lipid regioisomers and fatty acyl chain composition can be implemented as their molecular composition is associated with the original identity of the precursor lipids used to source the final products. Thus, researchers often take advantage of the unique characteristics of local lipidomes to surmise the regioisomerism of lipids of interest existing in that cellular space.

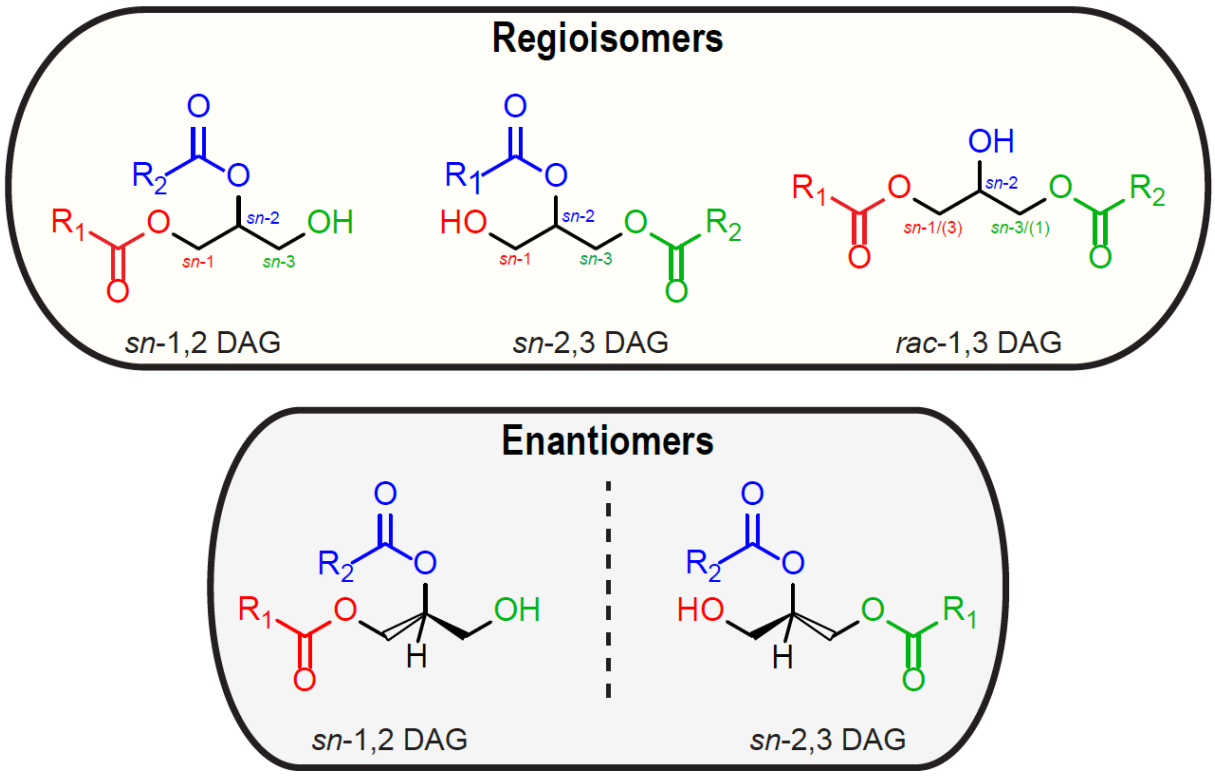

Figure 1.1 Diacylglycerol isomer structures. Structural depictions of DAG regio- and stereoisomers demonstrating the diversity in molecular composition these lipids can possess. A chiral center is present (although not displayed) at the *sn*-2 carbon along the glycerol backbone.

1.1.1 *Intracellular Origins of Diacylglycerol*

DAG is generated intracellularly in several distinct subcellular compartments, including the Golgi network, the endoplasmic reticulum (ER), the plasma membrane, and lipid droplets (LDs) via different chemical reactions from diverse lipid sources[3]. These sources can include membrane-associated phospholipids (PLs), triacylglycerol (TAG) stored in cytoplasmic or ER-associated LD or even basic glycerol-backbone containing building blocks[3]. Lipases or acyltransferases can subsequently generate DAG through the removal or addition of fatty acyl chains or a phospholipid head group moiety[4,5] (**Figure 1.2**). These enzymes that regulate the formation of DAG and its related lipid species follow well-characterized stereo/regiochemical-specific pathways at these subcellular locales[6]. As such, it is often inferred from these source pathways the stereo/regiochemical properties of subsequent DAG species related to particular biological systems and processes.

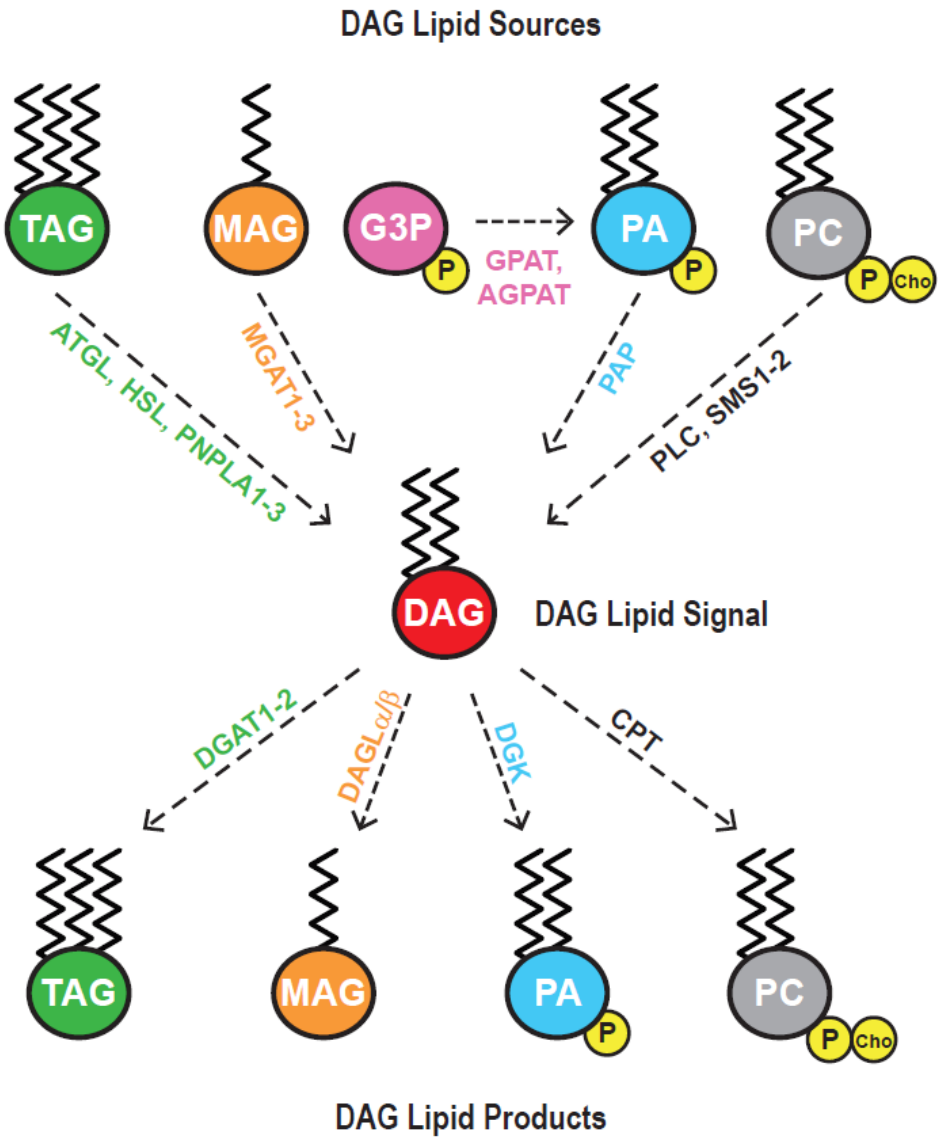

Figure 1.2 Summary of DAG metabolic pathways. DAG-mediated signaling is initiated once the lipid has been synthesized via a variety of metabolic enzymes (e.g., lipases, acyltransferases, phosphatases). Moreover, DAG-mediated signaling is attenuated through depletion of DAG pools via conversion of DAG into new lipid products, again through the action of lipid metabolizing enzymes.

1.1.1a *Diacylglycerols Sourced from Triacylglycerols*

In adipocytes, constituents of white adipose tissue (WAT), adipose triglyceride lipase (ATGL) regulates energy storage and utilization homeostasis through its catalytic action against TAGs[7]. Since excess energy is often stored in the form of TAGs, specifically in LDs, lipase-dependent action against these lipids is crucial to maintaining cellular viability and proper functionality through the release of energy metabolites, predominately fatty acids (FAs). ATGL, in particular exhibits its highest hydrolytic activity for TAGs with no observable activity for other neutral lipids such as DAGs, monoacylglycerols (MAGs), and cholesterol esters (CEs)[8]. ATGL preferentially hydrolyzes long-chain fatty acids of various length and saturation[9]. Furthermore, ATGL is unique among mammalian lipases as it hydrolyzes TAGs selectively at the *sn*-2 position, generating *rac*-1,3 DAGs. Interestingly, ATGL can expands its regioselectivity to include the *sn*-1 position, generating *sn*-2,3 DAGs following co-activation by ABHD5[9]. Importantly, ATGL does not hydrolyze fatty acyl chains at the *sn*-3 position of TAGs, therefore this particular lipase does not generate *sn*-1,2 DAGs[9].

Hormone-sensitive lipase (HSL) is expressed in many tissues with its highest in WAT and brown adipose tissue (BAT)[10]. HSL-dependent activity is strongly regulated by hormones although several phosphorylation events similarly control its activity by influencing both protein–protein interactions and intracellular localization[11,12]. HSL can be activated by catecholamines, which bind to β-adrenergic receptors during times of fasting to permit HSL to be translocated to the LD surface and perform its lipolytic action[13]. Interestingly, *in vivo* HSL exhibits a uniquely broad substrate spectrum which includes TAGs, DAGs, MAGs, and CEs[14]. However, *in vitro* HSL exhibits its greatest activity against DAG exceeding those against TAG and MAG almost tenfold with a distinct preference for polyunsaturated FAs at the *sn*-3 position[14,15]. Taken together, both ATGL and HSL constitute more than 90% of TAG hydrolase activity as determined in cultured adipocytes and murine WAT for the generation of different DAG isomers[16].

Several members of the PNPLA protein family are proposed TAG hydrolases as they have exhibited such catalytic activity *in vitro* or implicate TAG catabolism in knockout models, and as a result, may contribute to the generation of DAGs *in vivo*[7]. PNPLA4 demonstrates activity against a variety of substrates, including TAGs, retinyl esters (REs), and PLs[17]. Human PNPLA4 is reported to hydrolyze TAGs at *sn*-1/(3) and *sn*-2 position, generating an assortment of *rac*-1,3 and *sn*-1,2/(2,3) DAGs[17]. PNPLA5 does not exhibit direct TAG hydrolase activity *in vitro*, although its expression does lower TAG accumulation in cells[17]. Lastly, PNPLA3 catabolizes a diverse array of lipid substrates including TAG, DAG, MAG, and RE species with a distinct preference for TAG species composed of long-chain unsaturated FAs (e.g., C18:1)[18]. Importantly, since these enantiotopic FAs (C18:1) are often positioned in the *sn*-1 or *sn*-3 position, the resulting DAGs generated are chiral with *sn*-1,2/(2,3) orientations[18,19].

1.1.1b *Diacylglycerols Sourced from Phospholipids*

Phospholipases specifically hydrolyze PLs at distinct positions along the classical phospholipid backbone configuration. There are four major classes of phospholipases that each catalyze the hydrolytic cleavage of specific bonds. PLA_1 and PLA_2 catalyze the hydrolytic cleavage of the fatty acyl chains at either the *sn*-1 or *sn*-2 position, respectively. Phospholipase C (PLC) and D (PLD), in contrast, cleave respective phospho-glycerol and phospho-headgroup esters. Thus, as it pertains to DAGs generated from PLs, only PLCs directly contribute to intracellular DAG formation. Furthermore, all resulting DAGs will be produced at the plasma membrane and possess *sn*-1,2 stereochemistry, reflecting the stereochemistry of their original PL precursors[20].

Phosphatidylcholine-specific PLC (PC-PLC) isoforms are expressed in many organisms including mammals and exhibit a variety of localization and activity behaviors highly dependent on the system[21]. Notably, PC-PLC expression and activity appears to be concentrated at perinuclear areas and following mitogen-mediated cell receptor stimulation translocates to the

outer leaflet of the plasma membrane[21]. Relatively little is known about the physiological role of mammalian PC-PLCs however, they do contribute to the catabolic formation of DAGs *in vivo*[21]. In contrast, much more information has been reported on the role of phosphatidylinositol-specific PLC (PI-PLC) isozymes. For instance, thirteen PI-PLC isoforms have been identified and assigned to six subclasses with various tissue expression and subcellular localization profiles[22]. Importantly, upon cell activation PI-PLCs translocate to the plasma membrane and catalyze the hydrolysis of phosphatidylinositol 4,5-bisphosphate (PIP_2), a plasma membrane-associated PL, producing DAG and inositol 1,4,5-triphosphate (IP_3)[23]. Due to the *sn*-3 position of the phospho-headgroup residues of PLs, both PC-PLC and PI-PLC generate exclusively *sn*-1,2 DAGs[23].

Apart from direct hydrolysis of phospho-headgroups, other forms of PL-derived metabolism exist to generate DAG species. Sphingomyelin synthases (SMSs) are one such example as they catalyze the transfer of the phosphorylcholine headgroup from PC to a ceramide scaffold to generate sphingomyelin (SM) and *sn*-1,2 DAG[24]. Two mammalian enzymes, SMS1 and SMS2 have been described[25]. Localization of SMS1/2 proteins also dictates the role the resulting DAG exhibits in cellular signaling and lipid flux. For example, SMS1 localizes exclusively to the luminal side of the *trans*-Golgi and DAGs produced there may promote protein kinase D (PKD) translocation and the resultant formation of secretory vesicles[25]. In contrast, SMS2 additionally localizes to the extracellular leaflet of the plasma membrane where the DAGs it generates are utilized to replenish depleted SM levels following sphingomyelinase activity[26]. Similar to PLCs, even though SMS1/2 exhibit diverse substrate specificity, the resulting DAG intermediates are *sn*-1,2 isomers since their source lipids were originally PLs.

Phosphatidic acid phosphatase (PAP) catalyzes the dephosphorylation of PA to generate DAG[27]. PAP activity is positioned in the center of lipid flux pathways as its activity regulates not only TAG production, but additionally PLs. PAPs can be separated into two types based on their cellular localization and substrate specificity[27]. Type 1 PAPs are cytosolic enzymes that can

associate with plasma and nuclear membranes[28]. These enzymes are encoded by the *Lpin* genes and only catalyze the dephosphorylation of PA in a Mg^{2+}-dependent manner[29]. In contrast, type 2 PAPs are transmembrane enzymes that are localized in the plasma membrane, are able to dephosphorylate additional PL substrates, and are therefore also known as lipid phosphate phosphatases[30]. Furthermore, unlike type 1 PAPs, type 2 PAPs proceed via a Mg^{2+}-independent reactions[30]. Regardless, both type 1 and type 2 PAPs generate *sn*-1,2 DAGs following dephosphorylation of PA or alternative PL substrates, similar to previously described enzymes.

1.1.1c de novo *Biosynthesis of Diacylglycerols*

Thus far the generation of DAGs has been described via catabolic process (e.g., hydrolases, phosphatases) mainly with regard to bioenergetic production however, DAGs can also be produced via anabolic processes. Two main pathways through which DAG is produced as an intermediate in *de novo* lipid biosynthesis is unsurprisingly, related to TAG and PL[31]. TAG synthesis in most tissues, primarily in WAT and the liver involves the glyceraldehyde 3-phosphate (G3P) pathway[32]. Wherein G3P undergoes consecutive acylation reactions, catalyzed first by acyl-CoA-dependent glycerol-3-phosphate acyltransferase (GPAT) and subsequently by acyl-CoA acylglycerol-3-phosphate acyltransferase (AGPAT)[31]. The product of these acylation reactions is PA which, as previously described, is dephosphorylated to DAG by PAPs[29]. Since the biosynthetic pathway utilizes an *sn*-3 modified G3P substrate to begin with, the final DAG isomers are exclusively in the *sn*-1,2 conformations.

In contrast, the other major *de novo* DAG pathway often begins with *sn*-2 esterified MAGs, localized to the digestive tract[31]. In this MAG-pathway long-chain fatty acyl-CoAs are esterified in either the *sn*-1 or *sn*-2 positions to generate *sn*-1,2/(2,3) DAGs. Three enzymes have been reported to exhibit MGAT activity with all three demonstrating intracellular localization to the ER[33-35]. Where MGAT isoform diversity is evident is in their tissue-specific expression patterns and substrate specificities. MGAT1 is predominately expressed in stomach, adipocytes, and kidneys

whereas MGAT2 and MGAT3 demonstrate their highest expression in small intestine[33-35]. Notably, MGAT3 is the more biologically relevant isoform with regards to human biology as it is exclusively expressed in higher mammals[34]. MGAT3 prefers *sn*-2 MAG substrates along with palmitic acid-CoA (C16:0-CoA) and oleic acid-CoA (C18:1-CoA) acyl donors to generate *sn*-1,2 or *sn*-2,3 DAG isomers[34]. Interestingly, MGAT3 also functions as a TAG synthase as it exhibits significantly higher DAG-acyltransferase activity in comparison to other MGAT isoforms[36].

Where MGAT3 has strict substrate preferences, MGAT2 does not exhibit any significant selectivity involving fatty acyl chain-length or degree of unsaturation of the FA-CoA substrates[33]. Thus, MGAT2 can catalyze the esterification of any position along the glycerol backbone to create any DAG isomer if the corresponding MAG substrate is readily available. MGAT1, in comparison, exhibits high selectivity for long-chain unsaturated FA-CoAs, in particular arachidonic acid-CoA (C20:4-CoA)[35]. In addition, MGAT1 preferentially modifies at the *sn*-1 or *sn*-3 position of MAG substrates[35]. Thus, unlike the G3P pathway, which is limited to generating *sn*-1,2 DAGs at the plasma membrane interface, the MAG-pathway is readily capable of generating any variation of DAG isomer for translocation through the ER-Golgi complex.

1.1.2 *Role of Diacylglycerol in Intracellular Lipid Signaling*

DAG primarily influences intracellular signaling through the activation of distinct effector proteins[3]. In response to G-coupled protein receptor (GPCR) or tyrosine kinase (RTK) receptor activation by external agonists, such as hormones, PLC isoforms are activated and subsequently catalyze the hydrolysis of PIP_2 to generate DAG and IP_3[4]. Where IP_3 initiates Ca^{2+}-dependent cascades through the release of ER-stored Ca^{2+} ions into the cytosol, membrane-bound DAG instead functions as a plasma membrane translocator for nearby effector proteins[4]. While in most cases DAG does not directly activate these effector proteins, their binding at a conserved cysteine rich (C1) domain is critical in bringing these proteins in proximity to signaling partners that would promote their activation[37]. Following activation these effector proteins then regulate many diverse facets of cellular biology including, but not limited to, cell proliferation, differentiation, receptor desensitization, metastases dissemination, and immunity. Furthermore, many of the signaling effects by these effector proteins are system specific as expression profiles of signaling partners are highly dependent on the cell/tissue type. Several of these DAG effector proteins have been reported to serve critical roles in promoting tumorigenesis and immunological-based pathologies[3]. Thus, understanding how DAG specificity influences effector protein activation and regulation could be key to developing efficacious therapies that attenuate its aberrant signaling effects following maladaptive changes to its processing.

1.1.2a *Protein Kinase C Family*

One of the most well-characterized DAG effector proteins are isozymes that belong to the protein kinase C (PKC) family. PKC isoforms function as protein kinases that attenuate several signaling pathways through phosphorylation of critical serine and threonine residues[38]. In humans, there are fifteen PKC isoforms divided into three subfamilies, based on their secondary messenger activators. Both classical PKCs (cPKCs) (α, β, γ) and novel PKCs (nPKCs) (δ, ε, η, θ) are DAG

sensitive with cPKCs also necessitating Ca^{2+} and a phospholipid such as phosphatidylserine (PS) for proper activation[39]. Atypical PKCs (aPKCs) (ι, ζ) instead solely utilize PS for activation and therefore do not follow the canonical PLC activation pathway[39]. Interestingly, studies have shown that only *sn*-1,2 DAG species are able to be recognized by PKC C1 domains where other DAG isomers, *rac*-1,3 and *sn*-2,3 are inactive[40,41]. PKC family proteins demonstrate diverse expression profiles where its isoforms are nearly represented in all biological systems and cell types, including neurons, platelets, smooth muscle cells, and adipocytes.

1.1.2b *Protein Kinase D Family*

Protein kinase D (PKD) exhibits structural, enzymological, and regulatory properties different from the related PKC family members[42]. However similar to PKC isoforms, PKD mediates a diverse array of normal and abnormal biological functions through its distinct substrate specificity and dynamic changes in spatiotemporal localization[42]. Interestingly, PKD isoforms exist in an autoinhibited state via interactions between its C1-containing N-terminus and catalytic domains[43]. Activation of PKD requires a dual-mode mechanism mediated by DAG wherein it 1) directly promotes translocation of PKD from the cytosol to the plasma membrane and 2) activates PKC isoforms that would relieve the autoinhibited state of PKD via phosphorylation of serine residues located in the catalytic domain[43,44]. Thus, in this example DAG promotes PKD activation through secondary effector protein signals demonstrating an intersecting of signaling cascades that contribute to the complexity of its overall regulation. In support of this it has been observed that PKD1 is implicated in the regulation of a complex array of fundamental biological processes, on the level of PKC family members[42]. Additionally, PKD members can be selectively translocated to intracellular membranes such as the trans-Golgi network via interactions between DAG and a specific C1 domain moiety[45].

1.1.2c *Ras guanyl nucleotide releasing proteins*

Similar to membrane translocation and PKC-mediated activation of PKD, Ras guanyl nucleotide releasing proteins (RasGRPs) similarly rely on both DAG-C1 domain interactions for membrane translocation and PKC-mediated phosphorylation for proper functionality[46,47]. RasGRPs regulate the activation of small GTPase Ras signaling, which in turn modulates its effectors such as ERK1/2[46]. In mammals, four isoforms (RasGRP1-4) are expressed with certain isozymes playing predominant roles in certain cell types and being susceptible to different upstream activators. For instance, RasGRP1 functions downstream of both T-cell receptor (TCR) and B-cell receptor (BCR) whereas RasGRP3 acts downstream of solely BCR[48,49]. Regardless, both of these isoforms regulate Ras signaling in adaptive immunity as well as B-cell mitogenesis via downstream transcription factor activation[39]. Similarly, RasGRP4 primarily attenuates Ras signaling in mast cells, highlighting the diversity in immunological systems these enzymes affect[46]. Interestingly, RasGRP2 C1 domains are phorbol ester (a DAG-mimetic) insensitive suggesting a predominant role of PKC activation for its Ras activity[50].

1.1.2d *β-chimaerins*

The name of β-chimaerins is derived from first being identified as a “chimaera” between the C1 domains of PKC family members and the GTPase activating protein domain (GAP) of BCR protein[51]. In mammals, there are four expressible chimaerin isoforms (α1, α2, β1, and β2) from two splice variants. These enzymes are responsible for the negative regulation of small G-protein signaling through Rac, a small G protein that acts through ERK signaling[52]. β-chimaerins are translocated to the plasma membrane through the canonical PLC-DAG activation pathway mediated upstream through both GPCRs and RTKs, bringing them in proximity to Rac[52]. β-chimaerins inactivate Rac via its GAP domain which catalyzes the hydrolysis of GTP bound to

active Rac[53]. In this way, chimaerins regulate Rac-dependent processes such as cell-cycle progression, actin-cytoskeletal expansion, and tumorigenesis.

1.1.2e *Munc13 Proteins*

Apart from its role in intracellular effector protein signaling cascades, DAG also regulates membrane fusion and vesicular trafficking. The Munc13 protein family possess a single DAG/phorbol ester sensitive C1 domain which allows intracellular DAG to regulate the translocation and site of activity for Munc proteins[50]. In mammals there are three Munc isoforms expressed (Munc13-1-3) in the brain that regulates much of the synaptic function of neurons. In particular, Munc13-1 has been extensively described to interact with syntaxin 1 of the SNARE complex, a process essential to synaptic release[54]. Moreover, these Munc family proteins are located at the presynaptic interface and as such are critical to vesicle maturation and fusion[54]. Unlike with PKD and RasGRP enzymes, Munc13 isoform-specific activity is not additionally affected by PKC activation following DAG signaling[55]. While PKC-mediated phosphorylation does regulate SNARE complex formation, the engagement of Munc13 with SNARE-related components solely requires translocation to the presynaptic membrane via DAG/phorbol ester engagement with its C1 domain[55].

1.1.3 *Diacylglycerol Metabolizing Enzyme Pathways*

Since DAG is a widely utilized secondary messenger for signal transduction, its downregulation must be tightly controlled to prevent excessive and non-specific effector protein engagement and therefore downstream signaling effects. However, unlike with protein signals, there is no universal degradation complex (i.e., proteasomes and ubiquitylation) readily available to remove these lipid messengers apart from specific metabolic processes. As such, inactivation of lipid-mediated signaling pathways often occurs through manipulation of the chemical state of the lipid signal itself to make it unrecognizable to its original effector proteins (e.g., hydrolysis, acylation, phosphorylation-based modifications). In the case of DAGs, there exist four major pathways through which DAG may be depleted from the local lipid environment to produce a new lipid product thereby inactivating its original effector signal[3] (**Figure 1.2**). Conversion of DAG into new lipid products, however, brings additional complexity as these new molecules may function as lipid precursors or even cellular signals themselves to alternative pathways.

1.1.3a *Diacylglycerol-O-acyltransferases*

In the TAG biosynthetic pathway, the acylation of DAG is the final step and is catalyzed by enzymes known as diacylglycerol-*O*-acyltransferases (DGATs). In mammals, two DGAT enzymes have been characterized (DGAT1 and DGAT2)[56]. DGAT1 exclusively localizes to the ER whereas DGAT2 may localize to the ER, mitochondria-associated membranes, and LD membranes[57]. The C-terminal active site of DGAT1 faces the ER lumen while the N-terminal region faces the cytoplasm and permits association with long-chain FA-CoAs[57]. DGAT2 shares closer homology with MGAT proteins in comparison to DGAT1, primarily through a conserved HPHG region of its active site[56]. Moreover, DGAT2 contains a consensus region that functions as a neutral lipid-binding domain similar to one found in HSL[57]. Unlike DGAT2, which exclusively produces TAGs, DGAT1 can acylate other lipid substrates such as MAG to produce DAG[5].

DGAT1 and DGAT2 demonstrate different preferences with respect to their DAG substrates and FA-CoA donors during acylation. While human DGAT1 does not exhibit preferences for any particular FA-CoA donor, it does prefer *sn*-2 MAGs over *sn*-3 MAGs as substrates for the production of *sn*-1,2 DAGs in the intestine[58]. DGAT2 demonstrates a preference for medium-chained FA-CoAs (C12:0-CoA) as acyl donors[58]. DGAT enzymes exhibit differential DAG isomer preferences wherein DGAT1 catalyze *sn*-1,2/2,3 DAGs more efficiently than *rac*-1,3 DAGs whereas DGAT2 prefers *rac*-1,3 DAGs over other isomers[58]. The differences between DGAT substrate specificity may be directly linked to its accessibility to particular DAG isomer pools. For instance, only DGAT2 localizes to LDs and subsequently displays a preference for *rac*-1,3 DAGs. At this locale, ATGL catalyzes the hydrolysis of TAGs to produce both *rac*-1,3 and *sn*-2,3 DAGs, suggesting a purposeful futile cycle to exchange long-chain unsaturated FAs with medium-chain FAs at the *sn*-2 position[9]. In contrast, *sn*-1,2 DAGs present at the ER membranes, derived from *de novo* PL synthesis is accessible to both DGAT1 and DGAT2.

1.1.3b *Diacylglycerol Lipases*

In humans, there are two DAG lipases (DAGLα and DAGLβ) expressed that exhibit preferences for the hydrolysis of *sn*-1 positioned fatty acyl chains[59]. DAGLα and DAGLβ are serine hydrolases that preferentially hydrolyze arachidonic acid (AA)-esterified diacylglycerols (DAGs) to produce *sn*-2 esterified arachidonoylglycerol (2-AG)[59]. *In vitro*, DAGLs preferentially hydrolyze DAGs at the *sn*-1 position, can be stimulated with Ca^{2+}, and have negligible activity against other lipids including MAGs and PLs[60]. Mammalian DAGLs are expressed as transmembrane proteins composed of a 4-transmembrane domain region at the N-terminus followed by a canonical α/β hydrolase domain (containing the nucleophilic serine residue)[60].

DAGLα is highly expressed in brain and pancreas, while DAGLβ is highly expressed in bone marrow, spleen, liver, and lymph nodes[59,61]. Both enzymes hydrolyze *sn*-1,2 DAG isomers

with DAGLβ demonstrating preferences for DAG species containing linoleic acid (C18:2), oleic acid (C18:1) and AA (C20:4) at the *sn*-2 position[59]. In contrast, DAGLα does not exhibit preferences for particular DAG species based on *sn*-2 fatty acyl esterification[59]. DAGLα localizes to the plasma membrane, whereas DAGLβ can similarly localize to the plasma membrane and to LDs[61]. Since PLs exhibit a high abundance of AA (C20:4) at the *sn*-2 position, and DAGLs mediate the hydrolysis of PL-derived *sn*-1,2 DAGs, a large proportion of resulting *sn*-2 MAGs will be 2-AG. Notably, 2-AG is both a major endocannabinoid that functions as a CB_1 and CB_2 receptor agonist as well the major eicosanoid precursor lipid involved in inflammatory signaling. Thus, through dual regulation of 2-AG and AA pools, DAGLs, in particular, DAGLβ are important for mediating the crosstalk between endocannabinoid and eicosanoid signaling in immune cells.

1.1.3c *Choline Phosphotransferases*

The cytidine diphosphate (CDP)-choline or Kennedy pathway utilizes DAG species to generate the majority of intracellular PC in mammals[62]. The enzyme class that mediates this reaction is known as choline phosphotransferase (CPT) of which two proteins are expressed in humans. CPT1 is a CDP-choline-specific enzyme whereas CEPT1 functions to generate both PC and phosphatidylethanolamine (PE) using CDP-choline or CDP-ethanolamine, respectively[63,64]. CPT1 localizes to the Golgi network while CEPT1 localizes to the ER membrane[65]. In the yeast ortholog of CPT1, the protein exhibits a preference for *sn*-1,2 DAGs containing medium-chain length monounsaturated FAs (e.g., C16:1)[66]. Similarly, CEPT1 acts against *sn*-1,2 DAGs with a strong preference for dipalmitolein species (diC16:1)[65]. Since CPT activity is involved in PL biosynthesis at the ER and Golgi network, these enzymes exclusively deplete local *sn*-1,2 DAGs.

1.1.3d *Diacylglycerol Kinases*

Diacylglycerol kinases (DGKs) catalyze the phosphorylation of DAG into PA through the consumption of ATP[67]. There are ten (α, β, γ, δ, ε, ζ, η, θ, ι, and κ) isoforms across five subtypes of DGKs in mammals, suggesting that nature has intended for these distinct isozymes to phosphorylate specific DAG species at predetermined locales and times in the cell[68]. These structural motifs have imparted distinct DGK isoform localization and function as a result, and thus suggest that they may affect regulation of specific catalytic activity. DAG specificity has only recently been demonstrated for DGKε in regulation of *sn*-2 AA- (C20:4)-containing DAGs produced as byproducts in the PI cycle[69]. Additional studies have hinted at DAG specificity for other DGKs including DGKδ however, no comprehensive investigations have been capable of explicitly annotating these numerous lipid-protein interactions in their native state[70].

All DGK family members possess a conserved catalytic domain displaying a GGDGXXG motif that is essential for transferring the γ-PO3 of ATP to a nucleophilic hydroxyl on the accepting substrate via a conserved catalytic lysine residue[68]. Another well characterized and consistent feature within this family, as well as in other lipid binding protein families, is the cysteine-rich motif (CRM). The CRM domains present in DGKs share a homology to the DAG/phorbol ester binding exhibited by protein kinase C isoform C1-type motifs[71]. This discovery initially led researchers to suspect that DAG binding occurred at these C1 domain sites. However, further characterization studies revealed that only the C1A domains, those proximal to the C-terminus, of DGKβ and DGKγ displayed this “typical” DAG binding or phorbol ester sensitive behavior. Whereas all other isoforms were henceforth classified as possessing “atypical”, or non-DAG binding or phorbol ester insensitive C1 domains[72]. Nonetheless, like closely related PKC family members, DGK isoforms preferentially act against *sn*-1,2 DAG isomers, likely through its conserved C1 domain features.

1.2 *References*

1 Sato, M., Ueda, Y. & Umezawa, Y. Imaging diacylglycerol dynamics at organelle membranes. *Nat Methods* **3**, 797-799, doi:10.1038/nmeth930 (2006).

2 Kunkel, M. T. & Newton, A. C. Calcium transduces plasma membrane receptor signals to produce diacylglycerol at Golgi membranes. *J Biol Chem* **285**, 22748-22752, doi:10.1074/jbc.C110.123133 (2010).

3 Carrasco, S. & Merida, I. Diacylglycerol, when simplicity becomes complex. *Trends Biochem Sci* **32**, 27-36, doi:10.1016/j.tibs.2006.11.004 (2007).

4 Kadamur, G. & Ross, E. M. Mammalian phospholipase C. *Annu Rev Physiol* **75**, 127-154, doi:10.1146/annurev-physiol-030212-183750 (2013).

5 Cheng, D. *et al.* Acylation of acylglycerols by acyl coenzyme A:diacylglycerol acyltransferase 1 (DGAT1). Functional importance of DGAT1 in the intestinal fat absorption. *J Biol Chem* **283**, 29802-29811, doi:10.1074/jbc.M800494200 (2008).

6 Eichmann, T. O. & Lass, A. DAG tales: the multiple faces of diacylglycerol--stereochemistry, metabolism, and signaling. *Cell Mol Life Sci* **72**, 3931-3952, doi:10.1007/s00018-015-1982-3 (2015).

7 Wilson, P. A., Gardner, S. D., Lambie, N. M., Commans, S. A. & Crowther, D. J. Characterization of the human patatin-like phospholipase family. *J Lipid Res* **47**, 1940-1949, doi:10.1194/jlr.M600185-JLR200 (2006).

8 Taschler, U. *et al.* Adipose triglyceride lipase is involved in the mobilization of triglyceride and retinoid stores of hepatic stellate cells. *Biochim Biophys Acta* **1851**, 937-945, doi:10.1016/j.bbalip.2015.02.017 (2015).

9 Eichmann, T. O. *et al.* Studies on the substrate and stereo/regioselectivity of adipose triglyceride lipase, hormone-sensitive lipase, and diacylglycerol-O-acyltransferases. *J Biol Chem* **287**, 41446-41457, doi:10.1074/jbc.M112.400416 (2012).

10 Vaughan, M., Berger, J. E. & Steinberg, D. Hormone-sensitive Lipase and Monoglyceride Lipase Activities in Adipose Tissue. *Journal of Biological Chemistry* **239**, 401-409, doi:10.1016/s0021-9258(18)51692-6 (1964).

11 Anthonsen, M. W., Ronnstrand, L., Wernstedt, C., Degerman, E. & Holm, C. Identification of novel phosphorylation sites in hormone-sensitive lipase that are phosphorylated in response to isoproterenol and govern activation properties in vitro. *J Biol Chem* **273**, 215-221, doi:10.1074/jbc.273.1.215 (1998).

12 Nagayama, M., Shimizu, K., Taira, T., Uchida, T. & Gohara, K. Shrinking and development of lipid droplets in adipocytes during catecholamine-induced lipolysis. *FEBS Lett* **584**, 86-92, doi:10.1016/j.febslet.2009.10.088 (2010).

13 Su, C. L. *et al.* Mutational analysis of the hormone-sensitive lipase translocation reaction in adipocytes. *J Biol Chem* **278**, 43615-43619, doi:10.1074/jbc.M301809200 (2003).

14 Fredrikson, G., Strålfors, P., Nilsson, N. O. & Belfrage, P. Hormone-sensitive lipase of rat adipose tissue. Purification and some properties. *Journal of Biological Chemistry* **256**, 6311-6320, doi:10.1016/s0021-9258(19)69164-7 (1981).

15 Rodriguez, J. A. *et al.* In vitro stereoselective hydrolysis of diacylglycerols by hormone-sensitive lipase. *Biochim Biophys Acta* **1801**, 77-83, doi:10.1016/j.bbalip.2009.09.020 (2010).

16 Schweiger, M. *et al.* Adipose triglyceride lipase and hormone-sensitive lipase are the major enzymes in adipose tissue triacylglycerol catabolism. *J Biol Chem* **281**, 40236-40241, doi:10.1074/jbc.M608048200 (2006).

17 Gao, J. G. & Simon, M. A comparative study of human GS2, its paralogues, and its rat orthologue. *Biochem Biophys Res Commun* **360**, 501-506, doi:10.1016/j.bbrc.2007.06.089 (2007).

18 Lake, A. C. *et al.* Expression, regulation, and triglyceride hydrolase activity of Adiponutrin family members. *J Lipid Res* **46**, 2477-2487, doi:10.1194/jlr.M500290-JLR200 (2005).

19 Huang, Y., Cohen, J. C. & Hobbs, H. H. Expression and characterization of a PNPLA3 protein isoform (I148M) associated with nonalcoholic fatty liver disease. *J Biol Chem* **286**, 37085-37093, doi:10.1074/jbc.M111.290114 (2011).

20 Rhee, S. G. REGULATION OFPHOSPHOINOSITIDE-SPECIFICPHOSPHOLIPASEC. *Annu. Rev. Biochem.* **70**, 281-312 (2001).

21 Ramoni, C., Spadaro, F., Barletta, B., Dupuis, M. L. & Podo, F. Phosphatidylcholine-specific phospholipase C in mitogen-stimulated fibroblasts. *Exp Cell Res* **299**, 370-382, doi:10.1016/j.yexcr.2004.05.037 (2004).

22 Rhee, S. G. REGULATION OF PHOSPHOINOSITIDE-SPECIFIC PHOSPHOLIPASE C. *Annu. Rev. Biochem.* **70**, 281-312 (2001).

23 Fukami, K., Inanobe, S., Kanemaru, K. & Nakamura, Y. Phospholipase C is a key enzyme regulating intracellular calcium and modulating the phosphoinositide balance. *Progress in Lipid Research* **49**, 429-437 (2010).

24 Ullman, M. D. & Radin, N. S. The Enzymatic Formation of Sphingomyelin from Ceramide and Lecithin in Mouse Liver. *Journal of Biological Chemistry* **249**, 1506-1512, doi:10.1016/s0021-9258(19)42911-6 (1974).

25 Huitema, K., van den Dikkenberg, J., Brouwers, J. F. & Holthuis, J. C. Identification of a family of animal sphingomyelin synthases. *EMBO J* **23**, 33-44, doi:10.1038/sj.emboj.7600034 (2004).

26 Tafesse, F. G. *et al.* Both sphingomyelin synthases SMS1 and SMS2 are required for sphingomyelin homeostasis and growth in human HeLa cells. *J Biol Chem* **282**, 17537-17547, doi:10.1074/jbc.M702423200 (2007).

27 Donkor, J., Sariahmetoglu, M., Dewald, J., Brindley, D. N. & Reue, K. Three mammalian lipins act as phosphatidate phosphatases with distinct tissue expression patterns. *J Biol Chem* **282**, 3450-3457, doi:10.1074/jbc.M610745200 (2007).

28 Ware, T. B. *et al.* Reprogramming fatty acyl specificity of lipid kinases via C1 domain engineering. *Nature Chemical Biology* **16**, 170-178, doi:10.1038/s41589-019-0445-9 (2020).

29 Harris, T. E. *et al.* Insulin controls subcellular localization and multisite phosphorylation of the phosphatidic acid phosphatase, lipin 1. *J Biol Chem* **282**, 277-286, doi:10.1074/jbc.M609537200 (2007).

30 Carman, G. M. & Han, G. S. Roles of phosphatidate phosphatase enzymes in lipid metabolism. *Trends Biochem Sci* **31**, 694-699, doi:10.1016/j.tibs.2006.10.003 (2006).

31 Coleman, R. A. & Mashek, D. G. Mammalian triacylglycerol metabolism: synthesis, lipolysis, and signaling. *Chem Rev* **111**, 6359-6386, doi:10.1021/cr100404w (2011).

32 Li, D. *et al.* ADVANCED IMAGING. Extended-resolution structured illumination imaging of endocytic and cytoskeletal dynamics. *Science* **349**, aab3500, doi:10.1126/science.aab3500 (2015).

33 Yen, C. L. & Farese, R. V., Jr. MGAT2, a monoacylglycerol acyltransferase expressed in the small intestine. *J Biol Chem* **278**, 18532-18537, doi:10.1074/jbc.M301633200 (2003).

34 Cheng, D. *et al.* Identification of acyl coenzyme A:monoacylglycerol acyltransferase 3, an intestinal specific enzyme implicated in dietary fat absorption. *J Biol Chem* **278**, 13611-13614, doi:10.1074/jbc.C300042200 (2003).

35 Yen, C., Stone, S., Cases, S., Zhou, P. & Farese Jr, R. Identification of a gene encoding MGAT1, a monoacylglycerol acyltransferase. *Proc Natl Acad Sci U S A* **99**, 8512-8517 (2002).

36 Cao, J., Cheng, L. & Shi, Y. Catalytic properties of MGAT3, a putative triacylgycerol synthase. *J Lipid Res* **48**, 583-591, doi:10.1194/jlr.M600331-JLR200 (2007).

37 Colon-Gonzalez, F. & Kazanietz, M. G. C1 domains exposed: from diacylglycerol binding to protein-protein interactions. *Biochim Biophys Acta* **1761**, 827-837, doi:10.1016/j.bbalip.2006.05.001 (2006).

38 Kikkawa, U., Takai, Y., Tanaka, Y., Miyake, R. & Nishizuka, Y. Protein kinase C as a possible receptor protein of tumor-promoting phorbol esters. *Journal of Biological Chemistry* **258**, 11442-11445, doi:10.1016/s0021-9258(17)44245-1 (1983).

39 Griner, E. M. & Kazanietz, M. G. Protein kinase C and other diacylglycerol effectors in cancer. *Nat Rev Cancer* **7**, 281-294, doi:10.1038/nrc2110 (2007).

40 Sharkey, N. A., Leach, K. L. & Blumberg, P. M. Competitive inhibition by diacylglycerol of specific phorbol ester binding. *Proc Natl Acad Sci U S A* **81**, 607-610 (1984).

41 Rando, R. & Young, N. THE STEREOSPECIFIC ACTIVATION OF PROTEIN KINASE C. *Biochemical and Biophysical Research Communications* **122**, 818-823 (1984).

42 Wang, Q. J. PKD at the crossroads of DAG and PKC signaling. *Trends Pharmacol Sci* **27**, 317-323, doi:10.1016/j.tips.2006.04.003 (2006).

43 Waldron, R. T. & Rozengurt, E. Protein kinase C phosphorylates protein kinase D activation loop Ser744 and Ser748 and releases autoinhibition by the pleckstrin homology domain. *J Biol Chem* **278**, 154-163, doi:10.1074/jbc.M208075200 (2003).

44 Zugaza, J., Sinnet-Smith, J., Van Lint, J. & Rozengurt, E. Protein kinase D (PKD activation in intact cells through a protein kinase C-dependent signal transduction pathway. *EMBO J* **15**, 6220-6230 (1996).

45 Jamora, C. *et al.* Gβγ-Mediated Regulation of Golgi Organization Is through the Direct Activation of Protein Kinase D. *Cell* **98**, 59-68, doi:10.1016/s0092-8674(00)80606-6 (1999).

46 Stone, J. Regulation of Ras in lymphocytes: get a GRP. *Biochemical Society Transactions* **34**, 858-861 (2006).

47 Ebinu, J. O. *et al.* RasGRP, a Ras Guanyl Nucleotide–Releasing Protein with Calcium- and Diacylglycerol-Binding Motifs. *Science* **280**, 1082-1086 (1998).

48 Ebinu, J. O. *et al.* RasGRP links T-cell receptor signaling to Ras. *Blood* **95**, 3199-3203, doi:10.1182/blood.V95.10.3199 (2000).

49 Coughlin, J., Stang, S., Dower, N. & Stone, J. RasGRP1 and RasGRP3 Regulate B Cell Proliferation by Facilitating B Cell Receptor-Ras Signaling. *The Journal of Immunology* **175**, 7179-7184 (2005).

50 Irie, K., Masuda, A., Shindo, M., Nakagawa, Y. & Ohigashi, H. Tumor promoter binding of the protein kinase C C1 homology domain peptides of RasGRPs, chimaerins, and Unc13s. *Bioorg Med Chem* **12**, 4575-4583, doi:10.1016/j.bmc.2004.07.008 (2004).

51 Hall, C. *et al.* Novel Human Brain cDNA encoding a 34,000 M Protein *n*-Chimaerin, Related to Both the Regulatiory Domain of Protein Kinase C and BCR, the Product of the Breakpoint Cluster Region Gene. *J. Mol. Biol.* **211**, 11-16 (1990).

52 Wang, H. *et al.* Phospholipase Cgamma/diacylglycerol-dependent activation of beta2-chimaerin restricts EGF-induced Rac signaling. *EMBO J* **25**, 2062-2074, doi:10.1038/sj.emboj.7601098 (2006).

53 Yang, C., Liu, Y., Leskow, F. C., Weaver, V. M. & Kazanietz, M. G. Rac-GAP-dependent inhibition of breast cancer cell proliferation by {beta}2-chimerin. *J Biol Chem* **280**, 24363-24370, doi:10.1074/jbc.M411629200 (2005).

54 Augustin, I., Rosenmund, C., Sudhof, T. C. & Brose, N. Munc13-1 is essential for fusion competence of glutamatergic synaptic vesicles. *Nature* **400**, 457-461 (1999).

55 Rhee, J. S. *et al.* β Phorbol Ester- and Diacylglycerol-Induced Augmentation of Transmitter Release is Mediated by Munc13s and Not by PKCs. *Cell* **108**, 121-133 (2002).

56 Hofmann, K. A superfamily of membrane-bound *O*-acyltransferases with implications for Wnt signaling. *Trends Biochem Sci* **25**, 111-112 (2000).

57 Yen, C. L., Stone, S. J., Koliwad, S., Harris, C. & Farese, R. V., Jr. Thematic review series: glycerolipids. DGAT enzymes and triacylglycerol biosynthesis. *J Lipid Res* **49**, 2283-2301, doi:10.1194/jlr.R800018-JLR200 (2008).

58 Hiramine, Y. & Tanabe, T. Characterization of acyl-coenzyme A:diacylglycerol acyltransferase (DGAT) enzyme of human small intestine. *J Physiol Biochem* **67**, 259-264, doi:10.1007/s13105-010-0071-1 (2011).

59 Bisogno, T. *et al.* Cloning of the first sn1-DAG lipases points to the spatial and temporal regulation of endocannabinoid signaling in the brain. *J Cell Biol* **163**, 463-468, doi:10.1083/jcb.200305129 (2003).

60 Reisenberg, M., Singh, P. K., Williams, G. & Doherty, P. The diacylglycerol lipases: structure, regulation and roles in and beyond endocannabinoid signalling. *Philos Trans R Soc Lond B Biol Sci* **367**, 3264-3275, doi:10.1098/rstb.2011.0387 (2012).

61 Jung, K. M., Astarita, G., Thongkham, D. & Piomelli, D. Diacylglycerol lipase-alpha and -beta control neurite outgrowth in neuro-2a cells through distinct molecular mechanisms. *Mol Pharmacol* **80**, 60-67, doi:10.1124/mol.110.070458 (2011).

62 Gibellini, F. & Smith, T. K. The Kennedy pathway--De novo synthesis of phosphatidylethanolamine and phosphatidylcholine. *IUBMB Life* **62**, 414-428, doi:10.1002/iub.337 (2010).

63 Henneberry, A. L., Wistow, G. & McMaster, C. R. Cloning, genomic organization, and characterization of a human cholinephosphotransferase. *J Biol Chem* **275**, 29808-29815, doi:10.1074/jbc.M005786200 (2000).

64 Henneberry, A. L. & McMaster, C. R. Cloning and expression of a human choline/ethanolaminephosphotransferase: synthesis of phosphatidylcholine and phosphatidylethanolamine. *Biochem J.* **339**, 291-298 (1999).

65 Henneberry, A. L., Wright, M. M. & McMaster, C. R. The major sites of cellular phospholipid synthesis and molecular determinants of Fatty Acid and lipid head group specificity. *Mol Biol Cell* **13**, 3148-3161, doi:10.1091/mbc.01-11-0540 (2002).

66 Hjelmstad, R. H., Morash, S. C., McMaster, C. R. & Bell, R. M. Chimeric enzymes. Structure-function analysis of segments of sn-1,2-diacylglycerol choline- and ethanolaminephosphotransferases. *Journal of Biological Chemistry* **269**, 20995-21002, doi:10.1016/s0021-9258(17)31920-8 (1994).

67 Topham, M. K. & Prescott, S. M. Mammalian Diacylglycerol Kinases, a Family of Lipid Kinases with SIgnaling Functions. *The Journal of biological chemistry* **274**, 11447-11450 (1999).

68 Topham, M. K. & Epand, R. M. Mammalian diacylglycerol kinases: molecular interactions and biological functions of selected isoforms. *Biochim Biophys Acta* **1790**, 416-424, doi:10.1016/j.bbagen.2009.01.010 (2009).

69 Lung, M. *et al.* Diacylglycerol kinase epsilon is selective for both acyl chains of phosphatidic acid or diacylglycerol. *J Biol Chem* **284**, 31062-31073, doi:10.1074/jbc.M109.050617 (2009).

70 Shulga, Y. V., Topham, M. K. & Epand, R. M. Regulation and functions of diacylglycerol kinases. *Chem Rev* **111**, 6186-6208, doi:10.1021/cr1004106 (2011).

71 Merino, E., Sanjuan, M. A., Moraga, I., Cipres, A. & Merida, I. Role of the diacylglycerol kinase alpha-conserved domains in membrane targeting in intact T cells. *J Biol Chem* **282**, 35396-35404, doi:10.1074/jbc.M702085200 (2007).

72 Sakane, F., Kai, M., Wada, I., Imai, S. & Kanoh, H. The C-terminal part of diacylglycerol kinase alpha lacking zinc fingers serves as a catalytic domain. *Biochem J* **318**, 583-590 (1996).

Chapter 2. Determination of Diacylglycerol Kinase Substrate Recognition Mechanism

Adapted from: Timothy B. Ware, Caroline E. Franks, Mitchell E. Granade, Mingxing Zhang, Kee-Beom Kim, Kwon-Sik Park, Andreas Gahlmann, Thurl E. Harris, and Ku-Lung Hsu. *Nature Chemical Biology* 16, 170-178 (2020).

2.1 *Abstract*

C1 domains are lipid-binding modules that regulate membrane activation of kinases, nucleotide exchange factors, and other C1-containing proteins to trigger signal transduction. Despite annotation of typical C1 domains as diacylglycerol (DAG) and phorbol ester sensors, the function of atypical counterparts remains ill-defined. Here, we assign a key role for atypical C1 domains in mediating DAG fatty acyl specificity of diacylglycerol kinases (DGKs) in live cells. Activity-based proteomics mapped C1 probe binding as a principal differentiator of type 1 DGK active sites that combined with global metabolomics revealed a role for C1s in lipid substrate recognition. Protein engineering by C1 domain swapping demonstrated that exchange of typical and atypical C1s is functionally tolerated and can directly program DAG fatty acyl specificity of type 1 DGKs. Collectively, we describe a protein engineering strategy for studying metabolic specificity of lipid kinases to assign a role for atypical C1 domains in cell metabolism.

2.2 *Introduction*

The chemical makeup of lipids can have profound effects on cell biology and physiology. Fatty acid (FA) length and unsaturation are important determinants of membrane fluidity, permeability and signaling activity of metabolic products. Cells must tightly regulate the ratio of saturated (devoid of *cis* double bonds) and unsaturated (mono- or poly-) FAs in order to maintain an optimal balance of fluidity to permit trafficking of proteins and lipids without compromising structural integrity and barrier function of membranes. Metabolic enzymes that regulate the FA composition and dynamics of membranes are directly involved in fine tuning membrane curvature, budding, and fusion that broadly impact transport, metabolism, and signal transduction[1,2,3]. The ability of metabolic enzymes to select lipid substrates based on FA composition at membranes remains a poorly understood process in need of new methodologies to uncover the structure-function relationships of lipids *in vivo*.

A case example is the diacylglycerol kinase (DGK) family of lipid kinases that catalyze ATP-dependent phosphorylation of diacylglycerol[4] (DAG) to produce phosphatidic acid[5] (PA, **Figure 2.1a**). To date, ten mammalian DGKs have been identified and divided into five subtypes (**Figure 2.2**) based on primary protein sequence that differentiate isoforms on the basis of regulatory domains remote from the conserved lipid kinase domain (Pfam PF00781[6]). Isoform-selective targeting of DGKs remains difficult as inhibitors often block the conserved catalytic domain, leading to off-target activity[7]. The non-catalytic domains of DGKs modulate Ca^{2+} activation[8], subcellular localization[9,10], oligomerization[11], and protein-protein interactions[12] and presumably control when and where these enzymes can access DAG substrates for phosphorylation. Understanding DGK specificity is important because altered function of individual isoforms has been implicated in impaired tumor immune responses[13,14,15,16,17,18,19], Parkinson's disease[20,21], bipolar disorder[22,23,24,25,26], asthma[27], and metabolic disease[28,29,30,31,32], suggesting that distinct DAG and/or PA species are mediating specific biology. Paradoxically,

DGKε, which lacks defined regulatory domains compared with other DGKs is the only isoform with reported DAG fatty acyl chain specificity[33,34,35].

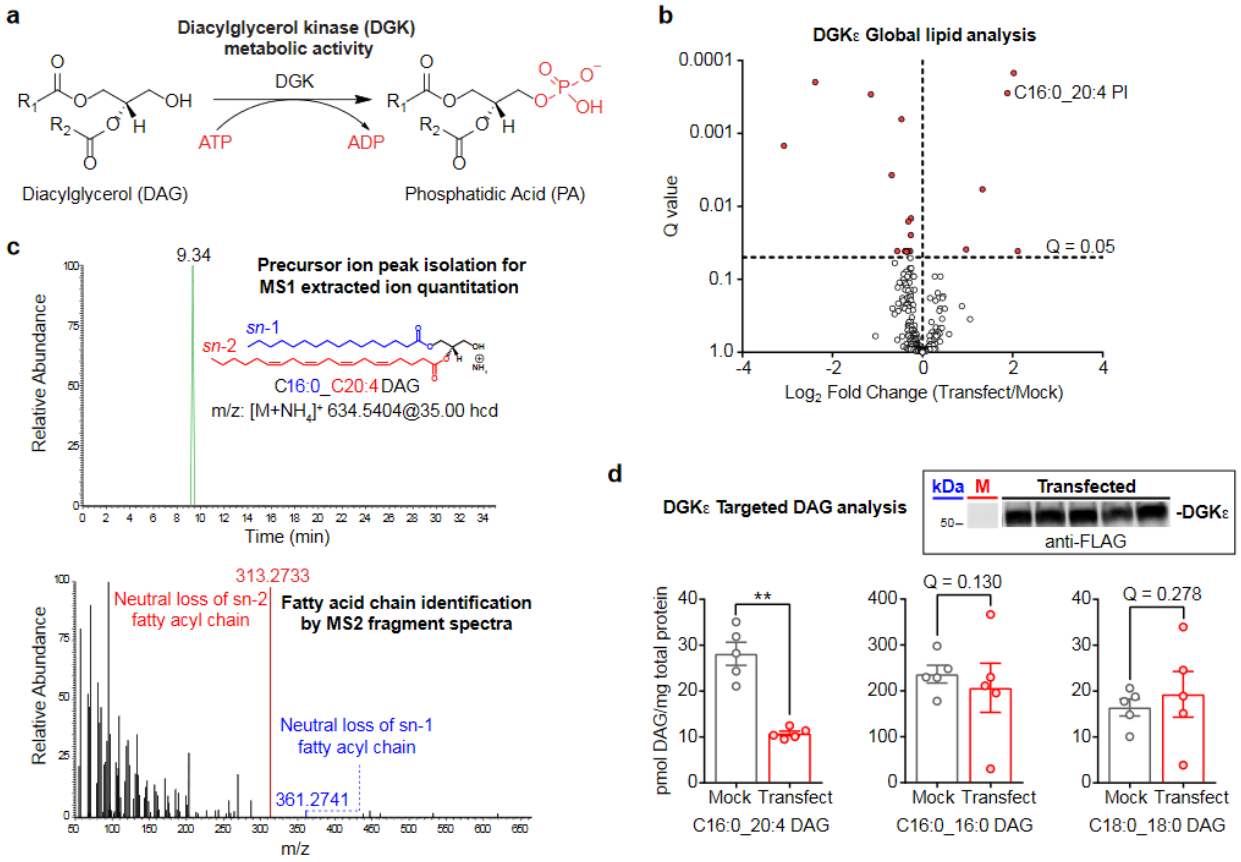

Figure 2.1 LC-MS/MS metabolomics for deciphering DGK isoform fatty acyl specificity. a) DGKs catalyze ATP-dependent phosphorylation of diacylglycerol to generate phosphatidic acid. b) Results from an untargeted lipidomics analysis of human DGKε overexpressed in HEK293T cells (*n*=5 biological samples). Significantly altered lipids were identified by a Q-value < 0.05 following a Benjamini-Hochberg correction of a two-sided binomial test. c) MS1 chromatogram (top) and MS2 fragmentation spectrum (bottom) obtained for identification and quantitative analysis of the DGKε substrate C16:0_C20:4 DAG. d) Targeted lipidomics analysis showed recombinant human DGKε substrate specificity for C16:0_C20:4 compared with C16:0_C16:0 and C18:0_C18:0 DAGs in live cells. Significance was determined using a Benjamini-Hochberg correction following a two-sided binomial test (**Q < 0.01). Data shown represents mean ± s.e.m.; (*n*=5 biological samples). Inset: western blot shows reproducible transient overexpression of recombinant DGKε in HEK293T cells (anti-FLAG antibody); "M" represents mock lane. All data shown are representative of two experiments (*n*=2 biologically independent experiments).

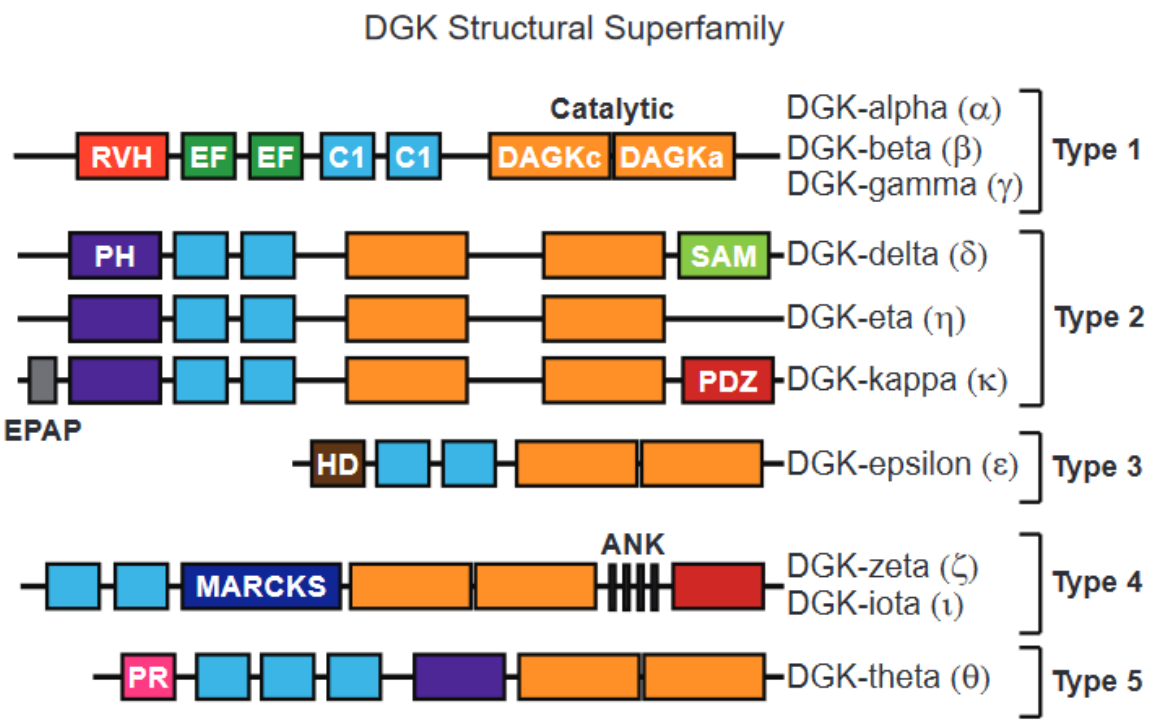

Figure 2.2 The diacylglycerol kinase superfamily regulates cell signaling via metabolism of lipid messengers. Classification of the 10 mammalian DGK isoforms into 5 subtypes based on structural motifs. RVH: recoverin homology domain; EF: EF Hand motif; C1: atypical/typical C1 domain; PH: pleckstrin homology domain; SAM: sterile alpha motif; EPAP: Glu-Pro-Ala-Pro repeats; PDZ: protein-protein interactions; HD: hydrophobic domain; MARCKS: myristolated alanine rich protein kinase C substrate domain; ANK: Ankyrin repeats; PR: proline-rich region.

DGKε shows preference for *sn*-2 arachidonic acid-esterified DAGs[33] (C20:4). The preference of DGKε for stearic acid (C18:0) at the *sn*-1 position led to discovery of its role in phosphorylating 1-stearoyl-2-arachidonoylglycerol (SAG) in the phosphatidylinositol (PI) cycle[36]. DGKε is unique among DGK isoforms as the smallest member composed of a hydrophobic domain, tandem cysteine rich (C1) domains, and the conserved lipid kinase domain. The small size of DGKε shows that acyl chain specificity can be achieved with a minimum domain topology. The C1 domains are promising candidates to function as lipid recognition modules based on their role in translocating target proteins to membranes during cellular activation[37,38] (e.g., protein kinase C or PKC). Unlike “typical” PKC C1s, the C1 domains of a majority of DGKs lack conserved amino acids needed for membrane association (presumably via DAG recognition)[37,38]. With the

exception of DGKβ and DGKγ, all DGK isoforms contain “atypical” C1s and the function of these domains with regards to metabolic function remains ill-defined in living systems.

Here, we annotate a new role for C1 domains in mediating DAG fatty acyl chain specificity of DGKs. We utilized chemical proteomics and metabolomics to reveal differences in molecular recognition of DGK active sites that correlate and potentially explain the distinct DAG substrate assignments in live cell gain-of-function studies. We performed C1 domain swapping experiments in type 1 DGKs to demonstrate that DAG fatty acyl chain specificity of DGKs is directly encoded by the identity of respective C1 domains independent of subcellular localization. The implication of our findings is establishment of C1 domains as a key component of DGK active sites that directs lipid substrate specificity and suggests that atypical and typical C1 domains are functionally interchangeable in terms of lipid kinase metabolic activity.

2.3 *Materials and Methods*

Reagents. Unless otherwise specified, all reagents were purchased from Fisher Scientific. Polyethyleneimine (Polysciences Inc., Cat# 24765), ritanserin ≥99% by HPLC (Tocris Bioscience, Cat# 1955), ketanserin tartrate ≥97% by HPLC (Tocris Bioscience, Cat# 0908), 1-stearoyl-2-arachidonoyl-d8-*sn*-glycerol (SAG-d8; Cayman Chemical Company, Cat# 10009872), and arachidonic acid-d8 (AA-d8; Cayman Chemical Company, Cat# 390010).

Cell culture. HEK293T cells were purchased from ATCC. *DGKA* Knockdown A549 cells were generated by Dr. Kwon-Sik Park Lab at University of Virginia. HEK293T cells were cultured in DMEM with 10% FBS (U.S. Source, Omega Scientific) and 1% L-glutamine (Thermo Fisher Scientific) in 10 cm^2 plates. Media in cell cultures were switched to serum-free DMEM 4 h prior to harvesting for all lipid analyses or 1 h for compound treatments. SILAC HEK293T cells were cultured in DMEM for SILAC (Fisher Scientific) supplemented with 10% dialyzed FBS (Omega Scientific) in 10 cm^2 plates. Light medium was supplemented with 100 μg ml^{-1} L-arginine and 100 μg ml^{-1} L-lysine. Heavy medium was supplemented with 100 μg ml^{-1} [$^{13}C_6{}^{15}N_4$]L-arginine and 100 μg ml^{-1} [$^{13}C_6{}^{15}N_2$]L-lysine. Light or heavy amino acids were incorporated for at least 5 passages prior to utilizing SILAC HEK293T cells for experiments. All cells were grown to ~80% confluency in a 37°C incubator with 5% CO_2. Cells were switched to serum-free DMEM media prior to compound treatments.

Transient transfection. Recombinant DGK proteins were produced by transient transfection of HEK293T cells with recombinant DNA. pDONR223-DGKK was a gift from William Hahn and David Root (Addgene plasmid # 23487). pCSF107mT-GATEWAY-3'-FLAG was a gift from Todd Stukenberg (Addgene plasmid # 67619). pCSF107mT-DGKK-FLAG construct was generated by recombination of the Addgene plasmids using the Gateway cloning system (Invitrogen). All other vectors were either developed by Dr. Thurl Harris (University of Virginia, School of Medicine) or gifted to Dr. Kevin Lynch (University of Virginia, School of Medicine) by Dr. Kaoru Goto (Yamagata

University, School of Medicine) and Dr. Fumio Sakane (Chiba University) and were kindly shared for these studies: pcDNA3-FLAG-DGKA (rat), pcDNA3-FLAG-DGKB (rat), pcDNA3-FLAG-DGKG (rat), pcDNA3.1-FLAG-DGKH (human), pCMV-Tag2B-FLAG-DGKQ (human), pGC-FLAG-DGKA (human), pGC-FLAG-DGKB (human), pGC-FLAG-DGKG (human), pcDNA3-DGKE-3xFlag (human), pCMV-HA-DGKI (human), and pCMV-SPORT6-HA-DGKZ (human). A549 cells with doxycycline-inducible knockdown of *DGKA* were developed and provided by Dr. Kwon-Sik Park (University of Virginia, School of Medicine). HEK293T cells were plated at a concentration of 440,000 cells in complete DMEM and grown to 50-60% confluency. A polyethyleneimine (PEI) stock solution was prepared (1 mg/mL, pH 7.4) and filter sterilized. Serum-free DMEM (600 µL) was mixed gently with 20 µL of sterile PEI (1 mg/mL, and pH 7.4), and 2.6 µg DNA in a sterile microfuge tube. Mixtures were incubated for 30 min at 25°C. The mixture was then added dropwise to each 10 cm^2 plate, rocked back and forth to mix, and placed back in the 37°C incubator. Cell pellets were harvested after two full days of growth, snap frozen in liquid N2, and stored at -80°C until use. Recombinant proteins were produced by transient transfection in SILAC HEK293T cells using the procedure described above, except that cells were plated at a concentration of 1 x 10^6 cells per 10 cm^2 plate and grown to ~70% confluency prior to introducing transfection mixture.

Western blot analysis of recombinant protein expression. The following antibodies were purchased for western blot studies: HA Epitope Tag Monoclonal Antibody (Thermo Fisher Scientific) Cat# PI26183; Anti-FLAG antibody produced in rabbit (Sigma-Aldrich) Cat# F7425; Goat anti-mouse DyLight 650 (Thermo Fisher Scientific) Cat# 84545; Goat anti-rabbit DyLight 550 (Thermo Fisher Scientific) Cat# 84541; DGKA Antibody Rabbit Polyclonal (Proteintech) Cat# 11547. Cell lysates were separated via ultracentrifugation at 100,000 x *g* for 45 min at 4°C. Proteins separated by SDS-PAGE (7.5% polyacrylamide, TGX Stain-Free Mini Gel) at 150 V for 55 min. Gel transfers were performed using the Bio-Rad Trans-Blot Turbo RTA Midi Nitrocellulose

Transfer Kit with a Bio-Rad Trans-Blot Turbo Transfer System (25V, 10 min). The nitrocellulose blot was then incubated in blocking solution (30 mL, 3% BSA in TBS-T (1.5 M NaCl, 0.25 M Tris pH 7.4 in ddH_2O)) for 1 h at 25°C with gentle shaking. The blot was then transferred immediately to primary antibody solution (1:1,000 anti-FLAG, 1:10,000 anti-HA or 1:1,000 anti-DGKα in TBS-T) and incubated overnight at 4°C with gentle shaking. The blot was then rinsed 5 times for 5 min in TBS-T, transferred immediately into secondary antibody solution (1:10,000 anti-species DyLight 550 or DyLight 650 in TBS-T), and incubated for 1 h at 25°C with gentle shaking. The blot was then rinsed 5 times for 5 min in TBS-T, transferred into ddH_2O, and imaged by in-blot fluorescence scanning on a ChemiDoc MP Imaging System. Each lane displayed in western blots represents an individual biological replicate of that overexpression/treatment condition.

Doxycycline-induced shRNA knockdown of DGKα in A549 cells. A549 cells were infected with lentiviral shRNAs targeting human *DGKA* gene in Tet-pLKO-puro plasmid (a gift from Dmitri Wiederschain; Addgene #21915). Oligonucleotide sequences for the target are as follows: shDGKA-1, 5′-CGGATTGACCCTGTTCCTAAC-3′, for shDGKA-2 5′-CGGCCAGAAGACAAGTTAGAA-3’. Lentiviral particles were produced by co-transfecting the lentiviral plasmid with 2 packaging plasmids (psPAX2 and pMD2.G) in HEK293T cells using PEI (Sigma-Aldrich, 408727). Supernatants containing the lentiviral particles were harvested 48 and 72 h after the transfection and filtered through 0.45 μm PVDF membrane. Infections were performed with viral supernatant in the presence of 5 μg/ml polybrene (Sigma-Aldrich, H9268). Puromycin with 2 μg/ml (A1113803, Thermo Fisher Scientific) was used to select stably transduced cells. *DGKA* knockdown in the selected cells was induced by adding doxycycline to culture media (Sigma-Aldrich, D9891) and was validated by immunoblot. A549 cells were cultured in a similar manner to HEK293T cells until they reached 80% confluency. Cells were treated with 10 μL of a 0.2 μg/μL doxycycline stock diluted in DMSO for 48 h. Following treatment, cells were

starved, harvested, and analyzed through either LC-MS/MS of lipid extracts or through western blot analysis of endogenous DGKα expression. DGKα knockdown was confirmed by western blot.

Site-directed mutagenesis. Primers for type 1 DGK lysine-alanine mutants were generated and purchased from Integrated DNA Technologies (IDT). The mutagenesis reaction was performed by combining the following in a PCR tube: MilliQ H_2O (34.8 µL), PfuUltra enzyme (1 µL), 10X PfuUltra buffer (5 µL), dNTP mix (1 µL), and template plasmid (5 µL). Primers were diluted to 10 µM in MilliQ H_2O and 1.6 µL of each (forward and reverse) were added to the mutagenesis master mix to bring the final volume to 50 µL. The mixture was placed in a thermocycler under the following protocol after being brought up to 98°C: 98°C (10 secs), 55°C (30 secs), 72°C (30 secs) for 35 cycles then left at 4°C overnight. Following PCR DpnI restriction enzyme (1 µL) was added, mixed, and incubated at 37°C for 1 h. This product was then transformed into electrocompetent E.coli cells (XL-1 from Agilent) and grown to obtain isolated mutated plasmid.

Lipid extraction. Modified Bligh Dyer method ($CHCl_3$:MeOH:H_2O/1:2:2; 0.1N HCl) was used to extract lipids from HEK293T cell pellets (~6.0 million cells). Antioxidant BHT (butylated hydroxy toluene) was added at 50 µg/mL during extraction. $CHCl_3$ (1 mL), and MeOH (2 mL) were added with 1.5 mL of ddH_2O containing resuspended HEK293T cells in a two-dram vial. 1N HCl (500 µL) was added last to bring the final concentration of acid to 0.1 N. Samples were vortexed, incubated on ice for 20 min, and centrifuged at 2,000 x *g* for 5 min at 4°C. Lipid standards (10 pmol each of AA-d8 and SAG-d8) were added to organic solvents prior to mixing and lipid extraction of cells. The organic layer was transferred, and aqueous layer extracted with addition of 1.5 mL of 1:2 $CHCl_3$:MeOH solution. The extracted organic layers were combined and dried down under nitrogen stream. Samples were resuspended in 240 µL of 1:1 MeOH:IPA and stored at −80°C until further analysis.

LC-MS/MS analysis of lipid extracts. The lipid samples were analyzed by LC-MS/MS. A Dionex Ultimate 3000 RS UHPLC system was used with an analytical column (Kinetex® 1.7 µm C18 100

Å, Phenomenex, LC column 100 x 2.1 mm) and reverse phase LC solvents (C: ACN:H_2O/50:50, 10 mM NH_4HCO_2, 1% formic acid; D: ACN:IPA:H_2O/10:88:2, 10 mM NH_4HCO_2, 1% formic acid) with the following gradient: Flowrate 0.25 mL/min, 0 min 65% C, 4 min 40% C, 12 min 15% C, 21 min 0% C, 24 min, 0% C, 24.1 min 100% C, 27 min 0% C, 30 min 100% C, 33 min 0% C, 35 min 65% C. The eluted lipids were ionized by electrospray using a HESI-II probe into an Orbitrap Q-Exactive Plus mass spectrometer (Thermo Scientific). Data acquisition was performed using both parallel reaction monitoring (PRM) targeted and Top10 data-dependent (ddMS2) global analysis methods. PRM targeting of diacylglycerol and phosphatidic acid lipid species was accomplished by filtering for the $[M+NH_4]+$ and [M-H]- adduct ions, respectively and subsequent MS2 detection of expected diagnostic fragment ions (neutral loss of fatty acyl chains in positive mode and loss of the fatty acyl chain along with H in the negative mode). Intensities of the lipid species were measured using TraceFinder™ software, which identified fragment ions across multiple samples based on the MS2 filter defined in a targeted list of lipids and aligned them according to the intensities of the ion species found in each raw file. Lipid identifications and peak alignments were performed using LipidSearch™ software while quantitative analysis of the aligned intensities was exported and analyzed using Prism GraphPad version 7.03. Positive and negative ion annotations for each sample were combined and aligned within a chromatographic time window to allow greater confidence in lipid identifications using appropriate MS2 product ions and neutral losses from the compiled dataset in LipidSearch™ analysis software. Aligned results were further filtered by retention time constraints, signal to noise ratio, intensity ratio of diagnostic ion, main adduct ion, ID quality, and peak quality specifications.

Sample preparation for quantitative LC-MS/MS analysis using ATP acyl phosphate probes. Proteomes were diluted to 2 mg/mL in kinase buffer. The light and heavy proteomes (0.5 mg, 250 µL total reaction volume) were pre-treated with vehicle or compound, respectively (5 µL, DMSO (light) or 50X stock in DMSO (heavy)), mixed gently, and incubated at 25°C for 30 min.

Desthiobiotin ATP acyl phosphate nucleotide probe (0.5 mM in ddH_2O) was then added to each sample (5 µL, 10 µM final), mixed gently, and allowed to incubate at 25°C for 30 min. After incubation, matched light and heavy proteomes were transferred and mixed in a 1:1 ratio in a two-dram vial containing 4:1:3 MeOH/$CHCl_3$/H_2O (2 mL MeOH, 500 µL $CHCl_3$, 1.5 mL H_2O) for extraction of proteins to remove excess probe, quickly vortexed, and centrifuged at 1,400 x *g* for 3 min to pellet protein. Organic and aqueous layers were removed using a Pasteur pipette, and the protein pellet was transferred to a screw-top tube in 600 µL MeOH. A second extraction was performed by adding $CHCl_3$ (150 µL) and H_2O (600 µL) to each sample, vortexed, and centrifuged at 1,400 x *g* for 3 min to pellet protein. Organic and aqueous layers were removed by pipetting, MeOH added to pellet (600 µL) and pellets were re-suspended by sonication (3 × 1 sec pulse, 20% amplitude) for a final extraction. Samples were then centrifuged at 17,000 x *g* for 5 min to pellet protein and MeOH was removed by pipetting. The pellets were re-suspended in 10 M urea/25 mM ammonium bicarbonate (500 mL), brought to a final volume of 1 mL with 25 mM ammonium bicarbonate, reduced with 10 mM DTT for 15 min at 65°C, allowed to cool, and then alkylated with 40 mM iodoacetamide for 30 min at 25°C in the dark. To de salt the samples, each was transferred to a two-dram glass vial, and to the vial 4:1:2 MeOH/$CHCl_3$/H_2O (2 mL MeOH, 500 µL $CHCl_3$, 1 mL H_2O) was added. The vials were vortexed quickly, spun at 1,400 x *g* for 3 min to pellet protein, and aqueous and organic layers were removed using a Pasteur pipette. The resulting protein pellet was transferred to a screw-top tube in 600 µL MeOH, and then $CHCl_3$ (150 µL) and H_2O (600 µL) were added to extract protein a second time. The samples were vortexed quickly, centrifuged at 1,400 x *g* to pellet protein, and the aqueous and organic layers were removed by pipetting. Resulting protein pellet was suspended in MeOH (600 µL) via sonication (3 × 1sec pulse, 20% amplitude), centrifuged at 17,000 x *g* for 5 min to pellet protein, and MeOH removed by pipetting. Protein pellets were then re-suspended in 25 mM ammonium bicarbonate (500 µL) and digested with 7.5 µg Trypsin/Lys-C (Promega, 15 µL, 0.5 µg/µL) for 3 h at 37°C. Avidin-agarose beads (Thermo Scientific Pierce, 100 µL aliquot per sample) were washed three

times by adding 10 mL DPBS, centrifuged at 1,400 x *g* for 1 min, and decanting. This wash step was repeated for a total of 3 times. Digested protein samples were mixed with washed avidin beads (100 µL) and brought to a volume of 5.5 mL with DPBS in a 15 mL conical and rotated for 1 h to enrich samples for the covalent desthiobiotin modification. The beads were washed with 25 mM ammonium bicarbonate (3X with 10 mL, centrifuge at 1,400 x *g* for 3 min, decant) and then H_2O (3X with 10 mL, centrifuge at 1,400 x *g* for 3 min, decant). Washed beads were then transferred to a low-bind microfuge tube, centrifuged at 1,400 x *g* for 3 min, allowed to rest for 1 min to settle beads, and then excess H_2O was removed *carefully* using a gel-loading pipette tip. To elute peptides, 100 µL of elution buffer (50% acetonitrile, ACN; 0.1% formic acid) was added to each sample and incubated for 3 min. Beads were spun down at 1,400 x *g* for 3 min, allowed to rest for 1 min to settle beads, and then 75 µL of peptide-containing supernatant was removed carefully using a gel-loading pipette tip and transferred to a new low bind centrifuge tube. This step was repeated two more times with 75 µL of elution buffer and all eluents were collected into the same centrifuge tube (~225 µL total). Peptides were dried on a speed vacuum, resulting peptide samples acidified in 5% (v/v) formic acid, and stored at −80°C until analysis.

LC-MS/MS analysis of SILAC samples. The peptide samples were analyzed by liquid chromatography-mass spectrometry. An integrated autosampler-LC (Ultimate 3000 RSLC nanoSystem, Dionex) was used to load the peptides onto a trap column (Nano-Trap, Thermo Scientific, 2 cm, 5 µm C18) and washed for 2 minutes with 1% B (80% ACN, 1% formic acid). The peptides were eluted from the trap column and through a homemade nanocapillary analytical column (20 cm, 5 µm C18 packed in 360 µm o.d. x 75 µm i.d. fused silica), with an integrated electrospray tip, using a 180 min 1–95% reverse-phase LC gradient (A: 0.1% formic acid; B: 80% ACN, 0.1% formic acid) with the following parameters: 0–2 min 1% B, 400 nL/min; 2–144 min to 95% B, 300 nL/min; 144.1–180 min 1% B, 400 nL/min. The eluting peptides were electrosprayed into an Orbitrap Q Exactive Plus mass spectrometer (Thermo Scientific), which was operated with

a top 10 data-dependent acquisition method that consisted of one full MS1 scan (375 – 1,500 m/z) followed by 10 MS2 scans of the most abundant ions recorded in the MS1 scan. For recombinant DGKE samples, a data-independent parallel reaction monitoring (PRM) method was used to detect DGKE peptides. One full MS1 scan (375 – 1,500 m/z) was followed by MS2 scans of targeted parent ions from a curated inclusion list (DGKE: EKAPSLFSSR, +2 charge state, 659.3617 m/z (light), 668.3729 m/z (heavy), 103.00–110.00 min). Data analysis was accomplished using the IP2 (Integrated Proteomics Applications) software package, in which RawConverter was used to generate searchable MS1 and MS2 data from the .raw file followed by using the ProLuCID algorithm to search the data against a modified human protein database (UniProt human protein database with rat DGKs, angiotensin I and vasoactive intestinal peptide standards; 40,660 proteins) with the following parameters: static carbamidomethyl modification of cysteine (+57.0142 Da), differential modifications of oxidized methionine (+15.9949 Da) and desthiobiotin-labeled lysine residues (+196.1212 Da), added masses of the SILAC “heavy”-labeled amino acids (+10.0083 Da for R, +8.0142 Da for K), and trypsin enzyme specificity with 2 missed cleavages. The resulting MS2 spectra matches were assembled into protein identifications and filtered using DTA Select 2.0 using the --mass, --modstat, and --trypstat options with a 1% peptide FDR. mzIdent files corresponding to searches were generated in IP2-Integrated Proteomics Pipeline, mzXML spectra data was extracted from the raw file using RawConverter and uploaded into Skyline-daily to determine SILAC ratios (SR) of light/heavy (vehicle/compound treated) peptides. Peptides used for analysis were assessed for quality in Skyline by the following criteria: isotope dot-product (iDOTP) ≥ 0.8, ratio dot-product (rDOTP) ≥ 0.8, and singletons defined by L/H ratios > 20 were set to 20. Dot-product values are measures of similarity between the precursor peak area and expected isotope distribution (iDOTP) and between the light and heavy peak area (rDOTP) as calculated in Skyline and described by Schilling et al. Probe-modified peptides that met these criteria were manually inspected and integrated. Peptide ratios reported were normalized to DMSO/DMSO peptide ratios to account for potential variations in

mixing and sample preparations. Additionally, reported DGK and FER peptides were verified by manual inspection of the raw data (MS1 and MS2).

Immunofluorescence microscopy. HEK293T cells were seeded at 50,000 cells/mL on sterile 22 mm borosilicate glass coverslips (Fisher Scientific) in 6-well dishes with 3 mL of complete DMEM or at 10,000 cells/mL on sterile 5 mm borosilicate glass coverslips in 24-well dishes with 1 mL of complete DMEM. Once cells reached 60% confluency, they were transfected with desired recombinant DGK isoform for 48 h. Cells were washed in PBS (2X), fixed with 4% formaldehyde in PBS for 20 mins, washed in PBS (2X), and stained with a 1:2,000 wheat germ agglutinin (WGA) stain conjugated to either an Alexa 350 fluorophore (Thermo Fisher Scientific) or Alexa 488 fluorophore (Biotium) in PBS at 37°C for 15 mins. Fixed cells were again washed in PBS (2X), permeabilized with 0.125% Triton X-100 in PBS for 5 mins, and subsequently washed in PBS (2X). Cells were incubated with 1:1,000 anti-FLAG antibody from rabbit (Thermo Fisher Scientific) diluted in 3% (w/v) BSA-PBS at 37°C for 3 h. Cells were washed in 0.1% Tween 20-PBS (5X), incubated with 1:10,000 goat anti-rabbit antibody (Thermo Fisher Scientific) diluted in PBS at 37°C for 1 h, and washed in 0.1% Tween 20-PBS (5X). Coverslips were mounted (cell side down) to glass slides using mounting media (Thermo Fisher Scientific) and stored at 25°C until analysis on a Zeiss 780 NLO Confocal microscope or stored in PBS at 4°C away from light until analysis with a home-built lattice light sheet microscope.

Lattice-light sheet microscopy image acquisition and data processing. Cell samples were imaged with a home-made lattice light sheet microscope. The square lattice pattern was applied to generate the excitation light sheet. The angle between the excitation light sheet and the glass coverslip is 31.8 degrees. The 3D image is produced from a stack of 2D slices by translating the specimen with a piezo stage (Physik Instrumente, P-621.1CD) through the stationary light sheet horizontally in the plane of the specimen coverslip. Typically, 400 2D slices were collected for one data set with a step size of 200 nm. The illumination intensity of the excitation beam (561 nm) at

the sample was about 1 W/cm^2. Images were acquired with the exposure time of 100 ms. The raw 3D image data was de-skewed and deconvolved as described previously[45,46] by using the Richardson-Lucy algorithm and the reconstructed 3D images were rendered using the 3D Viewer plugin in Fiji.

Liposomal DAG kinase assay. The liposomal method for measuring DAG kinase activity was modified from previously reported method[44]. Briefly, lipids were prepared for liposome formation by dissolving dioleoyl phosphatidylcholine (DOPC), dioleoyl phosphatidylserine (DOPS), and the appropriate DAG species in chloroform, combining, and drying *in vacuo* to remove all solvent. The surface concentration of lipids within the liposomes was 10 mol% DAG, 20 mol% DOPS, and 70 mol% DOPC. The lipids were then hydrated to 10 mM in liposome buffer (50 mM (3-(*N*-morpholino)propanesulfonic acid) (MOPS), pH 7.5, 100 mM NaCl and 5 mM $MgCl_2$). The hydrated lipids were subjected to five freeze-thaw cycles in liquid nitrogen, followed by extrusion through a 100 nm polycarbonate filter 11 times. The measurement of DGK activity was determined by following the incorporation of the γ-Phosphate from [γ-^{32}P]ATP into DAG to form a radiolabeled PA product. Immediately prior to running assays, [γ-^{32}P]ATP was prepared by adding 0.5 – 2 µL of [γ-^{32}P]ATP (6000 Ci/mmol) to 500 µL of 10 mM ATP. The assays were run as 100 µL reactions and contained liposome buffer, 0.1 mM $CaCl_2$, 1 mM dithiothreitol (DTT), appropriate cell lysate (4.4 µg total protein), 40 µL liposomes (4 mM lipids), and were initiated with the addition of 10 µL prepared 10mM [γ-^{32}P] ATP. The reactions were allowed to proceed for 20 min at 30°C before being terminated with the addition of 0.5 mL methanol with 0.1 N HCl, followed by 1 mL of ethyl acetate. Phase separation was achieved with the addition of 1 mL 1 M $MgCl_2$, and the organic phase was washed by thoroughly vortexing to remove soluble [γ-^{32}P] ATP. To measure the incorporation of [^{32}P] into DAG, the extract was centrifuged at 200 x *g* for 1 min, and 0.5 ml of the organic phase was removed, and the radioactivity was measured using a scintillation counter. The activity of each DGK expressing lysate was normalized to GFP expressing lysates as

background. Activity was calculated as nmol of PA produced per minute per mg of total protein present in the assay.

Sequence alignments. Lipid kinase sequences were obtained from Uniprot (https://www.uniprot.org) and aligned using Clustal Omega.

Hierarchical clustering. Calculation and generation of hierarchical clustering dendrograms was done using R with the following publicly available packages: 'cluster', 'factoextra', and 'tidyverse'. A Euclidean method was used to calculate distance measurements while the 'ward.D2' agglomeration method was utilized to calculate the dissimilarity values between observed parameters of the lipid analysis for hierarchical clustering.

Quantification and statistical analysis. For the lipid analyses, the intensities of targeted lipid species and their deuterated counterparts obtained from the LC-MS/MS analysis were used for the semi-quantitative determination of lipid concentrations within a sample. Intensities of lipid species were divided by the intensities of deuterated standards (AA-d8 for negative mode and SAG-d8 for positive mode; 10 pmol). The calculated lipid amounts were normalized based on total protein concentration of respective samples. Statistical analyses were performed in GraphPad Prism (v7.03). In order to determine statistically significant differences between groups analyzing multiple lipid species, a multiple hypothesis t-test (Dunnett's test) with Benjamini-Hochberg correction for false discovery rates (do not assume consistent standard deviation, confidence interval of 95%) was applied. Otherwise, a one-way ANOVA test was implemented to demonstrate significant differences between multiple groups with respect to individual lipid changes. Statistical significance was set at $P < 0.05$. The number of experimental biological replicates of cell populations in each sample group are indicated by *n* and can be found in respective figure legends. Data are shown as mean ± standard error of mean (s.e.m.).

Software and algorithms. In-gel/in-blot fluorescence scanning and normalization; Image Lab software (Bio-Rad). MS1 and MS2 file conversion; RawConverter (RawConverter). MS data protein search algorithm; ProLuCID (Integrated Proteomics Applications – IP2). MS data lipid search algorithm; LipidSearch (Thermo Fisher Scientific). MS data acquisition; Xcalibur (Thermo Fisher Scientific). MS data protein analysis; Skyline-daily (MacCoss Lab Software). MS data lipid analysis; TraceFinder (Thermo Fisher Scientific). Super-resolution microscopy image analysis – Fiji (ImageJ). Confocal microscopy image analysis – CZI (Zeiss). Sequence alignment software; Clustal Omega (EMBL-EBI). Statistical analysis calculation; Prism (GraphPad). Hierarchical clustering analysis; R (RStudio).

2.4 *Results*

2.4.1 *Evaluation of DGK Substrate Specificity Using Metabolomics-Based LC-MS/MS Analysis*

We employed a tandem liquid chromatography-mass spectrometry (LC-MS/MS) platform[39] for comparing DAG fatty acyl specificity across all ten mammalian DGKs (**Figure 2.3**). We reasoned that a gain of function approach would permit systematic evaluation of live cell changes in the lipidome in response to DGK activity that would help normalize differences in endogenous expression of isoforms. Individual human DGK isoforms were transiently overexpressed in HEK293T cells and recombinant protein expression confirmed by western blot. In general, we observed maximal overexpression at 48 h for several DGK isoforms and selected this time point for our lipidomics study (**Figure 2.4a**). We also found that overexpression of recombinant DGKs does not affect expression of an endogenous DGK (**Figure 2.4b**). Using our approach, we could detect on average ~600 distinct lipids per sample, based on fatty acyl composition, across 25 lipid classes in both positive and negative ion modes by global untargeted analyses.

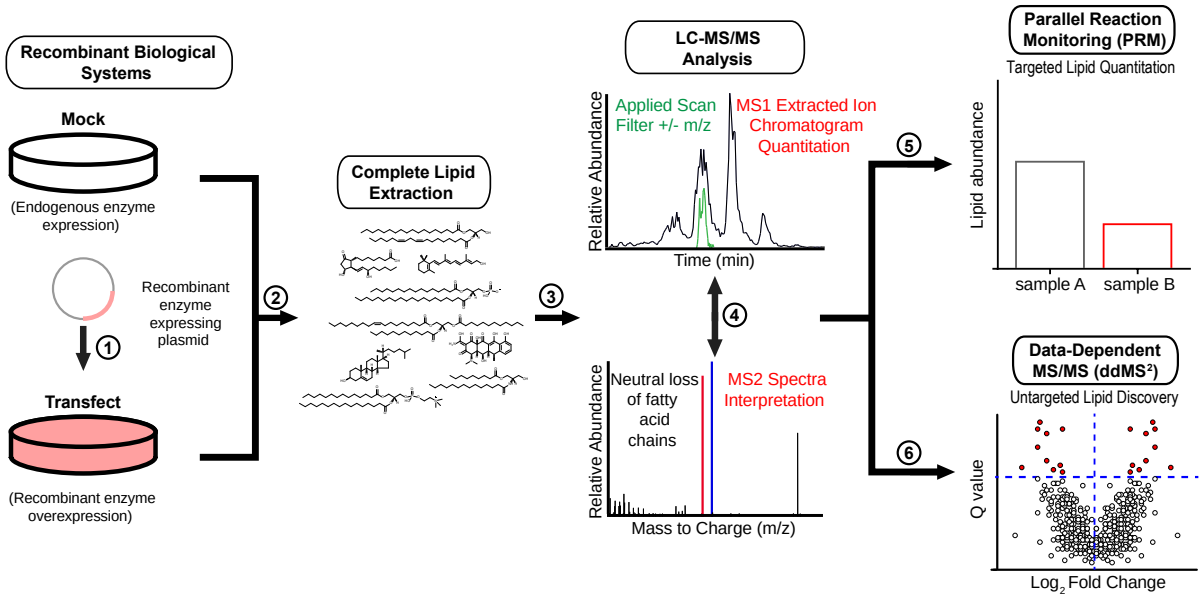

Figure 2.3 Metabolomics platform for quantitative evaluation of the DGK-regulated lipidome. Evaluation of DGK metabolic activity in live cells was achieved by: (1) recombinant overexpression of individual DGK isoforms via transient transfection. (2) Lipid extraction using a

modified Bligh Dyer method. (3) Quantitative analysis of cellular lipids using tandem LC-MS/MS for the separation of lipids and subsequent detection of MS1 precursor ions and MS2 fragment ions. (4) Lipid identification using LipidSearch™, which matched MS1 and MS2 ions with library spectra, followed by quantitation of lipid abundance by peak area. Diagnostic ions (i.e., loss of fatty acid chains) were used to distinguish closely related lipid species. (5) Parallel-reaction monitoring (PRM) for targeted quantitation of changes in low abundance and/or co-eluting lipid species. (6) Top10 data-dependent method (i.e., ddMS2) to acquire MS2 spectra for the 10 most abundant ions from each MS1 scan event for discovery-based, global lipidome profiling. Mock data shown in workflow (5, 6) are representative of analyses performed using LC-MS/MS.

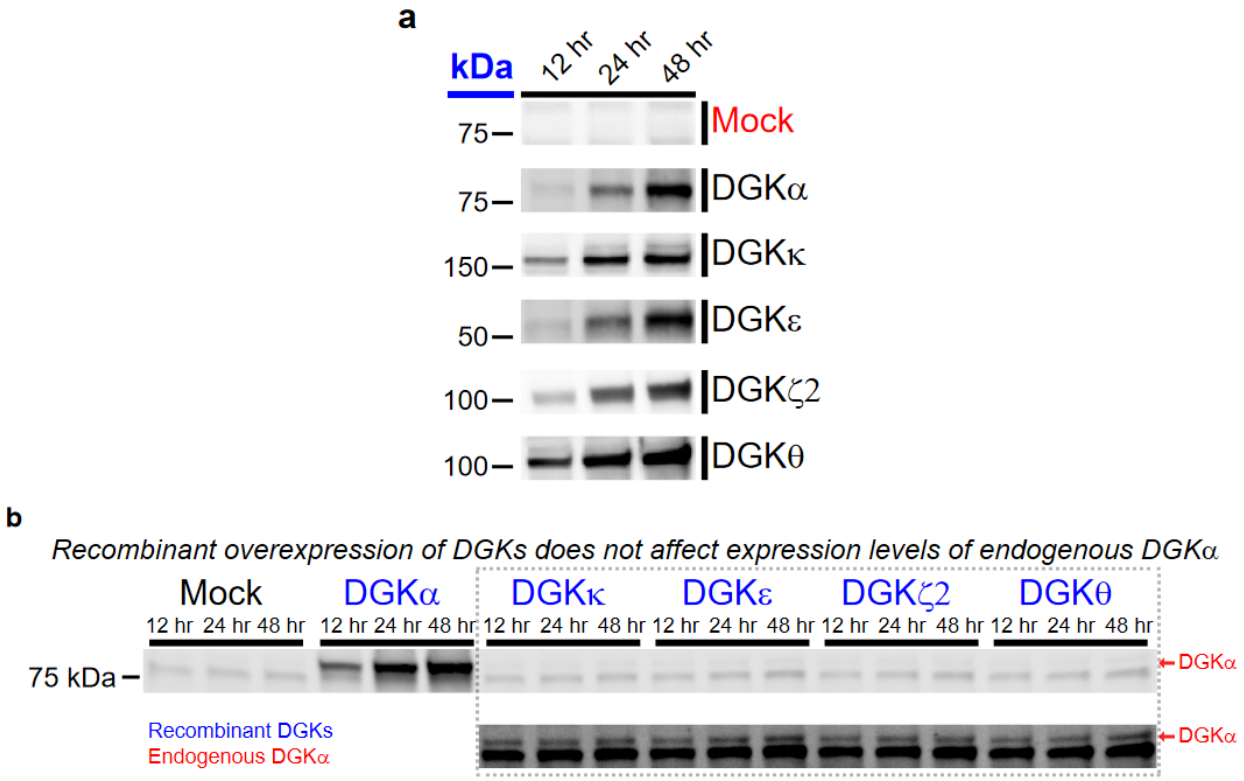

Figure 2.4 Time-course of recombinant overexpression of mammalian DGK isoforms in HEK293T cells. a) Western blots showing the expression of a representative human DGK isoform from each subtype over a 48-h time course after transient transfection. Recombinant DGKs were detected using anti-FLAG (DGKα, DGKκ, DGKε, DGKθ) or anti-HA (DGKζ2) antibodies. Soluble fractions are shown for DGKs except for DGKε, which is expressed in the membrane fraction. b) Western blot showing expression levels of endogenous DGKα were not changed upon overexpression of individual recombinant human DGK isoforms in HEK293T cells over a 48-h time course. The molecular weight (MW) of endogenous DGKα (red) matched the MW of recombinant DGKα (blue) using a polyclonal anti-DGKα antibody. The bottom panel is the same blot with enhanced contrast to highlight the endogenous DGKα band. Data shown are representative of two experiments (*n*=2 biologically independent experiments).

We proceeded with proof-of-concept studies on DGKε, which is the only reported isoform with DAG fatty acyl specificity[33,34,35]. Our untargeted analyses identified several lipid species with levels that were significantly altered in recombinant DGKε- versus mock-transfected HEK293T cells ($Q < 0.05$, **Figure 2.1b**). Notably, recombinant overexpression of DGKε resulted in elevations in cellular levels of a C16:0_C20:4 phosphatidylinositol (PI), which supports previous findings of DGKε involvement in the PI cycle[34,35]. We used a targeted parallel reaction monitoring (PRM[39]) approach to quantitate 34 DAG and 30 PA species with FA identities that were assigned by neutral loss fragmentation of fatty acids from the $[M+NH4]^+$ DAG adduct ions (**Figure 2.1c** and **Figure 2.5**). As expected based on previous reports[40], we discovered that recombinant DGKε overexpression resulted in reductions in cellular levels of the arachidonic acid-containing DAG species (C16:0_C20:4, **Figure 2.1d**). In contrast, saturated DAGs including C16:0_C16:0 and C18:0_C18:0 species were largely unaffected showing DGKε-mediated changes were fatty acyl chain specific (**Figure 2.1d**).

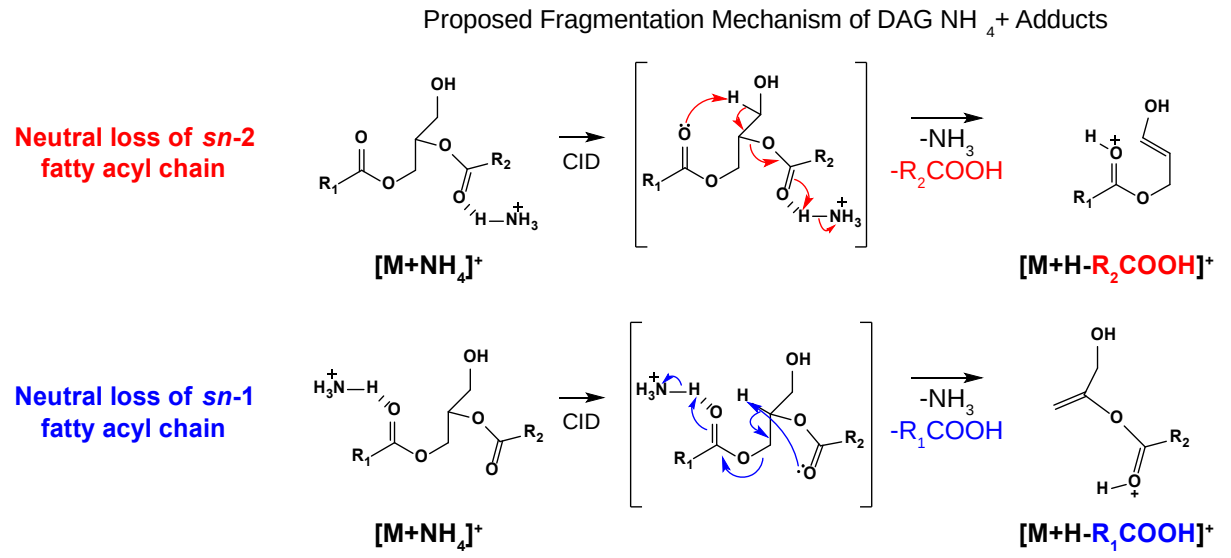

Figure 2.5 HCD-induced fragmentation of ammoniated glycerolipid products. Fragmentation spectra produced by loss of ammonia and a *sn*-1 or *sn*-2 fatty acyl chain of an ammoniated diacylglycerol (DAG) precursor ion are shown with proposed fragmentation mechanisms (red and blue peaks). All subsequent DAG identifications were confirmed by the

fragment ions that resulted from the losses of both fatty acid chains from the ammoniated precursor ion.

Collectively, our metabolomics strategy to assign endogenous DAG substrates for DGKs, which are identified by cellular depletion, confirms specificity of DGKε for arachidonoyl-containing DAGs in live cells.

2.4.2 *Assigning DAG Acyl Specificity to the DGK Superfamily*

We next applied our metabolomics platform to assign DAG substrates to additional DGK isoforms overexpressed in live HEK293T cells (**Figure 2.6a** and **Figure 2.6b**). To compare substrate fatty acyl specificity across the DGK family, we first identified putative DAG substrates by selecting lipids that showed >15% reduction in cellular levels in recombinant DGK- versus mock-transfected lipidomes (log_2 fold change of -0.23, **Figure 2.6c**). We compared whether these DAG substrates were unique, shared within subtype, or shared across subtypes based on fatty acyl chain length and unsaturation. Generally, we discovered minimal overlap in DAG substrates across the DGK superfamily. A few exceptions were noted including overlap in DAG substrates between type 3 and 5 DGKs (C18:1_C20:3 DAG for DGKε and DGKθ) as well as DAGs shared across type 3, 4, and 5 DGKs (C18:0_C22:6 and C16:0_C22:6 for DGKε, DGKζ2, and DGKθ, **Figure 2.6c**). In support of distinct DGK specificities, we identified DAG lipids uniquely regulated by DGKθ (C16:1_C18:1), DGKη (C16:0_C20:2), and DGKε (C16:0_C20:4) that exhibited diversity in fatty acyl chain length and unsaturation (**Figure 2.6c**). We could not detect depletions in any detected DAGs in DGKδ1- and DGKι-transfected cells suggesting that further optimization of conditions is needed to study these isoforms (**Figure 2.6a**).

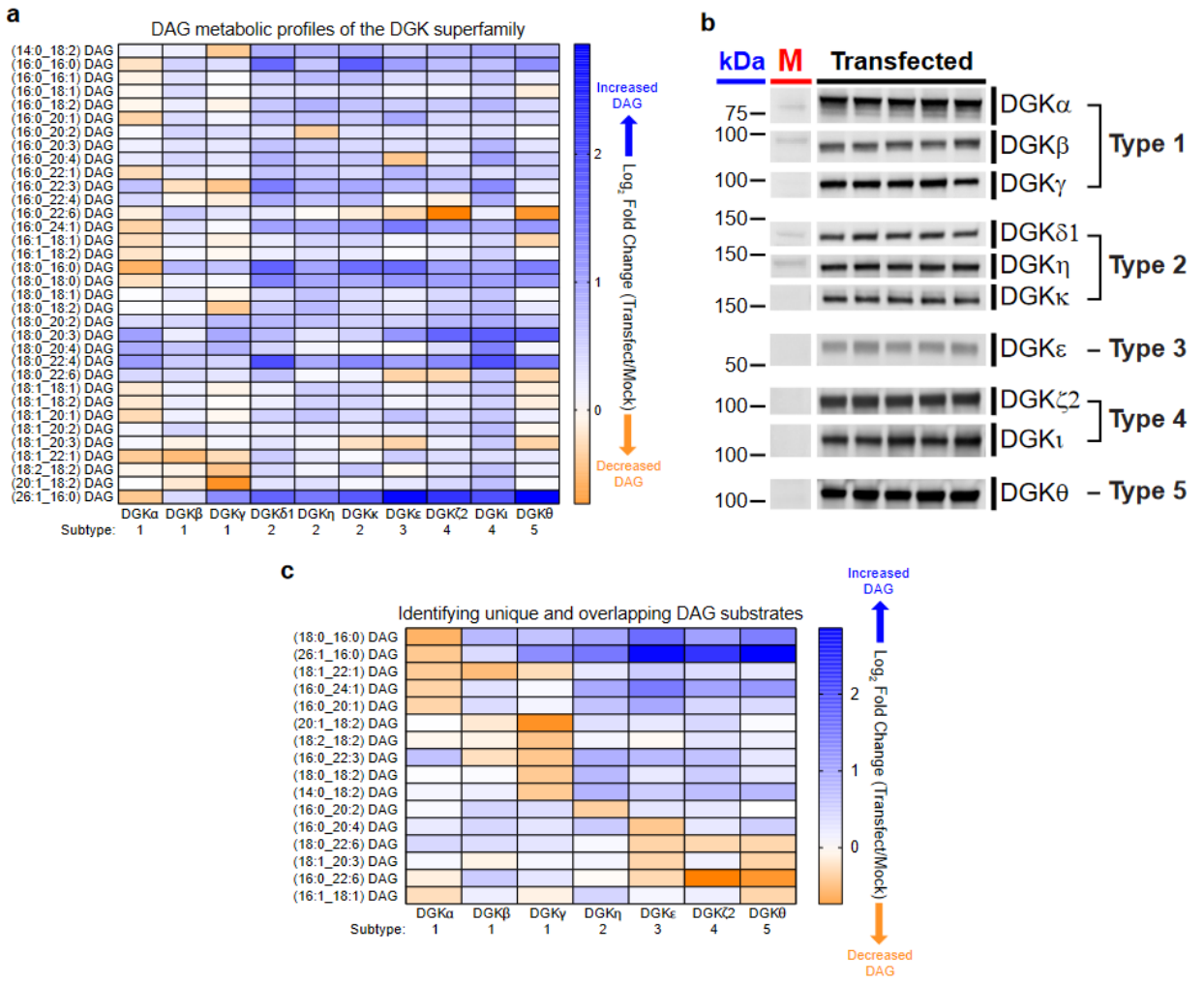

Figure 2.6 Assigning DAG substrate specificity to the DGK superfamily. a) Heat map displaying live cell alterations in the DAG lipidome (log_2 fold change) in recombinant human DGK overexpressed- compared with mock non-transfected-HEK293T cells (*n*=5 biological samples). All 10 isoforms from the DGK superfamily were analyzed by targeted lipidomics. b) Western blots showing recombinant overexpression of the 10 human DGK isoforms. Western blot data showed comparable expression of recombinant DGKs across 5 biological samples. All recombinant DGKs were detected using anti-FLAG antibody with the exception of DGKζ2 and DGKι, which were detected via an anti-HA antibody; "M" represents mock lane. All data shown are for soluble proteomes with the exception of recombinant DGKε, which is expressed in membrane fractions. c) Heat map highlighting altered DAGs that were unique and/or shared across DGK isoforms that showed at least a 15% change (log_2 fold change of -0.23) in cellular lipid abundance (*n*=5 biological samples). Note that C18:0_C22:6 (DGKζ2) and C16:0_C22:6 (DGKε) DAGs showed log_2 fold changes at the set cutoff (~0.23). All data shown are representative of two experiments (*n*=2 biologically independent experiments).

The DAG specificity observed across DGK subtypes was also observed between isoforms within members of type 1 DGKs. Specifically, DGKα and DGKγ each appeared to regulate a mutually exclusive set of DAG substrates that differed in terms of fatty acid makeup. DGKα substrates were enriched for long-chain saturated or monounsaturated fatty acids while DGKγ substrates contained more polyunsaturated fatty acid species with multiple DAGs containing linoleoyl FAs (**Figure 2.6c**). We did not detect any unique DAG substrates for DGKβ given that the sole DGKβ substrate (C18:1_C22:1) was also shared with DGKα (**Figure 2.6c**). We did not identify any DAG substrates that were shared between DGKα and DGKγ or across all 3 type 1 DGKs.

Hierarchical clustering of our targeted metabolomics results revealed interesting relationships with regard to the overall lipid changes when comparing DGK isoforms and the fatty acyl compositions of DAGs (**Figure 2.7a** and **Figure 2.7b**). For example, the type 1 and 2 DGK isoforms appeared to cluster within their respective subtypes as one would expect based on domain topology and sequence homology. However, DGKζ2 shared higher similarity with DGKε and DGKθ compared with type 4 DGKι as determined by DAG substrate profiles (**Figure 2.6c** and **Figure 2.7a**). We also measured cellular changes in lipid PA product in recombinant DGK- compared with mock-transfected cells (**Figure 2.8**). We identified cellular alterations in several DAG and PA lipid pairs with matching fatty acyl compositions that supports our gain-of-function lipidomics approach to capture DGK metabolic activity in live cells (i.e., DAG depletion and PA production, **Figure 2.8**). For several isoforms (e.g., DGKγ, DGKκ, and DGKι), we did not detect clear enhancements in cellular PA levels in response to DGK overexpression (**Figure 2.8**), which suggests further metabolism of this lipid intermediate as was observed for DGKε (i.e., C16:0_C20:4 PI, **Figure 2.1b**).

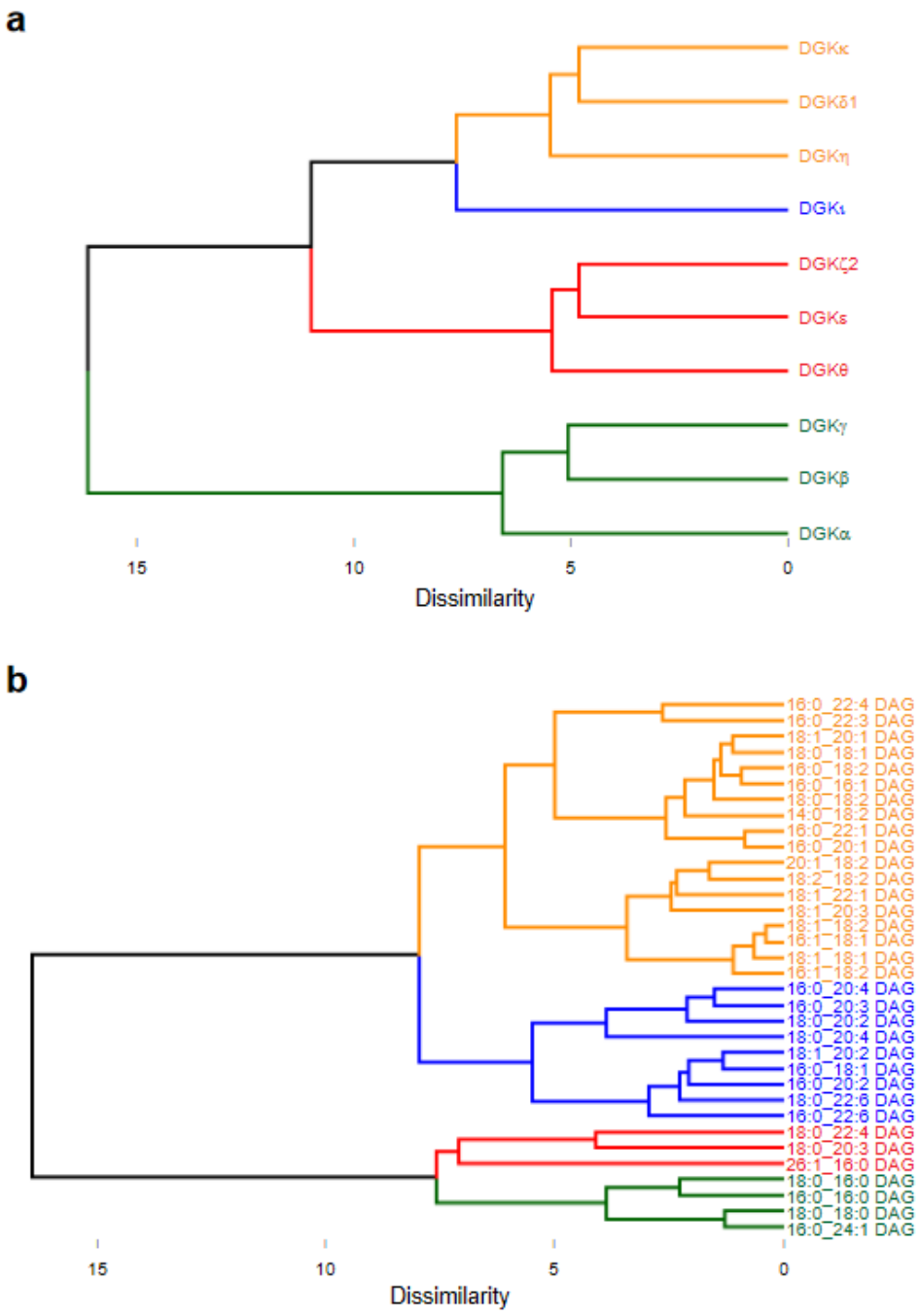

Figure 2.7 Hierarchical clustering of DGK superfamily LC-MS/MS analysis. a) Clustering data shows relationships between DGK isoforms with regards to the magnitude of changes in detected DAGs. b) Clustering data shows the relationship for metabolism by individual isoforms (DGKα, green cluster), their fatty acyl chain composition (orange and blue clusters), or through a combination of these two relationships (red cluster).

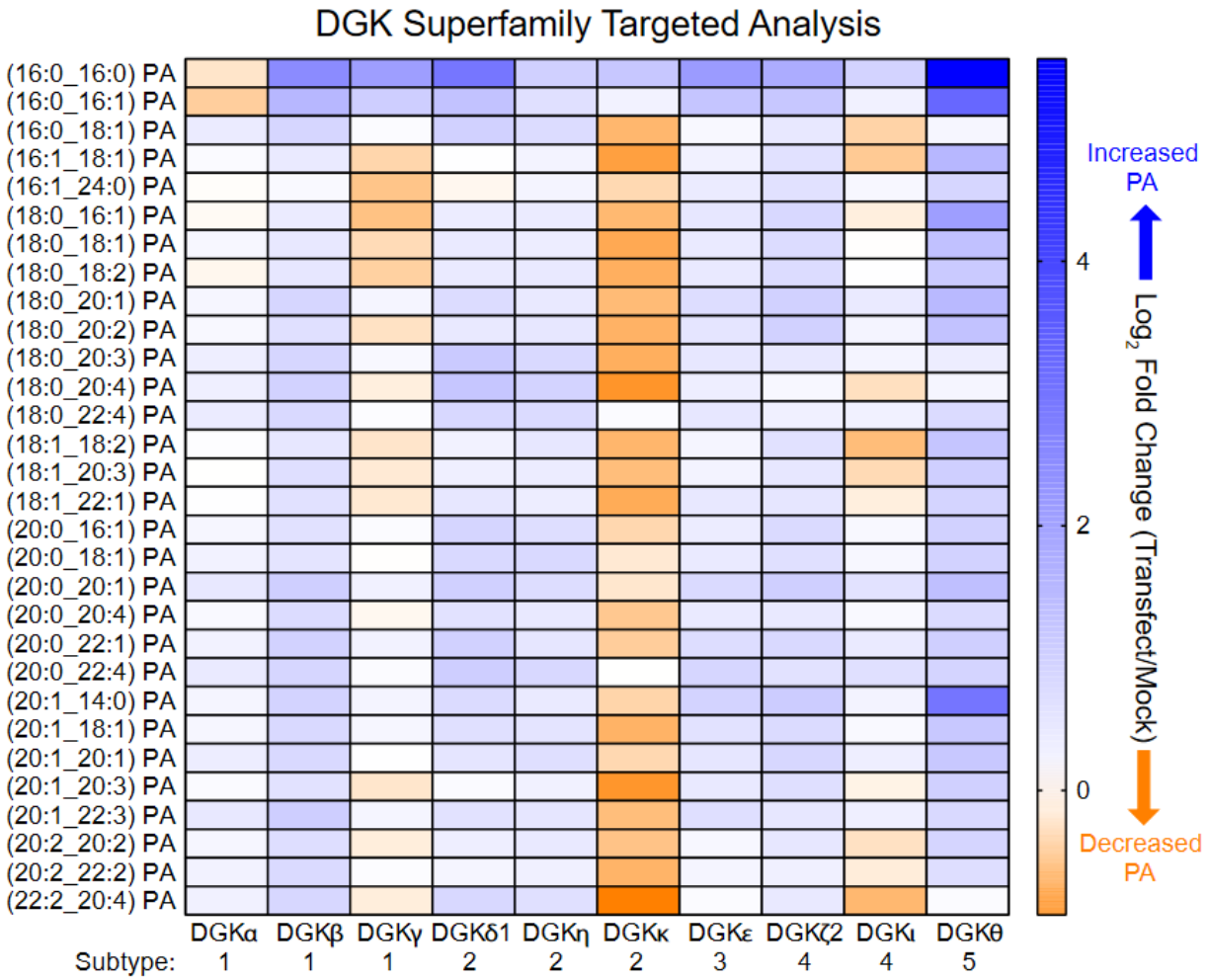

Figure 2.8 Phosphatidic acid (PA) metabolic profiles of the DGK superfamily. Heat map displaying the $\log_2$ fold change in cellular PA lipid levels in HEK293T cells expressing individual recombinant human DGK isoforms compared with non-transfected (mock) controls (*n*=5 biological samples). Data shown are representative of two experiments (*n*=2 biologically independent experiments).

Collectively, our findings show that DGK isoforms exhibit unique DAG fatty acyl specificity both within and across DGK subtypes in live cells, and for several of these DAG substrates we provide evidence of direct DAG to PA metabolism using our metabolomics strategy (**Figure 2.6** and **Figure 2.8**).

2.4.3 *Profiling of Type 1 DGK Active Sites Using Activity-Based Probes and LC-MS/MS Analysis*

We implemented a LC-MS/MS quantitative chemical proteomic assay using ATP acyl phosphates to probe ligand binding of DGKs as previously described[7,41]. Our goal was to identify functional differences in type 1 DGK active sites in order to understand how isoforms with high sequence homology are capable of exhibiting DAG fatty acyl specificity. Recombinant rat DGKα, DGKβ and DGKγ were transiently transfected in light and heavy SILAC[42] amino acid-labeled HEK293T cells. Light and heavy recombinant lysates were then treated with dimethyl sulfoxide (DMSO) vehicle or free ATP (1 mM), prior to addition of ATP acyl phosphate probe to label active site lysine residues. Light and heavy proteomes were combined in a 1:1 ratio, digested with protease, and desthiobiotin-modified tryptic peptides enriched using avidin affinity chromatography. Samples were then analyzed by LC-MS/MS to identify and quantify isotopically labeled active-site peptides as previously described[7,41]. See **2.3** ***Materials and Methods*** for additional details.

Using our quantitative chemical proteomic approach, we identified probe-modified sites in the lipid kinase domain (DAGKc/DAGKa region) of DGKβ and DGKγ that were highly competed by ATP as determined by SILAC ratios (SR) of MS1 chromatographic peak areas >5 in DMSO/ATP comparisons (**Figure 2.9**). In contrast to similar ATP binding profiles, we observed marked differences in probe modification of C1 domains across type 1 DGKs. Consistent with our previous results[7], we found a single probe-modified site in C1A for DGKα (K237, **Figure 2.9**). Extending our studies to the other type 1 isoforms revealed probe modifications located in C1A (K274) and C1B (K353) of DGKγ (**Figure 2.9**). We could not identify a probe modification site in either C1 domains of DGKβ (**Figure 2.9**). Pre-treatment with free ATP (1 mM) resulted in mild competition of DGKγ C1A (SR = 1.5) and C1B (SR = 1.4), which is comparable with the ATP sensitivity profile of DGKα C1A observed previously[7] (SR = 2.4, **Figure 2.9**). The differences in ATP probe binding across type 1 DGK C1s were not due solely to availability of lysine residues

given that these lysine sites are well conserved in type 1 DGKs and good tryptic peptide sequence overlap exists for likely LC-MS/MS detection (**Figure 2.10**).

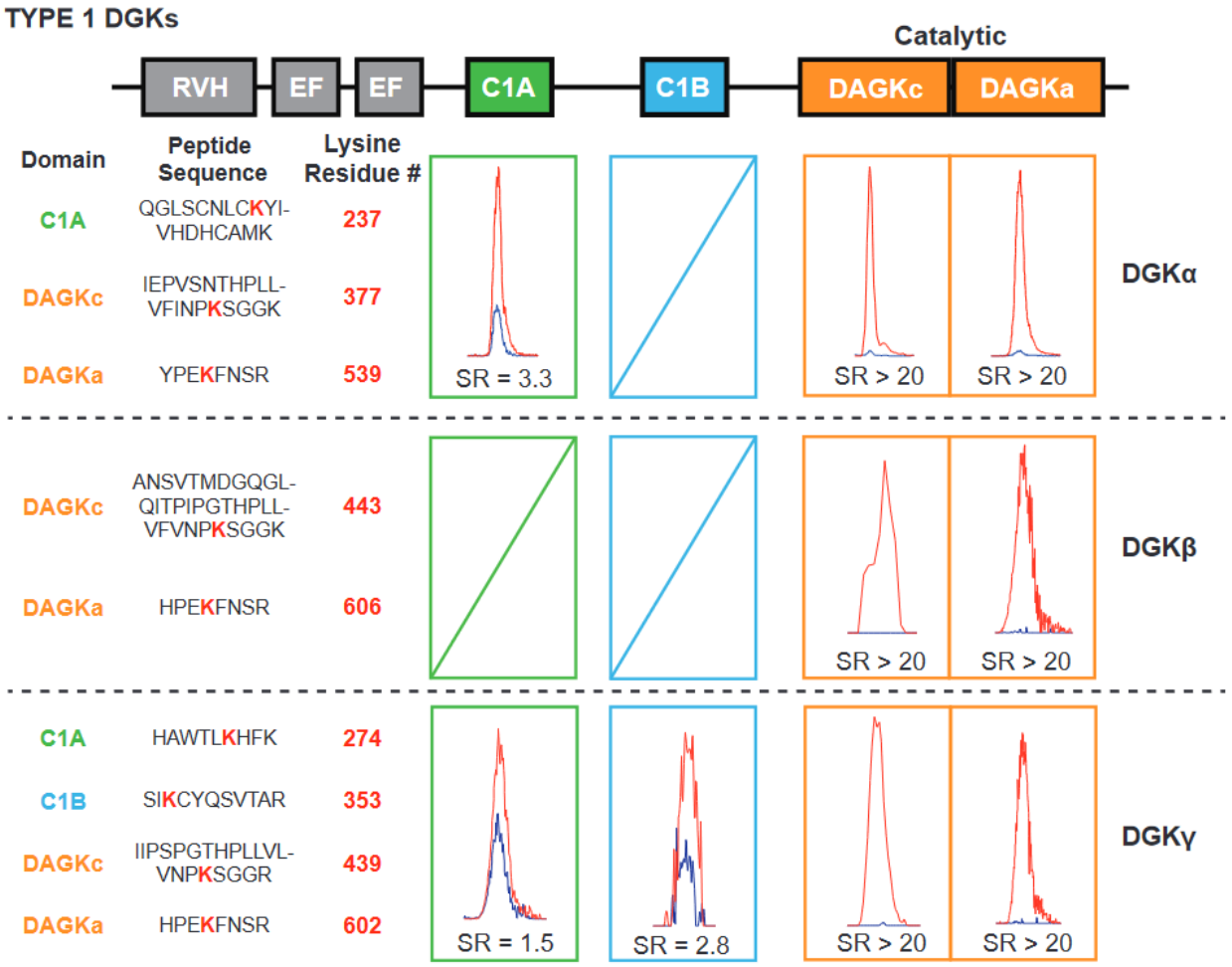

Figure 2.9 Activity-based profiling of functional binding sites in type 1 DGK active sites. Chemical proteomics with an ATP acyl phosphate probe was performed to map probe-binding sites of rat type 1 DGKs (DGKα, DGKβ and DGKγ). Competitive binding was measured between probe and free ATP (1 mM). MS1 extracted ion chromatograms of DGK probe-modified active site peptides are shown with corresponding SILAC light/heavy peptide abundance ratios (SR) from vehicle- (light, red peak) and free ATP-treated (heavy, blue peak) proteomes. Probe-modified sites highly competed by free ATP (SR >5) correspond to the ATP substrate binding sites of DGKs. Probe-modified sites that were not sensitive to ATP competition (SR <5) represent binding sites for alternative substrates and/or ligands. Data shown are representative of two experiments (*n*=2 biologically independent experiments).

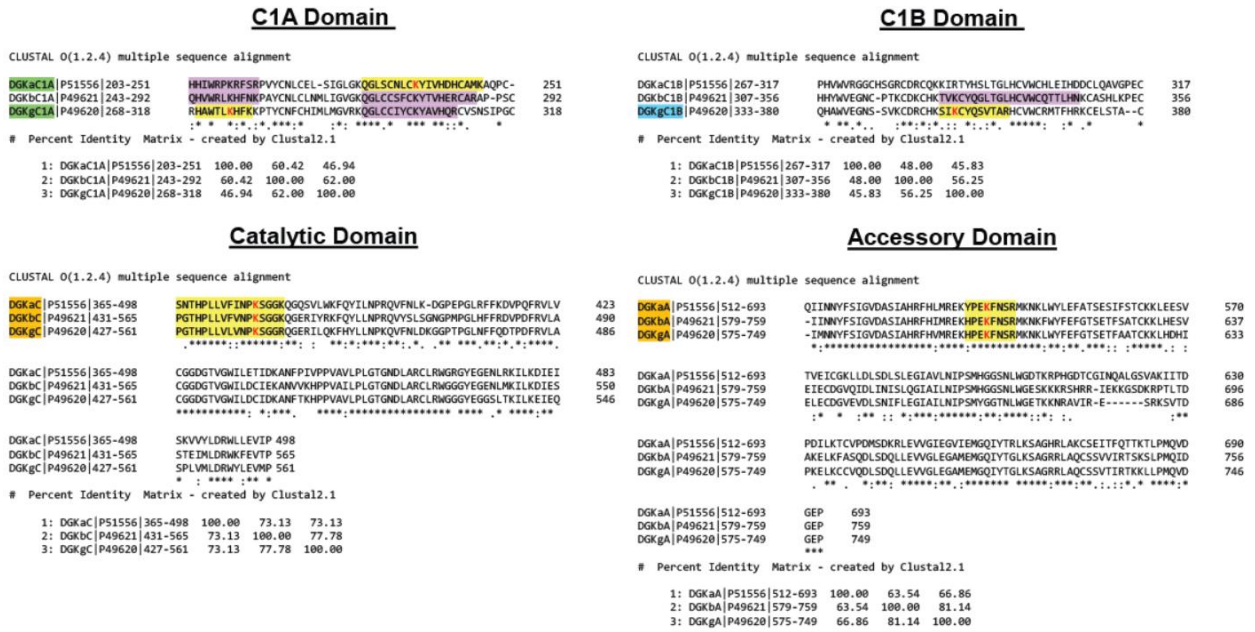

Figure 2.10 Sequence alignment of type 1 DGK domains containing probe-modified active site lysine residues detected by activity-based profiling with ATP acyl phosphates. Multiple protein sequence alignment of the type 1 rat DGK isoforms (DGKα, DGKβ, DGKγ) using Clustal Omega highlighting the sequence similarity within the conserved "archetypal" DGK superfamily domains; C1A (green), C1B (blue), catalytic (C, orange), and accessory (A, orange) domains. Regions highlighted in yellow indicate detected tryptic peptides containing probe-modified sites (lysine site of binding highlighted in red) while regions in purple indicate predicted tryptic peptide sequences that were not identified but still contain a conserved lysine residue that is available for probe modification.

In summary, our chemical proteomic studies revealed that type 1 DGK active sites differed principally in probe binding at C1A and C1B domains. Combined with the lack of potent ATP competition at C1 domains, our data suggest that alternative ligands and potentially substrates (i.e., lipids) are bound at these regions of type 1 DGK active sites.

2.4.4 *Both Typical and Atypical C1 domains are Required for Proper DGKα Metabolic Function*

Next, we tested whether C1 domains were necessary for DGK catalyzed metabolism of DAGs in live cells. We focused our efforts on DGKα because the C1A domain of this isoform has been shown to be a critical inhibitor-binding site from previous chemical proteomic studies[7,43]. We used

LC-MS/MS metabolomics to follow metabolism of the DGKα substrate C18:0_C18:0 DAG as a lipid biomarker of DGKα metabolic activity (**Figure 2.11a**). We confirmed C18:0_C18:0 DAG is an authentic substrate for native human DGKα by performing short hairpin RNA (shRNA) knockdown of endogenous DGKα in A549 cells. Doxycycline-inducible shRNA knockdown resulted in >80% knockdown of endogenous DGKα that was accompanied by a significant accumulation of cellular C18:0_C18:0 DAG in A549 cells (**Figure 2.11b** and **Figure 2.12a**). We identified additional DAG lipids that showed cellular accumulation or reduction upon DGKα knockdown or recombinant overexpression, respectively, which further supports our gain of function approach for mapping authentic lipid substrates of DGKs (**Figure 2.12b**).

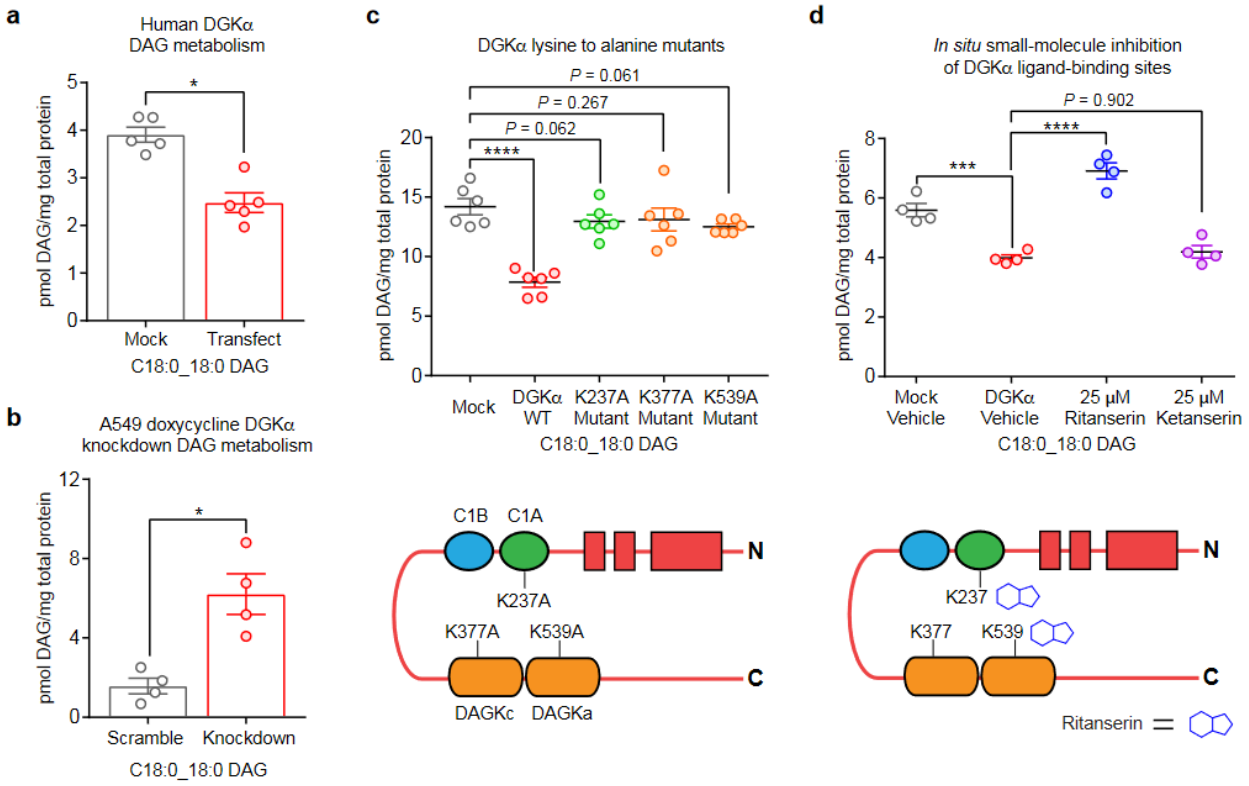

Figure 2.11 C1 domains are necessary and a druggable site for modulating DGKα metabolic function. a) Overexpression of recombinant human DGKα resulted in metabolism of C18:0_C18:0 DAG (*n*=5 biological samples). Statistical significance was determined using a Benjamini-Hochberg correction following a two-sided binomial test (*Q < 0.05). b) shRNA-mediated knockdown of endogenous DGKα in A549 cells (0.2 μg/mL doxycycline, 24 h, *n*=4 biological samples) resulted in accumulation of cellular C18:0_C18:0 DAG. Statistical significance was assessed using a Benjamini-Hochberg correction following a two-sided binomial test (*Q <

0.05). c) Site-directed mutagenesis (lysine to alanine) of ligand binding sites of rat DGKα resulted in perturbation of metabolic activity in live cells and supports a role for these domains in DGKα metabolic function (*n*=6 biological samples). Statistical significance was determined using a Dunnett multiple comparison correction following a one-way ANOVA test (****$P < 0.0001$). d) Treatment of rat DGKα-overexpressing HEK293T cells with ritanserin (blocks C1 and DAGKa sites[7]) but not the negative control molecule ketanserin disrupted DGKα metabolic activity as evaluated by the C18:0_C18:0 DAG biomarker. Compounds were treated at 25 µM final concentration for 1 h (*n*=4 biological samples). Statistical significance was determined using a Tukey's multiple comparison correction following a one-way ANOVA test (***$P < 0.001$, ****$P < 0.0001$). Data shown represent mean ± s.e.m. All data shown are representative of two experiments (*n*=2 biologically independent experiments).

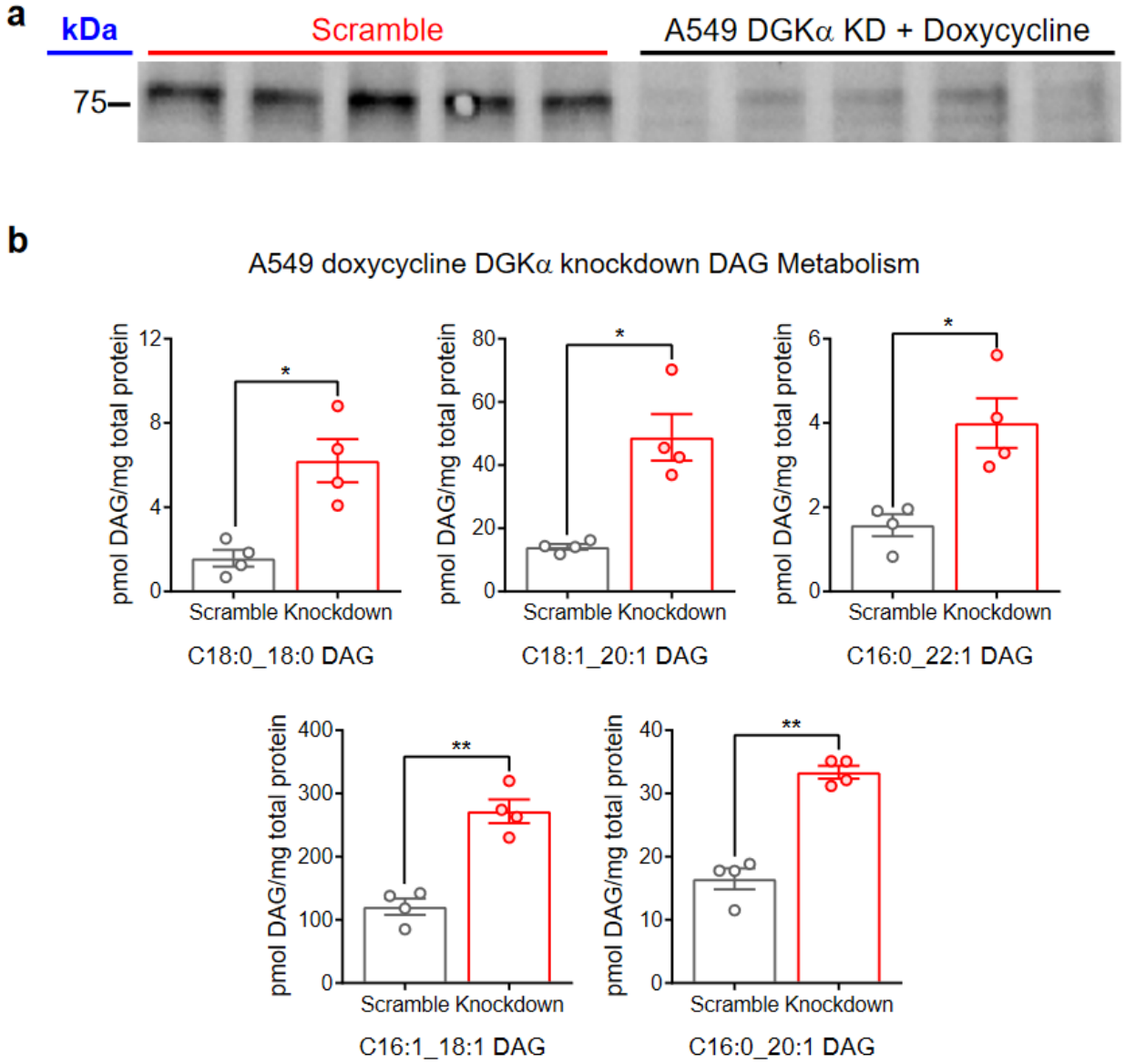

Figure 2.12 Doxycycline-inducible knockdown of DGKα in non-small cell lung cancer A549 cells. a) Western blot displaying shRNA-mediated knockdown (KD) of DGKα in A549 cells following 0.2 μg/mL treatment of doxycycline for 48 h. A DGKα-specific antibody was used to detect levels of endogenous DGKα (*n*=5 biological samples). b) Knockdown of endogenous DGKα in A549 cells (0.2 μg/mL doxycycline, 48 h, *n*=4 biological samples) resulted in accumulation of DAG lipids with the indicated fatty acyl composition. Cellular reductions in these same DAG species in gain of DGKα function studies support our metabolomics approach for mapping authentic DGK substrates in live cells. Significance of lipid alterations was determined using a Benjamini-Hochberg correction following a two-sided binomial test (*Q < 0.05, **Q < 0.01). Data shown represents mean ± s.e.m. Data shown are representative of two experiments (*n*=2 biologically independent experiments).

Our chemoproteomic results (**Figure 2.9**) identified probe-modified lysine sites in several domains implicated in the catalytic activity of DGKs. We performed site-directed mutagenesis (lysine to alanine) on DGKα to test the importance of these probe-modified sites for metabolic activity. Mutation of C1A (K237A) resulted in loss of DGKα metabolic activity as evidenced by cellular DAG levels that were comparable with mock controls (**Figure 2.11c**). As expected, mutation of individual DAGKc (K377A) or DAGKa (K539A) ATP binding sites also impaired DAG metabolic activity of DGKα (**Figure 2.11c**). We also show treatment with a DGKα inhibitor ritanserin that binds to C1A[7,44] can block DGKα metabolic activity. Pretreatment of recombinant DGKα-HEK293T cells with ritanserin but not the DGKα-inactive control molecule ketanserin resulted in blockade of C18:0_C18:0 DAG metabolism (**Figure 2.11d**).

In summary, our mutagenesis findings support C1 domains as a critical region necessary for DGKα metabolic function and C1-targeted inhibitors can be used to block DGKα-mediated metabolism in live cells.

2.4.5 *Engineering of DGK C1 Chimeras Reveals Mechanism of Fatty Acyl Specificity*

Here, we deployed a protein engineering strategy with C1 domain swapping to test whether 1) atypical (DGKα) and typical (DGKβ, DGKγ) C1s are functionally interchangeable between type 1

DGKs, and 2) C1s regulate DAG fatty acyl specificity of type 1 DGKs in live cells. Our approach is supported by evidence for DGK C1 involvement in ligand recognition and metabolism (**Figure 2.9** and **Figure 2.11**) and literature precedence for C1-DAG interactions of other proteins (e.g., PKC[38]).

We analyzed protein sequences of rat DGKα, DGKβ, and DGKγ to identify homologous regions before and after C1A and C1B, respectively, in order to swap the entire C1A/C1B unit (~150 amino acids) between type 1 isoforms. The result is production of hybrid DGK enzymes (dubbed DGK[α,β,γ]C1[α,β,γ] chimeras) containing native regulatory motifs (EF hands and RVH domain) and catalytic domains (DAGKc/DAGKa) but engrafted with C1 domains transplanted from a separate isoform (**Figure 2.13a**). First, we expressed the recombinant DGK chimeric proteins in HEK293T cells and found that their molecular weights matched their native DGK isoform counterparts with small deviations depending on the length of the exchanged C1 domains (**Figure 2.14a**). We confirmed that the domain swap of typical and atypical C1s was functionally tolerated by demonstrating catalytic activity of DGK chimeric proteins using a radiolabeled ATP substrate assay in DAG liposomes[44] (**Figure 2.14b**).

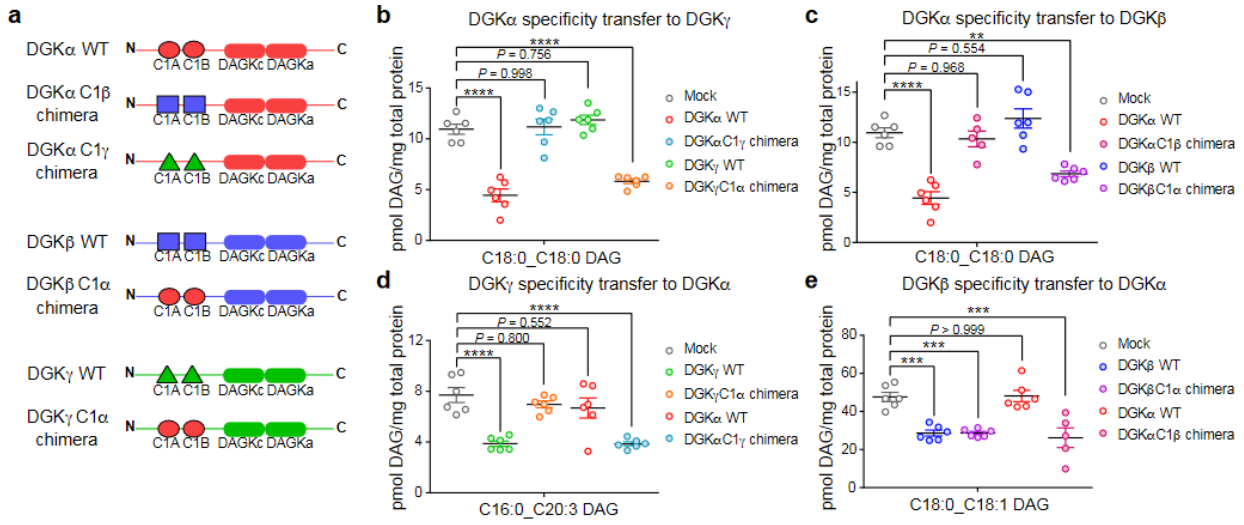

Figure 2.13 Programming DAG substrate specificity of DGKs in live cells by C1 domain engineering. a) Schematic of recombinant rat DGK wild-type (WT) and chimeric proteins used for metabolomics analyses. Targeted lipidomics demonstrated that DAG fatty acyl specificity of

type 1 DGKs can be engineered via C1 domain swapping: b) DGKα C18:0_C18:0 DAG specificity transferred to DGKγ; c) DGKα C18:0_C18:0 DAG specificity transferred to DGKβ; d) DGKγ C16:0_C20:3 DAG specificity transferred to DGKα; e) DGKβ C18:0_C18:1 DAG specificity transferred to DGKα. Significance of lipid species fluctuations was determined using a Tukey's multiple comparison correction following a one-way ANOVA test (***P* < 0.01, ****P* < 0.001, *****P* < 0.0001). All data shown represents mean ± s.e.m.; (*n*=5-6 biological samples). All data shown are representative of two experiments (*n*=2 biologically independent experiments).

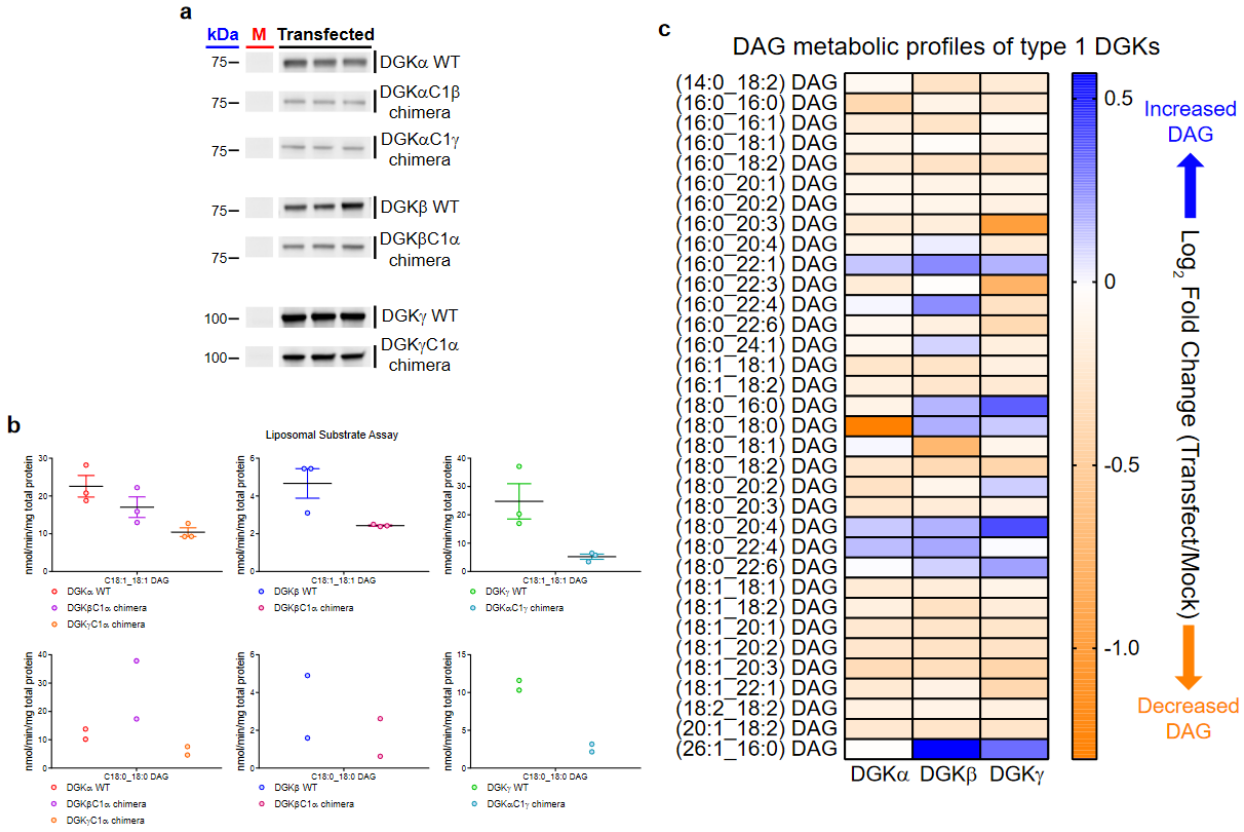

Figure 2.14 Expression and metabolomic profiling of type 1 recombinant DGK chimeras. a) Western blot analysis showing expression of recombinant rat DGK wild-type (WT) and C1 domain chimeras in proteomes from overexpressing HEK293T cells (*n*=3 biological samples). Detection was achieved using an anti-FLAG antibody. Data shown are representative of four experiments (*n*=4 biologically independent experiments). b) Recombinant DGK chimeras are catalytically active as judged by a liposomal substrate assay against both C18:1_C18:1 (*n*=3 biological samples) and C18:0_C18:0 (*n*=2 biological samples) DAG substrate. Liposomes used for substrate assays contained the following composition: 70% DOPC, 20% DOPS, and 10% DAG. Recombinant DGK overexpressed-HEK293T proteomes were used for substrate assays. Data shown represent mean ± s.e.m. Displayed activity (nmol/min/mg total protein) includes subtraction of mock background levels. Data shown are representative of one experiment (*n*=1 biologically independent experiment). c) Heat map displaying cellular alterations in the DAG lipidome (log_2 fold change) in recombinant rat type 1 DGK overexpressed- compared with mock

non-transfected-HEK293T cells (*n*=6 biological samples). Data shown are representative of two experiments (*n*=2 biologically independent experiments).

We performed targeted metabolomics profiling of rat WT DGKs to identify DAG substrates that were specific for each respective type 1 isoform: C18:0_C18:0 DAG, DGKα; C18:0_C18:1 DAG, DGKβ; C16:0_C20:3 DAG, DGKγ (**Figure 2.14c**). We used these DAGs as lipid biomarkers to probe how C1 domain exchange affects DGK lipid metabolism in live cells. Remarkably, we observed both loss and gain of DAG fatty acyl specificity for DAG biomarkers depending on C1 identity of the corresponding DGK chimeric protein (**Figure 2.13b-e**). Specifically, exchange of native C1 domains of DGKα with C1 domains from either DGKγ (DGKαC1γ chimera) or DGKβ (DGKαC1β chimera) resulted in loss of cellular metabolism for C18:0_18:0 DAG (**Figure 2.13b** and **Figure 2.13c**). In parallel, we observed a gain in DAG fatty acyl specificity for DGKα, which exhibited negligible activity towards C16:0_C20:3 DAG but gained this metabolic specificity upon engraftment of DGKγ C1s (DGKαC1γ chimera, **Figure 2.13d**).

We observed a similar metabolic effect for DGKγ that is characterized by gain of C18:0_C18:0 DAG specificity encoded by the transplanted DGKα C1s (**Figure 2.13b**) that is mirrored by loss of specificity for its C16:0_C20:3 DAG substrate (**Figure 2.13d**). In contrast, the exchange of C1 domains in DGKβ resulted in a different effect compared with DGKα and DGKγ. Specifically, DGKβ containing DGKα C1s (DGKβC1α chimera) gained specificity for C18:0_C18:0 DAG (**Figure 2.13c**) without loss of activity for its preferred C18:0_18:1 DAG substrate (**Figure 2.13e**). This result could possibly be due to other structural features inherent to DGKβ, which in addition to C1 domains can modulate DAG fatty acyl specificity of this isoform.

Given that C1 domains regulate membrane association[38], we performed lattice-light sheet microscopy[45,46] to determine whether the altered DAG specificity observed for DGK chimeric proteins was due to changes in subcellular localization. Cells were fixed using 4% formaldehyde

following 48 h of transfection to recapitulate the expression and activity profile used for our metabolomic analyses (**Figure 2.13b-e**). We found that DGKγC1α chimera showed distinct localization at the perimeter of what we suspect to be intracellular organelles, given the well-defined voids in the 3D fluorescence intensity distribution (**Figure 2.15**). In contrast, DGKαC1γ chimera displayed scattered localization throughout the cell and was not enriched for a particular subcellular locale. Neither chimera showed localization that was overtly akin to the behavior of WT DGKα or DGKγ. Our microscopy data shows subcellular localization of the C1 chimeras are different from each other and from wild-type C1 donor DGKs and supports a localization-independent mechanism for the engineered DAG substrate specificity observed by metabolomics (**Figure 2.15**).

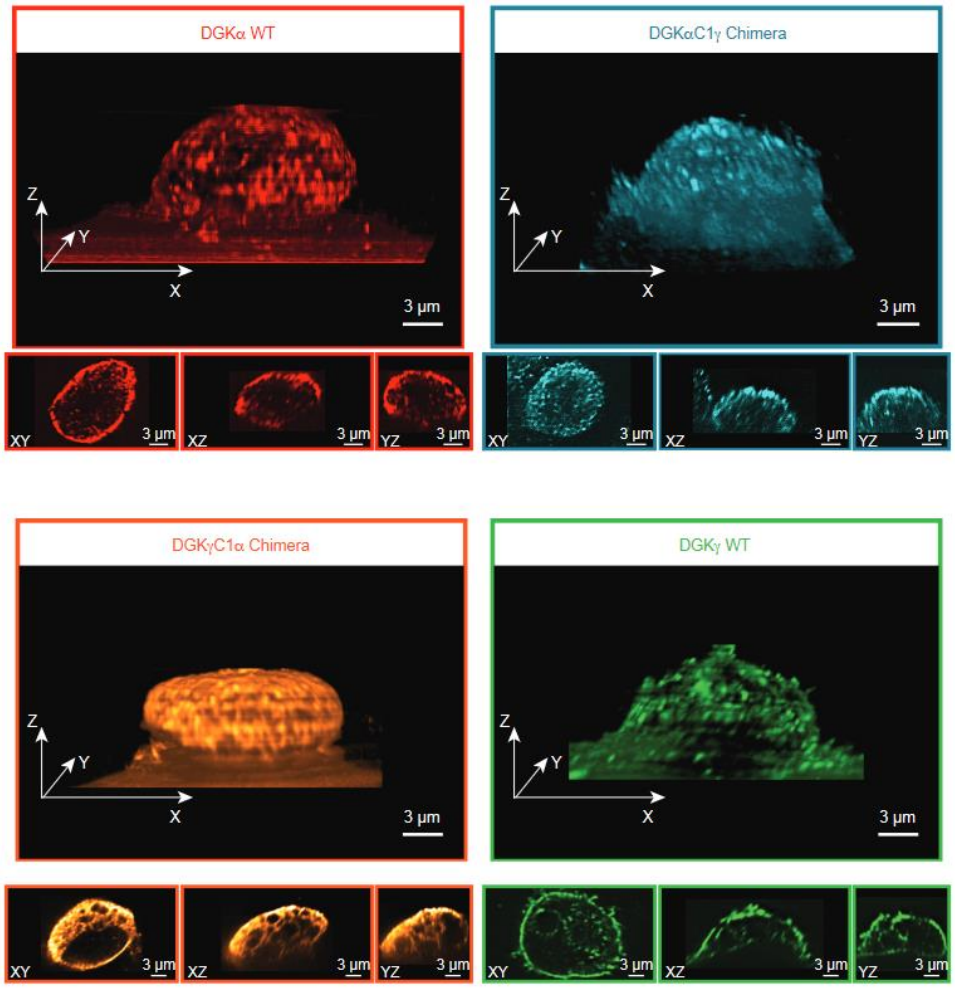

Figure 2.15 Lattice-light sheet microscopy shows DGK chimeras are not localized based on C1 identity. Recombinant rat DGK isoforms were imaged by immunofluorescence using an anti-FLAG primary and DyLight 550 secondary antibody staining. Images were acquired at 561 nm excitation using an illumination intensity of the sample at 1 W/cm^2. The raw 3D image data was de-skewed and deconvolved as described previously[45,46] and 3D images were rendered using the 3D Viewer plugin in Fiji (see Methods for details). The reconstructed voxel size of the 3D image is 100 by 100 by 100 nm. For each 3D image, three orthogonal cross sections through the cell center are also displayed. Microscopy results reveal that subcellular localization of the C1 chimeras are different from each other and from wild-type C1 donor DGKs. Data shown are representative of two experiments (*n*=2 biologically independent experiments).

In summary, our protein engineering, LC-MS/MS metabolomics, and microscopy data provide evidence that C1 domains directly mediate DAG fatty acyl specificity of type 1 DGKs in live cells and the programmable nature of the tandem C1s is not simply due to protein localization.

2.5 *Discussion*

DGKs are specialized multi-domain lipid kinases responsible for metabolizing lipid secondary messengers involved in cellular activation. Metabolic specificity of DGKs is believed to arise from diverse regulatory domains outside of the conserved catalytic core to control when and where these enzymes are active. Despite this widely accepted model, biochemical studies have shown that a minimal DGK architecture is sufficient for attaining DAG substrate specificity despite lack of elaborate regulatory domains[33,34,35]. Here, we applied chemical proteomics, metabolomics, and protein engineering to annotate a direct role for C1 domains in mediating DAG fatty acyl specificity of DGKs.

Given the variable expression of native DGKs in cell and tissues, we used a gain of function approach combined with LC-MS/MS metabolomics to enable assignment of lipid substrate specificity for all 10 mammalian enzymes in live cells. We validated lipids identified from recombinant overexpression as authentic substrates by showing that knockdown of endogenous DGKs resulted in accumulation of DAGs with identical fatty acyl composition (**Figure 2.12**). Our lipidomics approach was crucial for identifying isoform-specific biomarkers to track activity of individual DGK isoforms. Our initial proof of concept studies used DGKε to validate the capability of our method for quantitating changes in DAGs with fatty acyl chains that matched previous findings[33,34,35]. We observed depletion of arachidonic acid-containing DAG and accumulation of PI species with identical fatty acyl composition (C16:0 and C20:4 fatty acids, **Figure 2.1b** and **Figure 2.1d**) that agree with previous reports of regulation of the PI cycle by DGKε[34,35].

Our live cell lipidomics findings revealed several interesting and unexpected features of DGK specificity. First, we observed minimal overlap in DAG acyl specificity across isoforms (**Figure 2.6a**). Specifically, only a handful of identified DAGs were shared between isoforms from two or more subtypes (**Figure 2.6c**). Several isoforms including DGKδ1, DGKκ, and DGKι did not show appreciable changes in cellular DAGs in our recombinant system (**Figure 2.6a**).

Interestingly, the latter two isoforms showed a paradoxical depletion of cellular PA when overexpressed in cells (**Figure 2.8**). It is tempting to speculate that DGKκ may not function solely as a DAG kinase based on our metabolomic findings and its unique catalytic domain topology (i.e., peptide region separating DAGKc and DAGKa regions[47,48,49], **Figure 2.2**). Whether this effect is due to feedback regulation or an alternative metabolic function of DGKκ is a subject that will be explored in future studies.

The DAG fatty acyl specificity observed between type 1 DGKs was surprising and prompted us to explore ligand binding in their active sites to gain insights into how molecular specificity could be achieved. As expected, the ATP binding regions of DGKα, DGKβ, and DGKγ mapped to homologous regions including conserved probe-modified lysine sites (DAGKc and DAGKa sites, **Figure 2.9**). In contrast, we observed differential probe labeling in C1A and C1B of type 1 DGKs that correlated with the DAG acyl specificity observed by metabolomics. Specifically, DGK isoforms (DGKα and DGKγ) that showed programmable DAG specificity also contained C1 domains sensitive to covalent reaction with ATP acyl phosphate probe (**Figure 2.9**, **Figure 2.13b** and **Figure 2.13d**). Interestingly, the absence of probe binding at DGKβ C1s was correlated with a lesser effect of these domains in mediating DAG acyl specificity for this isoform (**Figure 2.9** and **Figure 2.13e**).

Although our metabolomics and proteomics data support C1 involvement in DGK specificity, we used protein engineering to provide direct evidence for this model. We generated DGK C1 chimeric proteins to demonstrate that the DAG fatty acyl specificity of DGKs could be programmed by exchanging C1 domains in live cells (**Figure 2.13**). Our studies suggest that C1s are a component of the DGK active site to help select lipid substrates and this hypothesis is supported by previous chemical proteomic findings of a putative DGKα interdomain active site composed of C1A and the catalytic domains[43]. Our previous and current findings present a working model whereby the regulatory domains could be involved in formation of DGK active sites

(**Figure 2.2**). This hypothesis would provide a framework for future studies to map additional ligand binding sites outside of the catalytic domain using existing as well as DGK-tailored activity-based probes to gain deeper understanding of mechanisms regulating DGK specificity in biological systems.

While our studies provide key insights into DGK lipid specificity, we recognize that recombinant overexpression systems can alter cellular localization, structure, and regulation of DGK isoforms, which could affect our lipid specificity assessments. We also acknowledge the potential for compensatory effects (e.g., feedback regulation) in our live cell lipidomics studies. Together, these limitations could explain the increases in DAGs with overexpression of certain DGKs (**Figure 2.6a**), the limited examples of direct DAG to PA conversion (**Figure 2.8**), and some differences in DGKε specificity (e.g. broader substrate profile and a preference for C16:0_C20:4 over C18:0_C20:4 DAG, **Figure 2.6a**) compared with previous findings[33,40]. Another caveat is overexpression of one recombinant DGK could affect expression of other native DGKs as well as proteins outside of the DGK superfamily. Despite validation that native DGKα expression was not affected (**Figure 2.4b**), additional studies evaluating proteome-wide changes (including additional endogenous DGK isoforms) are needed to rule out potential non-specific effects from our recombinant system. Although our current findings support DGK C1 domains as a principal determinant of DAG fatty acyl specificity, future studies aimed at integrating C1 biology with additional regulatory mechanisms including, e.g., subcellular localization and membrane curvature[50] are needed to decipher DGK function *in vivo*.

In summary, the DGK superfamily plays multifaceted roles in mammalian physiology and disease, and efforts are underway to target individual isoforms for therapeutic purposes. The identification of C1 domains as a key site for directing specificity of DGK activity is an important step toward advancing basic understanding of lipid signaling networks as well as the identification of ligand binding sites for developing isoform-selective inhibitors.

2.6 *Acknowledgments*

We thank Mark Ross and all members of the Hsu Lab for helpful discussions and review of the manuscript. We thank Sean Campbell for assistance in designing DGK chimera plasmids. This work was supported by the University of Virginia (start-up funds to K.-L.H.), National Institutes of Health Grants (DA035864 and DA043571 to K.-L.H.; GM801868 to T.B.W.), U.S. Department of Defense (Grant W81XWH-17-1-0487 to K.-L.H.), NCI Cancer Center Support Grant (5P30CA044579-27 to K.-L.H. and T.E.H.), and the Schiff Foundation (Brain Tumor Research Grant to K.-L.H. and T.E.H.). Images were acquired using the W.M. Keck Center for Cellular Imaging Zeiss 780 Confocal microscopy system at UVA (NIH OD016446).

Author Contributions

T.B.W. and K.-L.H. conceived of the project, designed experiments, and analyzed data. T.B.W performed all lipidomics experiments by mass spectrometry and analyzed all data from these studies. T.B.W performed cloning and expression of proteins, conducted inhibition studies, and performed biochemical assays. T.B.W. conducted cellular studies. T.B.W. performed all immunofluorescence experiments and analyzed results from these studies. T.B.W. performed bioinformatics analysis of DGK targeted metabolomics data. C.E.F. performed chemical proteomic experiments and data analysis. M.E.G. and T.E.H. performed liposome substrate assay and data analysis. M.Z. and A.G. performed lattice-light sheet microscopy and data analysis. K.B.K. and K.S.P. performed shRNA knockdown of endogenous DGKα in A549 cells. T.B.W. and K.-L.H. wrote the manuscript.

2.7 *References*

1. Aimon S, Callan-Jones A, Berthaud A, Pinot M, Toombes GE, Bassereau P. Membrane shape modulates transmembrane protein distribution. *Dev Cell* 2014, **28**(2): 212-218.
2. Di Paolo G, De Camilli P. Phosphoinositides in cell regulation and membrane dynamics. *Nature* 2006, **443**(7112): 651-657.
3. Lee MC, Orci L, Hamamoto S, Futai E, Ravazzola M, Schekman R. Sar1p N-terminal helix initiates membrane curvature and completes the fission of a COPII vesicle. *Cell* 2005, **122**(4): 605-617.
4. Almena M, Mérida I. Shaping up the membrane: diacylglycerol coordinates spatial orientation of signaling. *Trends Biochem Sci* 2011, **36**(11): 593-603.
5. Liu Y, Su Y, Wang X. Phosphatidic acid-mediated signaling. *Adv Exp Med Biol* 2013, **991**: 159-176.
6. van Blitterswijk WJ, Houssa B. Properties and functions of diacylglycerol kinases. *Cell Signal* 2000, **12**(9-10): 595-605.
7. Franks CE, Campbell ST, Purow BW, Harris TE, Hsu KL. The Ligand Binding Landscape of Diacylglycerol Kinases. *Cell Chem Biol* 2017, **24**(7): 870-880 e875.
8. Yamada K, Sakane F, Matsushima N, Kanoh H. EF-hand motifs of alpha, beta and gamma isoforms of diacylglycerol kinase bind calcium with different affinities and conformational changes. *Biochem J* 1997, **321**: 59-64.
9. Abramovici H, Hogan AB, Obagi C, Topham MK, Gee SH. Diacylglycerol kinase-zeta localization in skeletal muscle is regulated by phosphorylation and interaction with syntrophins. *Mol Biol Cell* 2003, **14**(11): 4499-4511.
10. Kume A, Kawase K, Komenoi S, Usuki T, Takeshita E, Sakai H, et al. The Pleckstrin Homology Domain of Diacylglycerol Kinase eta Strongly and Selectively Binds to Phosphatidylinositol 4,5-Bisphosphate. *J Biol Chem* 2016, **291**(15): 8150-8161.
11. Imai S, Sakane F, Kanoh H. Phorbol ester-regulated oligomerization of diacylglycerol kinase delta linked to its phosphorylation and translocation. *J Biol Chem* 2002, **277**(38): 35323-35332.
12. Harada BT, Knight MJ, Imai S, Qiao F, Ramachander R, Sawaya MR, et al. Regulation of enzyme localization by polymerization: polymer formation by the SAM domain of diacylglycerol kinase delta1. *Structure* 2008, **16**(3): 380-387.
13. Jing W, Gershan JA, Holzhauer S, Weber J, Palen K, McOlash L, et al. T cells deficient in diacylglycerol kinase-zeta are resistant to PD-1 inhibition and help create persistent host immunity to leukemia. *Cancer Res* 2017, **77**(20): 5676-5686.
14. Olenchock BA, Guo R, Carpenter JH, Jordan M, Topham MK, Koretzky GA, et al. Disruption of diacylglycerol metabolism impairs the induction of T cell anergy. *Nat Immunol* 2006, **7**(11): 1174-1181.
15. Zha Y, Marks R, Ho AW, Peterson AC, Janardhan S, Brown I, et al. T cell anergy is reversed by active Ras and is regulated by diacylglycerol kinase-alpha. *Nat Immunol* 2006, **7**(11): 1166-1173.
16. Merida I, Andrada E, Gharbi SI, Avila-Flores A. Redundant and specialized roles for diacylglycerol kinases alpha and zeta in the control of T cell functions. *Sci Signal* 2015, **8**(374): re6.
17. Prinz PU, Mendler AN, Masouris I, Durner L, Oberneder R, Noessner E. High DGK-alpha and disabled MAPK pathways cause dysfunction of human tumor-infiltrating CD8+ T cells that is reversible by pharmacologic intervention. *J Immunol* 2012, **188**(12): 5990-6000.
18. Riese MJ, Wang LC, Moon EK, Joshi RP, Ranganathan A, June CH, et al. Enhanced effector responses in activated CD8+ T cells deficient in diacylglycerol kinases. *Cancer Res* 2013, **73**(12): 3566-3577.

19. Guo R, Wan CK, Carpenter JH, Mousallem T, Boustany RM, Kuan CT, et al. Synergistic control of T cell development and tumor suppression by diacylglycerol kinase alpha and zeta. *Proc Natl Acad Sci U S A* 2008, **105**(33): 11909-11914.
20. Pankratz N, Wilk JB, Latourelle JC, DeStefano AL, Halter C, Pugh EW, et al. Genomewide association study for susceptibility genes contributing to familial Parkinson disease. *Hum Genet* 2009, **124**(6): 593-605.
21. Simon-Sanchez J, van Hilten JJ, van de Warrenburg B, Post B, Berendse HW, Arepalli S, et al. Genome-wide association study confirms extant PD risk loci among the Dutch. *Eur J Hum Genet* 2011, **19**(6): 655-661.
22. Baum AE, Akula N, Cabanero M, Cardona I, Corona W, Klemens B, et al. A genome-wide association study implicates diacylglycerol kinase eta (DGKH) and several other genes in the etiology of bipolar disorder. *Mol Psychiatry* 2008, **13**(2): 197-207.
23. Weber H, Kittel-Schneider S, Gessner A, Domschke K, Neuner M, Jacob CP, et al. Cross-disorder analysis of bipolar risk genes: further evidence of DGKH as a risk gene for bipolar disorder, but also unipolar depression and adult ADHD. *Neuropsychopharmacology* 2011, **36**(10): 2076-2085.
24. Squassina A, Manchia M, Congiu D, Severino G, Chillotti C, Ardau R, et al. The diacylglycerol kinase eta gene and bipolar disorder: a replication study in a Sardinian sample. *Mol Psychiatry* 2009, **14**(4): 350-351.
25. Zeng Z, Wang T, Li T, Li Y, Chen P, Zhao Q, et al. Common SNPs and haplotypes in DGKH are associated with bipolar disorder and schizophrenia in the Chinese Han population. *Mol Psychiatry* 2011, **16**(5): 473-475.
26. Moya PR, Murphy DL, McMahon FJ, Wendland JR. Increased gene expression of diacylglycerol kinase eta in bipolar disorder. *Int J Neuropsychopharmacol* 2010, **13**(8): 1127-1128.
27. Melen E, Himes BE, Brehm JM, Boutaoui N, Klanderman BJ, Sylvia JS, et al. Analyses of shared genetic factors between asthma and obesity in children. *J Allergy Clin Immunol* 2010, **126**(3): 631-637 e631-638.
28. Laramie JM, Wilk JB, Williamson SL, Nagle MW, Latourelle JC, Tobin JE, et al. Multiple genes influence BMI on chromosome 7q31-34: the NHLBI Family Heart Study. *Obesity (Silver Spring)* 2009, **17**(12): 2182-2189.
29. Jiang LQ, de Castro Barbosa T, Massart J, Deshmukh AS, Lofgren L, Duque-Guimaraes DE, et al. Diacylglycerol kinase-delta regulates AMPK signaling, lipid metabolism, and skeletal muscle energetics. *Am J Physiol Endocrinol Metab* 2016, **310**(1): E51-60.
30. Lowe CE, Zhang Q, Dennis RJ, Aubry EM, O'Rahilly S, Wakelam MJ, et al. Knockdown of diacylglycerol kinase delta inhibits adipocyte differentiation and alters lipid synthesis. *Obesity (Silver Spring)* 2013, **21**(9): 1823-1829.
31. Chibalin AV, Leng Y, Vieira E, Krook A, Bjornholm M, Long YC, et al. Downregulation of diacylglycerol kinase delta contributes to hyperglycemia-induced insulin resistance. *Cell* 2008, **132**(3): 375-386.
32. Liu Z, Chang GQ, Leibowitz SF. Diacylglycerol kinase zeta in hypothalamus interacts with long form leptin receptor. Relation to dietary fat and body weight regulation. *J Biol Chem* 2001, **276**(8): 5900-5907.
33. Lung M, Shulga YV, Ivanova PT, Myers DS, Milne SB, Brown HA, et al. Diacylglycerol kinase epsilon is selective for both acyl chains of phosphatidic acid or diacylglycerol. *J Biol Chem* 2009, **284**(45): 31062-31073.
34. Shulga YV, Topham MK, Epand RM. Study of arachidonoyl specificity in two enzymes of the PI cycle. *J Mol Biol* 2011, **409**(2): 101-112.
35. Shulga YV, Topham MK, Epand RM. Substrate specificity of diacylglycerol kinase-epsilon and the phosphatidylinositol cycle. *FEBS Lett* 2011, **585**(24): 4025-4028.

36. Rodriguez de Turco EB, Tang W, Topham MK, Sakane F, Marcheselli VL, Chen C, et al. Diacylglycerol kinase epsilon regulates seizure susceptibility and long-term potentiation through arachidonoyl- inositol lipid signaling. *Proc Natl Acad Sci U S A* 2001, **98**(8): 4740-4745.
37. Marquez VE, Blumberg PM. Synthetic diacylglycerols (DAG) and DAG-lactones as activators of protein kinase C (PK-C). *Acc Chem Res* 2003, **36**(6): 434-443.
38. Das J, Rahman GM. C1 domains: structure and ligand-binding properties. *Chem Rev* 2014, **114**(24): 12108-12131.
39. Ware TB, Shin M, Hsu K-L. Metabolomics analysis of lipid metabolizing enzyme activity. *Methods Enzymol* 2019, **626**: 407-428.
40. Pettitt TR, Wakelam MJO. Diacylglycerol kinase epsilon, but not zeta, selectively removes polyunsaturated diacylglycerol, inducing altered protein kinase C distribution in vivo. *J Biol Chem* 1999, **274**(51): 36181-36186.
41. Franks CE, Hsu KL. Activity-Based Kinome Profiling Using Chemical Proteomics and ATP Acyl Phosphates. *Curr Protoc Chem Biol* 2019, **11**(3): e72.
42. Mann M. Functional and quantitative proteomics using SILAC. *Nat Rev Mol Cell Biol* 2006, **7**(12): 952-958.
43. McCloud RL, Franks CE, Campbell ST, Purow BW, Harris TE, Hsu KL. Deconstructing Lipid Kinase Inhibitors by Chemical Proteomics. *Biochemistry* 2018, **57**(2): 231-236.
44. Boroda S, Niccum M, Raje V, Purow BW, Harris TE. Dual activities of ritanserin and R59022 as DGKalpha inhibitors and serotonin receptor antagonists. *Biochem Pharmacol* 2017, **123**: 29-39.
45. Chen BC, Legant WR, Wang K, Shao L, Milkie DE, Davidson MW, et al. Lattice light-sheet microscopy: imaging molecules to embryos at high spatiotemporal resolution. *Science* 2014, **346**(6208): 1257998.
46. Li D, Shao L, Chen BC, Zhang X, Zhang M, Moses B, et al. ADVANCED IMAGING. Extended-resolution structured illumination imaging of endocytic and cytoskeletal dynamics. *Science* 2015, **349**(6251): aab3500.
47. Imai S, Kai M, Yasuda S, Kanoh H, Sakane F. Identification and characterization of a novel human type II diacylglycerol kinase, DGK kappa. *J Biol Chem* 2005, **280**(48): 39870-39881.
48. Klauck TM, Xu X, Mousseau B, Jaken S. Cloning and characterization of a glucocorticoid-induced diacylglycerol kinase. *J Biol Chem* 1996, **271**(33): 19781-19788.
49. Sakane F, Imai S, Kai M, Wada I, Kanoh H. Molecular cloning of a novel diacylglycerol kinase isozyme with a pleckstrin homology domain and a C-terminal tail similar to those of the EPH family of protein-tyrosine kinases. *J Biol Chem* 1996, **271**(14): 8394-8401.
50. Bozelli JC, Jr., Jennings W, Black S, Hou YH, Lameire D, Chatha P, et al. Membrane curvature allosterically regulates the phosphatidylinositol cycle, controlling its rate and acyl-chain composition of its lipid intermediates. *J Biol Chem* 2018, **293**(46): 17780-17791.

Chapter 3. Characterization of Novel and Selective TAG Lipase Functionality of Diacylglycerol Lipase Beta in Macrophages

Adapted from: Myungsun Shin, Timothy B. Ware, Ku-Lung Hsu. *Cell Chemical Biology* 27 (3), 314-321 (2020).

3.1 *Abstract*

Here, we apply quantitative chemical proteomics and untargeted lipidomics to assign a polyunsaturated fatty acid (PUFA)-specific triacylglycerol (TAG) lipase activity for diacylglycerol lipase-beta (DAGLβ) in macrophages. We demonstrate that DAGLβ but not DAGLα is expressed and active in bone marrow-derived macrophages (BMDMs) as determined by activity-based protein profiling (ABPP) analysis of SILAC BMDMs. Genetic disruption of DAGLβ resulted in accumulation of cellular TAGs composed of PUFA but not saturated/low unsaturated FA counterparts, which is recapitulated in wild-type macrophages treated with a DAGLβ-selective inhibitor. Biochemical assays with synthetic substrates confirm PUFA-TAGs as authentic DAGLβ substrates. In summary, our findings identify DAGLβ as a PUFA-specific TAG lipase in primary macrophages.

3.2 *Introduction*

Diacylglycerol lipases (DAGLs) hydrolyze arachidonic acid (AA)-esterified diacylglycerols (DAGs) to biosynthesize the principal endocannabinoid 2-arachidonylglycerol (2-AG)[1,2]. DAGLs are members of the serine hydrolase superfamily that utilize a catalytic serine for calcium-dependent cleavage of DAGs in a *sn*-1 selective manner[3,4]. The function of DAGL isoforms is regulated by cell type- and tissue-specific expression in mammals. DAGLα expression is enriched in central tissues (e.g., brain and spinal cord) where this isoform regulates 2-AG involved in synaptic activity and neuroinflammation[1,2,5,6]. DAGLβ activity is enriched in macrophages[7], microglia[6], and dendritic cells[8] where this isoform regulates 2-AG and downstream metabolic products including prostaglandins important for innate immune responses underlying peripheral and central inflammation.

To date, the substrate specificity of DAGLs have been assigned principally by targeted liquid chromatography-mass spectrometry (LC-MS) metabolomics approaches[9]. These analyses were performed with a predefined set of lipids based on insights from prior studies of substrate specificity in cells and/or animals. Targeted metabolomics has been vital for identifying DAGs, endocannabinoids, and prostaglandins as DAGLα- and DAGLβ-regulated lipids involved in mediating cell biological and animal physiological functions[5-8,10]. While critical for understanding DAGL biology, this targeted approach is not well-suited for global discovery of new lipids regulated by these enzymes. Consequently, the full range of substrates regulated (directly or indirectly) by DAGLs remains underexplored.

Here, we performed untargeted metabolomics to map putative lipid substrates of DAGLβ in primary macrophages. Genetic disruption of DAGLβ resulted in cellular accumulation of a rare subset of triacylglycerols (TAGs) in primary macrophages. Specifically, our metabolomics profiling identified TAGs containing polyunsaturated fatty acids (PUFAs) as putative DAGLβ substrates, which we could recapitulate by pharmacology using DAGLβ-selective inhibitors. PUFA-TAGs

were confirmed as authentic DAGLβ substrates by biochemical assays using synthetic lipid standards. Collectively, our findings identify DAGLβ as a neutral lipase that is capable of hydrolyzing DAGs and TAGs with specificity that is dependent on fatty acyl composition.

3.3 *Materials and Methods*

Mice. All studies were conducted in 6-12-week-old C57BL/6J, DAGLβ, and DAGLα mice. Mice were housed in the MR6 animal facility (UVa), and Gilmer animal facility (UVa). All studies were carried out under a protocol approved by the ACUC/University of Virginia. All animals were allowed free access to a standard chow diet and water. The animals were housed according to the ACUC policy on social housing of animals. For experiments involving BMDMs, both male and female mice were used in performing described work. Each experiment was controlled by using same-sex littermates.

Bone Marrow Derived Macrophages (BMDMs) differentiation. Mice used to culture BMDMs were the same as described in the 'Animals' section. Both male and female mice were used in the following studies. BMDMs were cultured as previously described[11]. In brief, the bone marrow from the hind legs of mice was extracted and incubated for 5 min with 0.83% ammonium chloride, to clear erythrocyte progenitors. The bone marrow was cultured with RPMI media supplemented with 10% FBS (Omega Scientific), 5% HEPES (Gibco), 1% antibiotic-antimitotic (penicillin-streptomycin, Gibco), and 10% L929-conditioned media (L929 cells purchased from ATCC). For SILAC BMDMs, the L929-conditioned media was instead supplemented with 10% dialyzed FBS (Omega Scientific) and either "light" L-arginine and L-lysine (100 μg ml^{-1}) or "heavy" [$^{13}C_6{}^{15}N_4$]L-arginine and [$^{13}C_6{}^{15}N_2$]L-lysine (100 μg ml^{-1}). The culture continued for 7 days, with media changes every 3–4 days, after which the media was exchanged for one lacking L929-conditioned media. On day 7, the BMDMs were gently separated from petri dishes using 0.25% trypsin (Gibco), followed by centrifugation and media replacement. Finally, BMDMs were plated on non-tissue culture treated petri dishes for various treatments and analyses**.**

HEK293T Cells. HEK293T cells (gender: female) were obtained from ATCC and were not further authenticated. HEK293T cells were cultured in complete DMEM media (10% FBS (U.S. Source,

Omega Scientific) and 1% L-glutamine (Thermo Fisher Scientific)) in 10 cm^2 plates. All cells were grown to ~80% confluency in a 37°C incubator with 5% CO_2.

L929 Cells. L929 cells (gender: male) were obtained from ATCC and were not further authenticated. L929 cells were cultured in complete RPMI media (10% FBS (U.S. Source, Omega Scientific), 2 mM L-glutamine (Thermo Fisher Scientific), 100 µg mL^{-1} penicillin-streptomycin (Sigma-Aldrich), and 20 mM HEPES (pH 7.4)) in Corning™ CELLSTACK™ Culture Chambers. 678,400 cells were seeded across the two chambers of the cell stack in 423 mL of complete RPMI media in a 37°C incubator with 5% CO_2. Media was harvested from the cell stack after each week for two weeks and replaced with fresh complete RPMI media.

Reagents. Unless otherwise specified, reagents used were purchased from Fisher Scientific. Bio-beads SM-2 Adsorbants (Bio-Rad) catalog# 1528920. Polyethyleneimine (Polysciences, Inc.) catalog# 24765, 2-Mercaptoethanol (Sigma-Aldrich) catalog# M6250-250ML, recombinant M-CSF (Peprotech) catalog# 315-02. KT109 (synthesized in house), KT195 (Cayman Chemical Company) catalog# 14818. Anti-FLAG antibody produced in rabbit (Sigma-Aldrich) catalog# F7425, Goat anti-rabbit DyLight 550 (Thermo Fisher Scientific) catalog# 84541. PE/Cy7 anti-mouse/human CD11b antibody (Biolegend) catalog# 101215. Rat anti-mouse F4/80 antibody (Bio-Rad) catalog# MCA497A488T. Arachidonic acid-d8 (Cayman Chemical Company) catalog# 390010, 2-Arachidonyl glycerol-d5 (Cayman Chemical Company) catalog# 362162, Tritetradecanoin (C14:0) (Nu-Chek Prep) catalog# T-140, Trihexadecanoin (C16:0) (Nu-Chek Prep) catalog# T-150, Trioctadecanoin (C18:0) (Nu-Chek Prep) catalog# T-160, Trieicosanoin (C20:0) (Nu-Chek Prep) catalog# T-170, Tridocosanoin (C22:0) (Nu-Chek Prep) catalog# T-180, Triarachidonin (C20:4) (Nu-Chek Prep) catalog# T-295, Trieicosapentaenoin (C20:5) (Nu-Chek Prep) catalog# T-325, Tridocosahexaenoin (C22:6) (Nu-Chek Prep) catalog# T-310. Fetal bovine serum (FBS) and dialyzed FBS were obtained from Omega Scientific.

Overexpression of DAGLβ in HEK293T Cells. Recombinant mouse DAGLβ protein was produced by transient transfection of HEK293T cells with recombinant DNA. The transient transfection was performed as described previously[7] and in **2.3 *Materials and Methods***.

Western Blot Analysis. Western blots were prepared and analyzed as described previously, see **2.3 *Materials and Methods*** for additional details.

Lipid Extraction. BMDM and HEK293T cell pellets (3 million cells) were extracted using the Folch extraction method (2:1:1 chloroform:methanol:water) as previously described[13]. BHT (50 µg/ml) was added to organic solvents used for extraction. Chloroform/methanol solution (3 mL) was added with 1 mL of resuspended cells in water. Samples were briefly vortexed and centrifuged at 2,000 x *g* for 5 min. Organic layer was transferred and aqueous layer was added with 1.5 mL of additional 2:1 chloroform:methanol solution for extraction followed by centrifugation at 2,000 x *g* for 5 min. Organic layers were combined and dried under stream of nitrogen gas. Samples were resolubilized in 120 µL of 1:1 methanol:isopropanol solution and stored at -80°C until further analysis.

LC-MS/MS Lipidomics. A Dionex Ultimate 3000 RS UHPLC system was used with the analytical column (Kinetex® 1.7 µm C18 100 Å, LC column 100 X 2.1 mm) and reverse phase LC solvents (A: 0.1% formic acid, 10 mM ammonium formate, 50% water, 50% acetonitrile, B: 0.1% formic acid, 10 mM ammonium formate, 10% acetonitrile, 88% isopropanol, 2% water) and the following gradient: 0-4 min, 35% to 60% B; 4-12 min, 60% to 85% B; 12-24 min, 85% to 100% B, flow rate at 250 µL/min. The eluted lipids were electrosprayed using a HESI-II probe into an Orbitrap Q-Exactive Plus mass spectrometer (Thermo Scientific), which was operated under one of two methods: 1) A top 10 data-dependent (ddMS2) acquisition method that consisted of one full MS1 scan (250-1,200 m/z) followed by 10 MS2 scans of the most abundant ions recorded in the MS1 scan. 2) A targeted parallel reaction monitoring (PRM) acquisition method that performs multiple MS2 scans from a pre-specified MS1 precursor scan of a known ion m/z and retention window.

Isolation window was set at 1.2 m/z. Data acquisitions were performed using both ddMS2 global analysis and PRM targeted methods, in both positive and negative ionization modes to enhance the confidence of lipid identification. PRM targeting of diacylglycerol and triacylglycerol lipid species was accomplished by filtering for the $[M+NH_4]+$ adduct ions and subsequent MS2 detection of expected diagnostic fragment ions (neutral loss of fatty acyl chains in positive ion mode). Intensities of the lipid species were measured using TraceFinder™ software, which identified fragment ions across multiple samples based on the MS2 filter defined in a targeted list of lipids and aligned them according to the intensities of the ion species found in each raw file. Raw intensities were normalized to base peak ion intensities for each sample acquisition to account for instrument injection variation. Lipid identifications and peak alignments were performed using LipidSearch™ software while quantitative analysis of the aligned intensities was exported and analyzed using GraphPad Prism version 7.03.

Lipid Identification by LC-MS/MS. Data analysis was performed using the LipidSearch™ software package, which used MS1 monoisotopic precursor ions for the *in-silico* database search followed by the product ions search from MS2 spectra (search parameters: Target database: Q Exactive, SearchType: product, ExpType: LC-MS, Precursor tolerance 5.0 ppm, product tolerance 5.0 ppm, intensity threshold: product ion 1.0%, m-score threshold 2.0). Results from positive and negative ion mode analyses were merged to generate a matched lipid dataset. The searched data were aligned with selected parameters (ExpType: LC-MS, Alignment Method: Median, Toprank Filter: on, Main node Filter: Main isomer peak, m-Score Threshold: 5.0, ID quality filter: A, B, C, D) and curated with species with high-confidence grade scores “A” and “B” for further analysis.

Sample preparation for LC-MS/MS Substrate Assay. Cell pellets were dounce homogenized in lysis buffer (0.25 M sucrose, 20 mM HEPES at pH 7.4, 2 mM DTT) and ultracentrifuged at 100,000 x *g* for 45 min at 4°C. Pellets were resuspended by sonication in activity buffer (50 mM

HEPES at pH 7.4, 100 mM NaCl , 5 mM $CaCl_2$, 0.1% Triton X-100 v/v, 10% DMSO and 0.5 mM DTT). Protein concentration was standardized to 0.37 mg mL^{-1} (membrane fraction) and treated with respective inhibitors for 30 min (KT109 2 µM, KT195 2 µM). Lipid substrate was prepared as follows: 250 pmol of respective lipid substrate, dissolved in chloroform, was placed in a dram vial, dried under a stream of nitrogen gas, brought up in 460 µL of activity buffer, and briefly sonicated to create a turbid solution. 40 µL of the pre-treated lysates were then added to the lipid substrate mixture at a final volume of 500 µL in activity buffer. The reaction was vortexed and left to continue at room temperature for 4 h. The reaction was quenched via organic extraction. The extraction was carried out by adding 1.5 mL of hexane (3:1 hexane:H_2O) with 80 mg of bio-beads (Bio-Rad). Reaction mixture was vortexed and centrifuged at 2,000 x *g* for 5 min. Additional wash with 1.5 mL of hexane was performed and hexane layers were combined. Hexane layer was transferred to a new dram vial and added with 1 mL of water, and 80 mg of bio-beads. After vortex/centrifugation, hexane layer was transferred to a clean dram vial and dried down under nitrogen. Samples were resuspended in 1:1 isopropanol:methanol and stored at -80°C until further analysis.

LC-MS/MS Substrate Assay. LC-MS/MS conditions used for the substrate assay lipid identification are identical to the conditions described in “LC-MS/MS Lipidomics” with slight changes in LC configuration. External hardware divert valves were used to discard eluents from the initial 6 min of the analysis in order to prevent residual triton X-100 from being introduced to mass spectrometer.

Sample Preparation for Gel-based Competitive Activity Based Protein Profiling (ABPP). Cell pellets were processed using dounce homogenizer. Supernatant was isolated and centrifuged at 100,000 x *g* for 45 min. Resulting supernatant fraction and resuspended pellet solution were referred as soluble and membrane fraction, respectively. Proteomes (1 mg/mL) were treated with HT-01 probe at 1 µM final concentration for 30 min at 37°C. The reaction was

quenched using SDS-PAGE loading buffer. After separation by SDS-PAGE (10% acrylamide), samples were visualized by in-gel fluorescence scanning using ChemiDoc MP imaging system (Bio-Rad).

Sample preparation for quantitative LC-MS/MS analysis using Fluorophosphonate probes. SILAC proteomes were diluted to 1 mg/mL in PBS and sample aliquots (432 µl) were treated with fluorophosphonate (FP) alkyne probe at 100 µM (5 µl, 100X stock in DMSO; final concentration of 1 µM), mixed gently and incubated for 2 h at room temperature. Light and heavy probe-modified proteomes were mixed 1:1 and subjected to CuAAC conjugation to desthiobiotin-PEG3-azide (10 µl of 10 mM stock in DMSO; final concentration of 200 µM) using TCEP (10 µl of fresh 50 mM stock in water, 1 mM final concentration), TBTA ligand (33 µl of a 1.7 mM 4:1 *t*-butanol/DMSO stock, 100 µM final concentration) and $CuSO_4$ (10 µl of 50 mM stock, 1 mM final concentration). Samples were vortexed and then incubated for 1 h at room temperature. Excess reagents were removed by chloroform-methanol extraction. Protein pellets were resuspended in 500 µL of 6 M urea:25 mM ammonium bicarbonate followed by dithiothreitol reduction and iodoacetamide alkylation. Excess reagents were removed by chloroform-methanol extraction as described above, and the protein pellet was resuspended in 500 µL of 25 mM ammonium bicarbonate and then digested to peptides as trypsin/Lys-C (7.5 µg in 15 µL of ammonium bicarbonate, Promega catalog # V5073) was added to the mixture and incubated for 3 h at 37°C. Probe-modified peptides were enriched by avidin affinity chromatography, eluted, and prepared for LC-MS/MS analysis. Nano-electrospray ionization–LC–MS/MS analyses were performed using an Ultimate 3000 RSLC nanoSystem-Orbitrap Q Exactive Plus mass spectrometer (Thermo Scientific). The eluting peptides were electrosprayed into an Orbitrap Q Exactive Plus mass spectrometer (Thermo Scientific), which was operated with a top 10 data-dependent acquisition method that consisted of one full MS1 scan (375 - 1,500 m/z) followed by 10 MS2 scans of the most abundant ions recorded in the MS1 scan. Data analysis was accomplished using the IP2 (Integrated

Proteomics Applications) software package, in which RawConverter was used to generate searchable MS1 and MS2 data from the .raw file followed by using the ProLuCID algorithm to search the data against a mouse protein database (UniProt mouse protein database, angiotensin I and vasoactive intestinal peptide standards, 55,513 proteins) with the following parameters: static carbamidomethyl modification (+57.02146 Da), differential modification of oxidized methionine (+15.9949 Da), added masses of the SILAC “heavy”-labeled amino acids (+10.0083 Da for R, +8.0142 Da for K), and trypsin enzyme specificity with 1 missed cleavage. The resulting MS2 spectra matches used to generate SILAC ratios (SR) of light/heavy (vehicle/compound treated) peptides.

Flow Cytometry Cell Sample Preparation and Analysis. After BMDMs were differentiated, suspension cells were seeded in a 96-well plate in 50 mL volume at 100,000 cells per well in complete BMDM differentiation media. Supernatant was collected in V-bottom 96 well plate and centrifuged at 1,400 x *g* for 5 min to pellet residual BMDMs. Supernatant was transferred to a separate 96 well plate and stored at -80°C until further analysis. Cytokine profiling was performed at the UVa flow cytometry core. In brief, antibody-immobilized beads were prepared by sonication/vortexing for 1 min with 60 mL of each individual antibody-bead: PE/Cy7 anti-mouse/human CD11b [M1/70] (Catalog# 101215) and Rat anti Mouse F4/80 (Catalog# MCA497A488T) and combining them in a total volume of 3.0 mL of assay buffer (Millipore corporation, catalog# L-AB). Wells were washed, detected, and analyzed using the Luminex MAGPIX system following manufacturer’s recommended protocols. Samples were analyzed using median fluorescent intensity (MFI) data using a 5-parameter logistic for calculating the cytokine concentrations in samples. Exported data were analyzed using FloJo (version 10.6.1).

Quantification and Statistical Analysis. For the lipid analyses, the intensities of identified lipid species were used for the semi-quantitative determination of lipid concentrations within a sample. Intensities of lipid species were divided by the base peak intensities of each injected sample. The

calculated lipid amounts were normalized based on the number of cells for each respective sample. Statistical analyses were performed in GraphPad Prism version 7.03. In order to determine statistically significant differences between groups analyzing multiple lipid species, a Holm-Sidak multiple comparison test (do not assume consistent standard deviation, confidence interval of 95%) was applied. Otherwise, an unpaired t-test was implemented to demonstrate significant differences between two groups with respect to individual lipid changes while one-way ANOVA was used for comparisons across three or more conditions. Statistical significance was set at $P < 0.05$. The number of experimental biological replicates of cell populations in each sample group are indicated by *n* and can be found in respective figure legends as well as the number of times individual experiments were repeated with similar results. Data are shown as mean ± standard error of mean (s.e.m.).

3.4 *Results*

3.4.1 *Activity-Based Protein Profiling (ABPP) of DAGLs in Bone Marrow-Derived Macrophages*

Bone marrow-derived macrophages (BMDMs) were differentiated from bone marrow of mice using L929-supplemented media for 7 days following published procedures[11] (see **3.3 *Materials and Methods*** for additional details). We chose BMDMs for our global metabolomics studies because of the ability to generate homogeneous cultures of both wild-type (WT) and DAGLβ knockout (KO) primary macrophages. To determine whether BMDMs express active DAGLα and/or DAGLβ, we performed activity-based protein profiling (ABPP[12]) studies (**Figure 3.1a)** with our DAGL-tailored probe HT-01[7] (**Figure 3.1b**). We detected prominent HT-01 labeling of a ~70 kDa protein band that was present in proteomes from *Daglb*$^{+/+}$ but absent from *Daglb*$^{-/-}$ BMDMs (**Figure 3.1c**). We also performed HT-01-based ABPP comparisons of *Dagla*$^{+/+}$and *Dagla*$^{-/-}$ BMDM proteomes but could not detect active DAGLα (**Figure 3.1c**). These ABPP results are in contrast with brain proteomes where we could reliably measure endogenous DAGLα and DAGLβ using HT-01 (**Figure 3.1d**). Thus, we focused the remainder of our macrophage studies on the DAGLβ isoform.

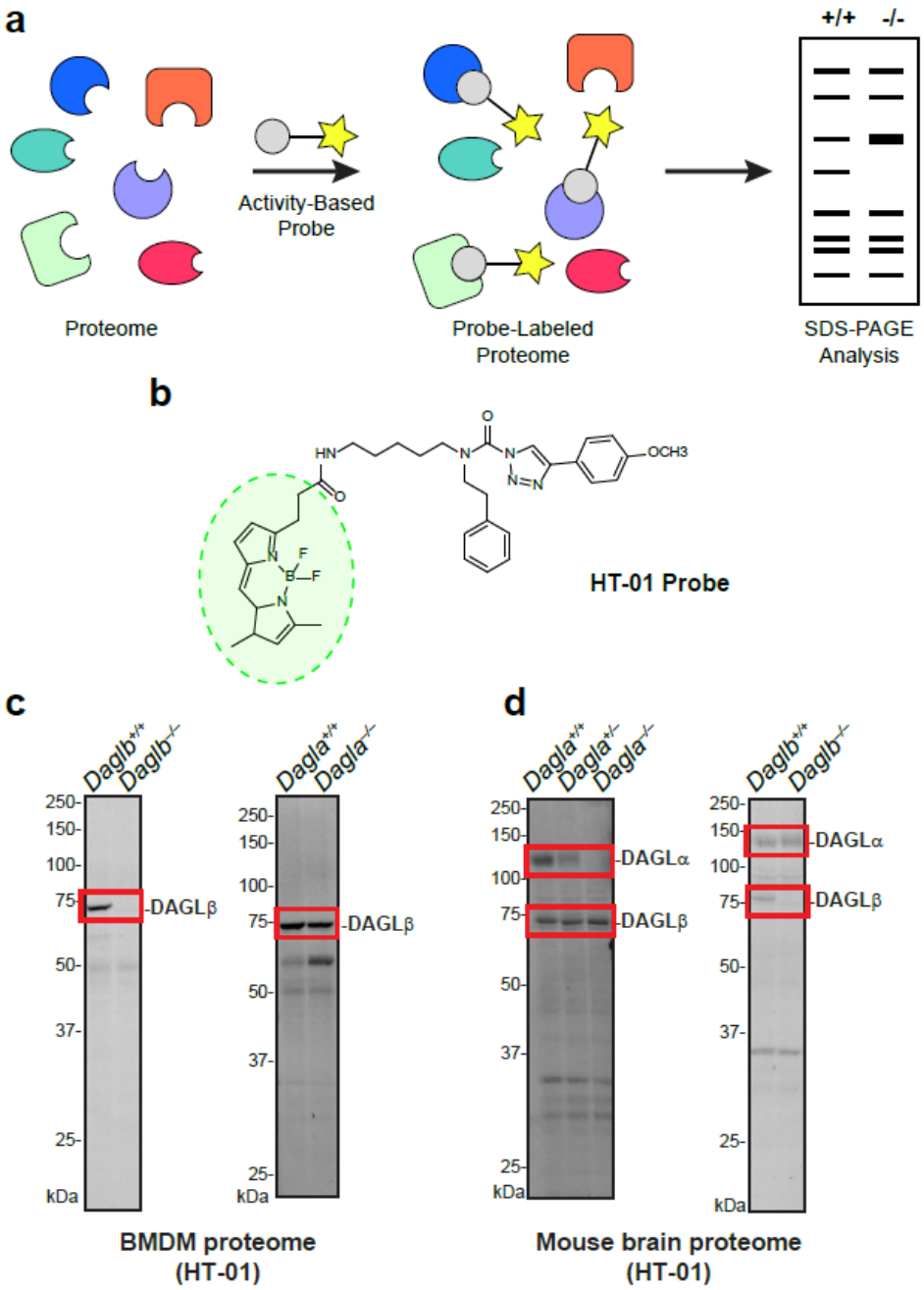

Figure 3.1 HT-01-based activity-based protein profiling (ABPP) of DAGL activity in primary macrophage and brain proteomes. a) Schematic workflow for gel-based ABPP analysis using a genetic model to assess differences in probe labeling of proteins. Band intensities reflect levels of probe labeling. b) Structure of the DAGL-tailored ABPP probe HT-01. c) Native DAGLβ but not DAGLα activity was detected in BMDMs as judged by gel-based ABPP analyses with HT-01. BMDM membrane proteomes were treated with the DAGL-tailored ABPP probe HT-01 (1 μM, 30 min, 37°C) followed by SDS-PAGE and in-gel fluorescence scanning to measure active DAGLs in BMDM proteomes. d) Native DAGLα and DAGLβ were active and detected in mouse brain proteomes. Gel-based ABPP analysis of brain membrane proteomes from DAGL wild-type (*Dagl*$^{+/+}$), heterozygous (*Dagl*$^{+/-}$), and knockout (*Dagl*$^{-/-}$) mice treated with HT-01 probe.

In summary, gel based ABPP profiling studies identified DAGLβ as a principal DAGL isoform expressed in BMDMs.

3.4.2 *LC-MS Metabolomics Identifies PUFA-TAGs as Putative DAGLβ Substrates in BMDMs*

Next, we deployed an untargeted MS-metabolomics approach to gain an unbiased global evaluation of alterations in lipid composition of DAGLβ-disrupted BMDMs. Total lipids (i.e. lipidome) were extracted from *Daglb*$^{+/+}$ and *Daglb*$^{-/-}$ BMDMs using the Folch method[13] and analyzed by liquid chromatography-mass spectrometry (LC-MS/MS) on a high-resolution Q-Exactive Plus mass spectrometer configured for untargeted data-dependent acquisition (ddMS2, **Figure 3.2a**). Lipid precursor ions (MS1) selected for fragmentation were identified using LipidSearch™ that matches precursor (MS1) and fragment (MS2) spectra to an *in-silico* database containing more than 1.5 million lipid molecules and their predicted precursor and fragment ions[14]. Identified lipids were scored based on fatty acid (FA) chain composition, which is determined from fragment ions corresponding to neutral loss of FAs, and only those with high quality (Grade A or B signifying 2-4 lipid class-specific diagnostic fragment ions and less than 5 ppm precursor mass deviation) were selected for further manual evaluation (**Figure 3.2b**; see **3.3 *Materials and Methods*** for details). We detected on average ~980 lipids per BMDM sample analysis, which consisted of positive and negative ion mode LC-MS/MS analyses.

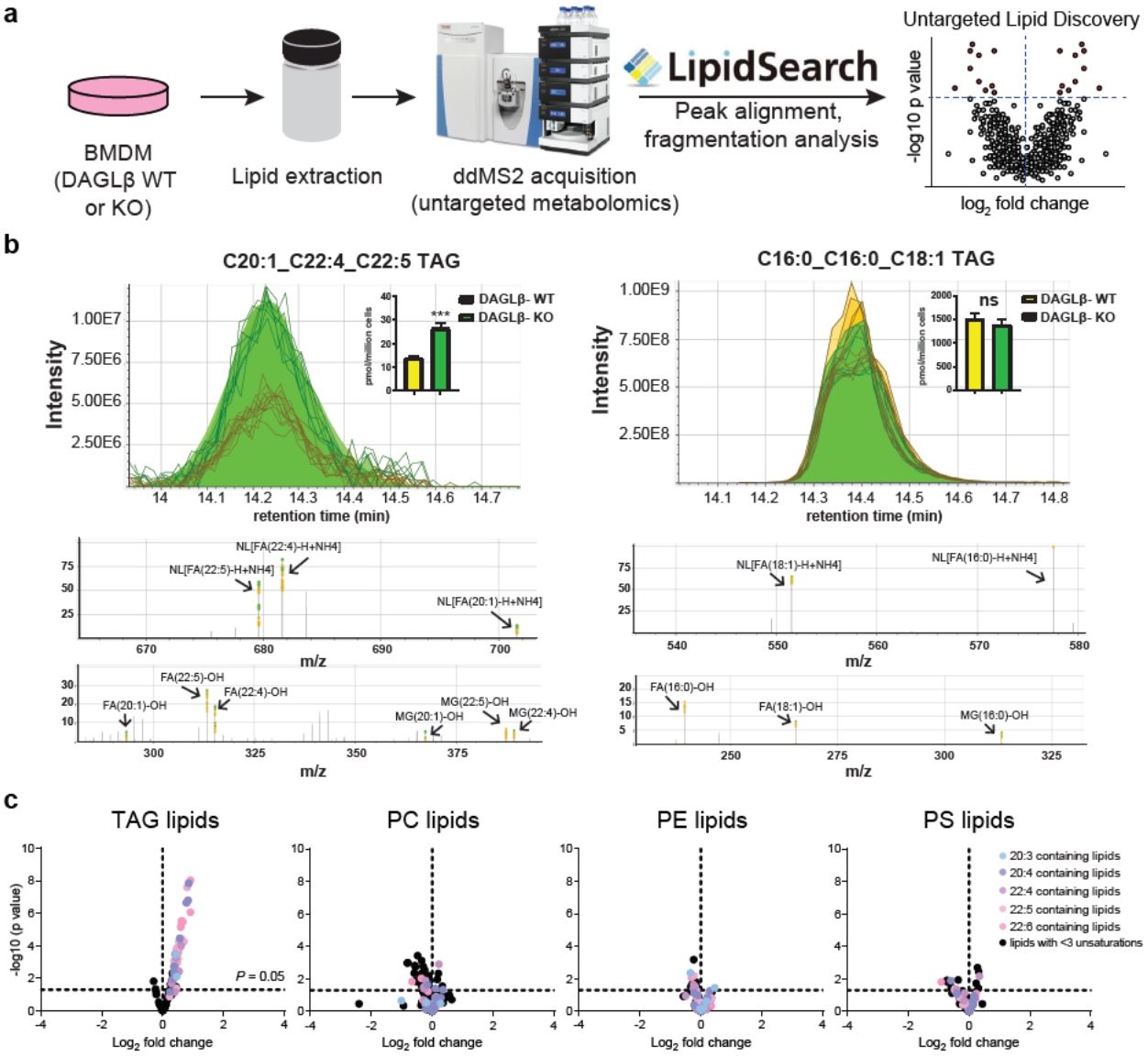

Figure 3.2 Untargeted lipidomics reveals PUFA-TAG accumulation in DAGLβ-disrupted BMDMs. a) Schematic of untargeted LC-MS lipidomic profiling platform. b) Representative peak alignments of MS1 chromatograms and MS2 fragmentation spectra observed for triacylglycerol (TAG) species from LipidSearch™ and manual analyses of the raw MS data. The following diagnostic ions enable confident TAG identification: neutral loss of each fatty acyl chain (NL[FA-H+NH4]), precursor ion ([TAG+NH4]+), and fragmentation of the remaining glycerol backbone and the released fatty acyl chains (monoacylglycerol (MG)-OH and FA-OH). Inset: bar graphs showing the abundances of each TAG species from the MS1 chromatograms (Data shown represent mean ± s.e.m.; *n*=5 biological samples). Statistical significance was determined using a Holm-Sidak correction following a two-sided binomial test (***$P < 0.001$). c) Volcano plot showing changes in abundance of lipid species detected in DAGLβ KO compared with WT BMDMs from global lipidomics analyses (*n*=5 biological samples). Dashed lines indicated statistical significance cutoff (horizontal; $P = 0.05$) and direction of fold change (vertical; left and right quadrant denote decreased and increased abundance, respectively, in KO/WT comparisons). Results show preferential accumulation of PUFA containing TAG species in

DAGLβ KO vs. WT BMDM lipidomes. Phosphatidylcholine (PC), phosphatidylethanolamine (PE), and phosphatidylserine (PS) lipids showed negligible changes in both PUFA (colored circles) and species with low units of unsaturation (lipids with <3 unsaturation units, black circles). Statistical significance was determined using a Holm-Sidak correction following a two-sided binomial test. All data shown are representative of two independent experiments (*n*=2 biologically independent experiments).

From these data, we could quantitate >750 distinct species after filtering for lipids with high quality annotations of FA composition. We validated our BMDM LC-MS metabolomics approach by demonstrating that genetic disruption of DAGLβ resulted in lipid alterations that matched previous reports in peritoneal macrophages[7]. Specifically, metabolomics analysis showed accumulation of AA-esterified DAG substrates along with cellular reduction of the downstream products 2-AG and AA (**Figure 3.3a**). Interestingly, our untargeted findings revealed a striking alteration in TAG lipid profiles in DAGLβ-disrupted BMDMs. We observed statistically significant accumulation of TAG species that contained polyunsaturated fatty acids (PUFAs) in *Daglb*$^{-/-}$ compared with *Daglb*$^{+/+}$ BMDMs (**Figure 3.2c**). Fatty acid composition of accumulated TAGs included species containing omega-6 (arachidonic acid, C20:4) and omega-3 fatty acids (docosapentaenoic acid, C22:5; **Figure 3.2c**). TAGs containing saturated or low degrees of unsaturation (<3) showed negligible differences in *Daglb*$^{-/-}$ compared with *Daglb*$^{+/+}$ lipidomes (**Figure 3.2c**). To determine if PUFA-TAG changes were due to general alterations in macrophage lipidomes, we compared levels of phospholipids between *Daglb*$^{-/-}$ and *Daglb*$^{+/+}$ lipidomes and observed negligible changes in phosphatidyl-ethanolamine (PE), -choline (PC), and -serine (PS) species (**Figure 3.2c**).

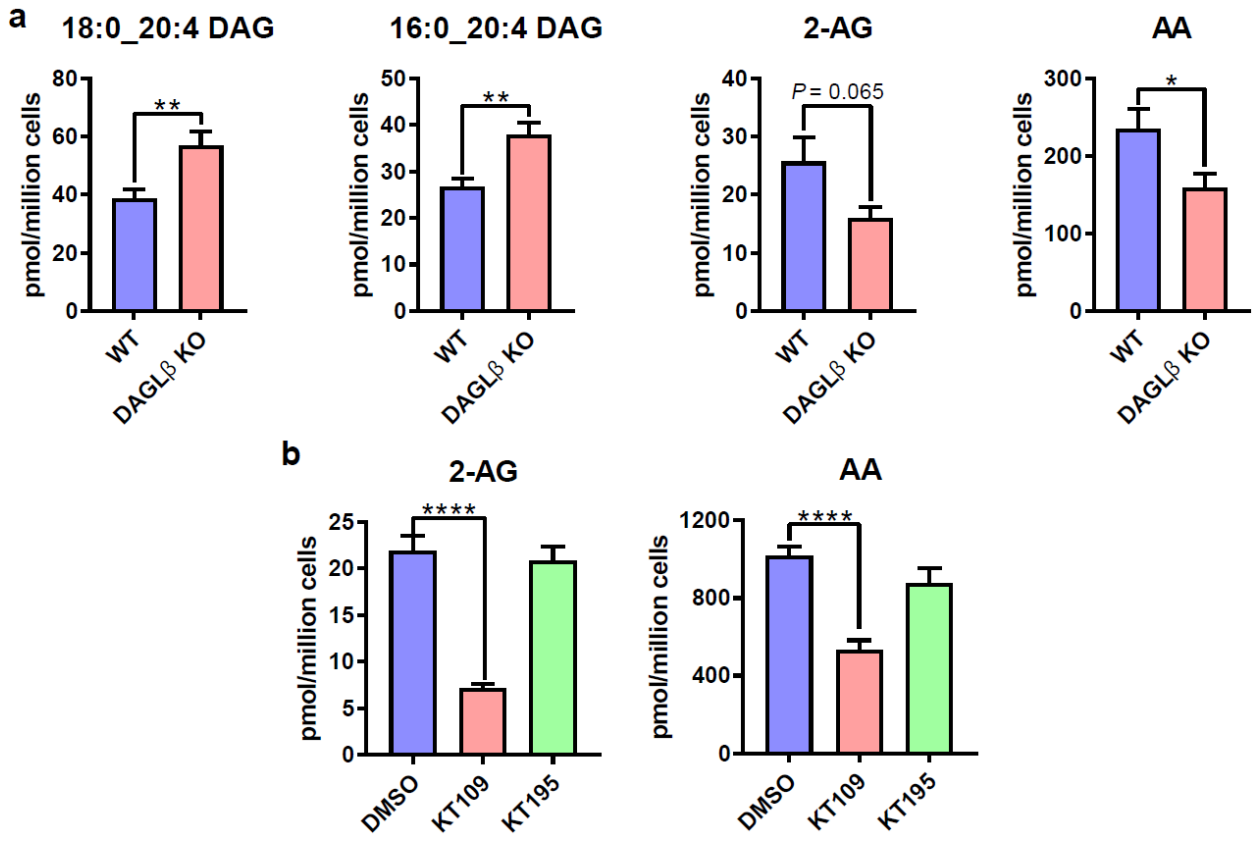

Figure 3.3 Metabolomics analysis of DAGLβ-disrupted BMDMs. a) Targeted metabolomics demonstrated that genetic knockout of DAGLβ resulted in cellular accumulation of lipid substrates (DAG) and depletion of products (2-AG, arachidonic acid, or AA) in BMDMs. Statistical significance was determined using a two-tailed t-test (*P < 0.05, **P < 0.01; n=5-10 biological samples). b) Targeted metabolomics showed that pharmacological blockade of DAGLβ reduced cellular 2-AG and AA in wild-type BMDMs as expected based on the role of DAGLβ in endocannabinoid biosynthesis (n=6-11 biological samples). Statistical significance was determined using a one-way ANOVA test with Dunnett multiple comparison correction (****P < 0.0001). All data shown represent mean ± s.e.m. and are representative of one or two independent experiments (n=1-2 biologically independent experiments).

3.4.3 *Differentiation of SILAC BMDMs for Quantitative Chemoproteomic Profiling*

To complement our genetic KO findings, we performed competitive ABPP gel-based analysis (**Figure 3.4a)** using our previously reported DAGLβ inhibitor KT109 and matching negative control compound KT195[7] (**Figure 3.4b**) to determine whether acute blockade of DAGLβ affected TAG levels in BMDMs. We determined by gel-based ABPP using HT-01 that treatment of BMDMs with

KT109 but not KT195 resulted in concentration-dependent blockade of DAGLβ (**Figure 3.4c**). From our gel-based ABPP studies, we selected optimal treatment conditions (200 nM compounds, 4 h, 37°C) for LC-MS ABPP to determine selectivity across the serine hydrolase family.

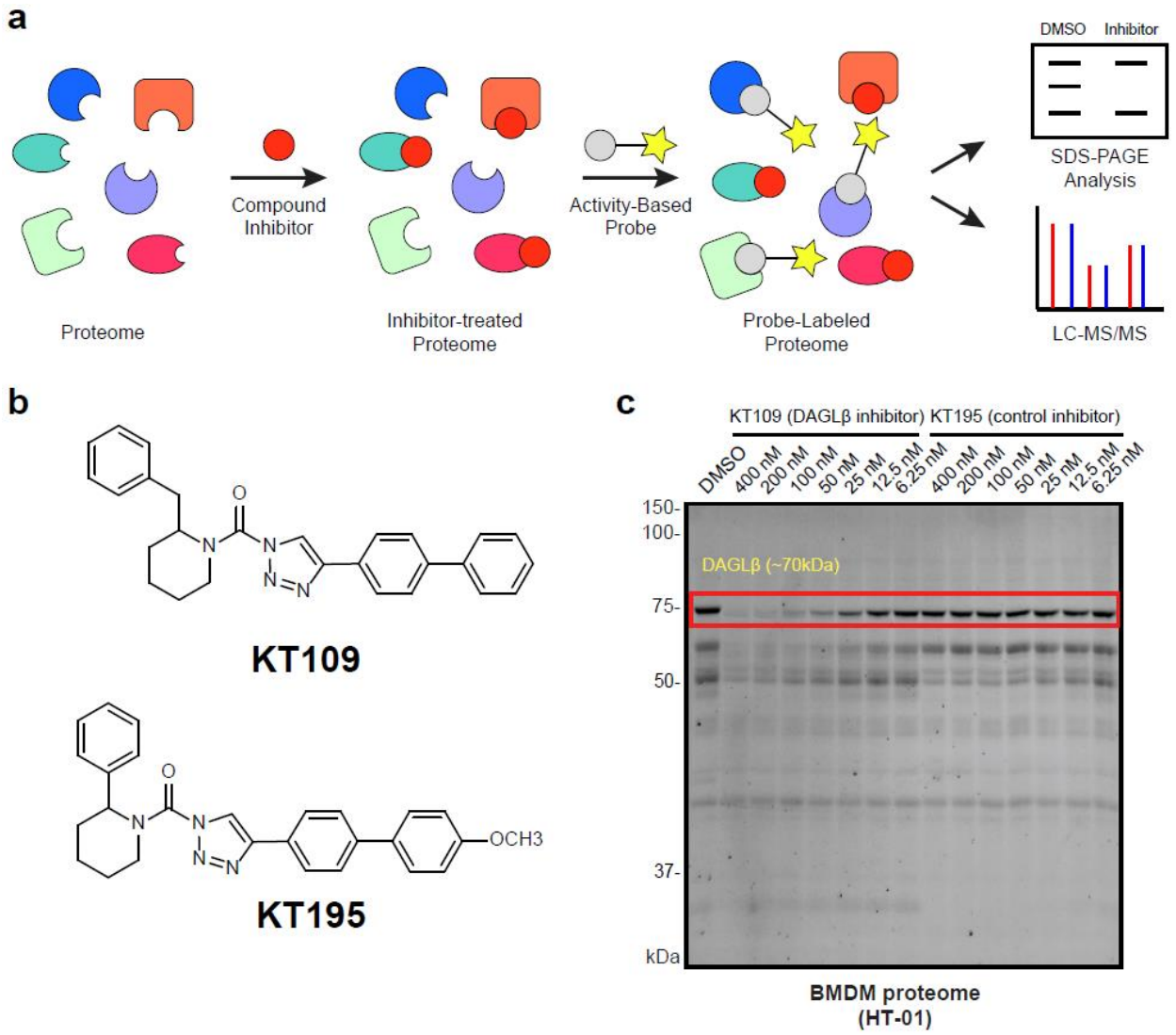

Figure 3.4 Competitive ABPP analysis of DAGLβ in BMDMs using HT-01 a) Schematic workflow for ABPP using small molecule inhibitors for competition of probe-accessible active sites. b) Structures of inhibitors used to assay DAGLβ-specific activity. KT109 is a DAGLβ-selective inhibitor whereas KT195 is a control inhibtor as it is selective for ABHD6, a serine hydrolase family member. c) BMDMs were treated with varying concentrations of the DAGLβ inhibitor (KT109) or matching negative control compound (KT195) for 4 h at 37°C followed by cell lysis and HT-01-based ABPP profiling of membrane proteomes (1 μM probe, 30 min, 37°C).

KT109 but not KT195 showed concentration-dependent blockade of HT-01 labeling of endogenous DAGLβ in proteomes from compound-treated cells.

Next, we established a quantitative proteomics strategy to assess compound potency and selectivity in inhibitor-treated primary macrophages (**Figure 3.5a**). We hypothesized that isotopically-labeled lysine and arginine (i.e. SILAC[15]) would be efficiently incorporated into macrophage proteomes during the rapid differentiation and proliferation of bone marrow stem cells to produce SILAC light- and heavy-labeled BMDMs. For these studies, BMDMs were differentiated from bone marrow of mice using L929 supplemented media (SILAC or standard media) for 7 days as depicted in **Figure 3.5a** and as described in **3.3 *Materials and Methods***. We used fluorescence activated cell sorting (FACS) and established markers for BMDMs (F4/80 and CD11b) to compare macrophage content under standard and SILAC differentiation conditions. We observed comparable numbers of $F4/80^{+}CD11b^{+}$ macrophages in standard and SILAC media (both light and heavy) conditions, which confirmed that BMDMs differentiated under SILAC media were phenotypically similar to standard media counterparts (**Figure 3.5b**).

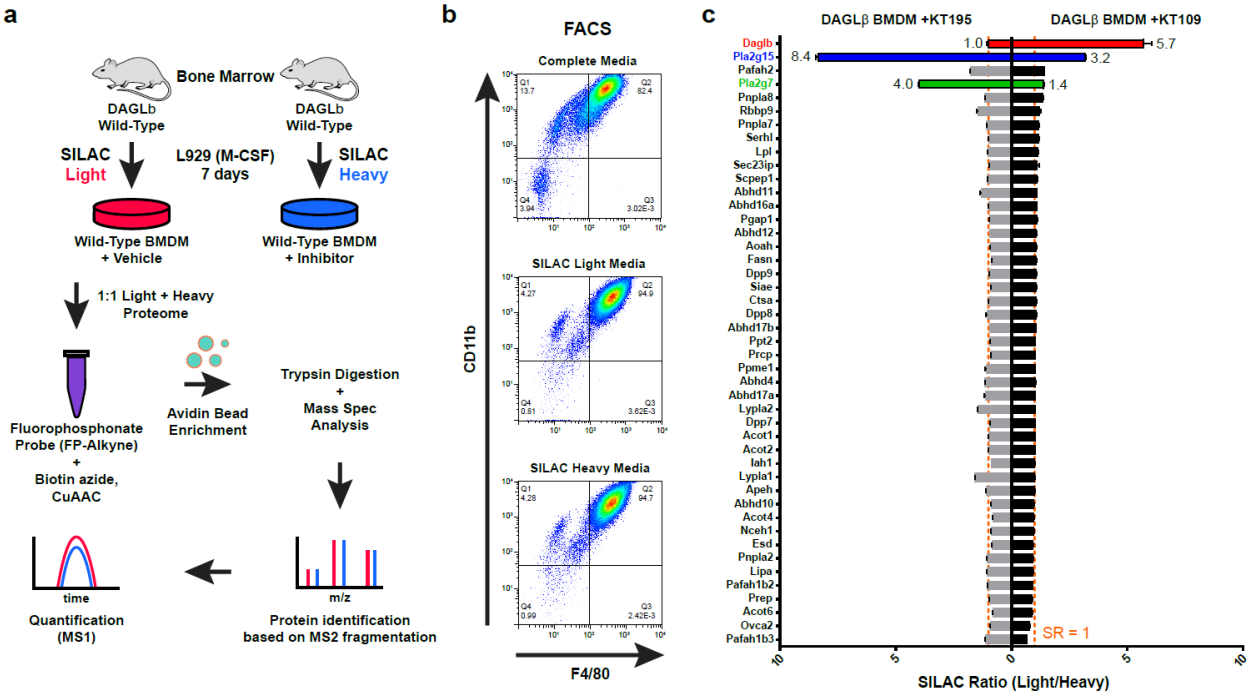

Figure 3.5 ABPP-SILAC analysis of inhibitor activity against serine hydrolases in SILAC BMDMs. a) Generation of SILAC primary macrophage via incorporation of isotopically labeled amino acids during BMDM differentiation. b) Flow cytometry analyses confirmed that BMDMs differentiated using standard or SILAC media are phenotypically equivalent as judged by analysis of macrophage cell surface markers (CD11b and F4/80). c) ABPP-SILAC analysis of BMDMs treated with DMSO (light) or inhibitor (heavy; 200 nM of KT109 or KT195, 4 h, 37°C) followed by labeling with FP-alkyne probe (10 μM, 2 h, 25°C). A SILAC ratio (SR) of ~1 indicates no change in serine hydrolase activity between treatment conditions (vertical dashed line; SR = 1). Data shown represent mean ± s.e.m. All data shown are representative of two independent experiments (*n*=2 biologically independent experiments).

Next, we evaluated global changes in serine hydrolase activity in proteomes from DMSO vehicle- (light) compared with KT109-treated (heavy) BMDMs. After inhibitor treatment, cells were lysed, proteomes labeled with the broad-spectrum serine hydrolase probe FP-alkyne, and SILAC light- and heavy-labeled samples combined. Next, biotin-azide was conjugated by copper catalyzed azide-alkyne cycloaddition (CuAAC[16]) followed by avidin enrichment, on-bead trypsin digestion, and tandem liquid chromatography-mass spectrometry LC-MS/MS ABPP to measure changes in serine hydrolase activity in BMDM proteomes (**Figure 3.5c**). The activity profiles across the 45 detected serine hydrolases in BMDMs were largely unchanged (median SILAC ratio (light/heavy) or SR of ~1) between proteomes from vehicle and KT109-treated cells with the exception of DAGLβ, which showed potent blockade of activity (SR >5, **Figure 3.5c**). We also identified PLA2G15 as a moderately-competed target of KT109 (SR >3, **Figure 3.5c**), which matched our previous ABPP studies in primary macrophages[7]. In contrast, the negative control molecule KT195 was largely inactive against DAGLβ (SR = 1) but showed potent and moderate activity against PLA2G15 and PLA2G7, respectively, in compound treated BMDMs (**Figure 3.5c**). Finally, we could not detect DAGLα activity in our LC-MS studies, which agrees with our HT-01-based ABPP studies (**Figure 3.1c** and **Figure 3.1d**).

In summary, our ABPP-SILAC studies identified DAGLβ as the active DAGL isoform in BMDMs and confirmed that KT109 and KT195 can be used as complementary probes to discern DAGLβ-specific from non-specific pharmacological effects in our metabolomics studies.

3.4.4 *DAGLβ Inhibitors Recapitulate PUFA-TAG Accumulation Observed in KO BMDMs*

From our ABPP-SILAC studies, we selected compound treatment conditions (200 nM compounds, 4 h, 37 °C) for untargeted metabolomics analyses of BMDMs. We first validated that treatment of BMDMs with KT109 but not KT195 resulted in lipid alterations that support functional blockade of DAGLβ (**Figure 3.3b**). Closer inspection of our untargeted metabolomics data revealed a moderate but statistically significant ($P < 0.05$) PUFA-TAG accumulation in KT109- but not KT195-treated BMDMs (**Figure 3.6a**). Akin to *Daglb*$^{-/-}$ BMDMs, we observed minimal accumulations in saturated-TAG species in KT109-treated cells (**Figure 3.6a**). Importantly, the PUFA-TAG changes observed were specific given that acute blockade of DAGLβ did not result in obvious perturbations in phospholipids detected including PS, PC, and PE species of varying fatty acyl compositions (**Figure 3.6b-d**).

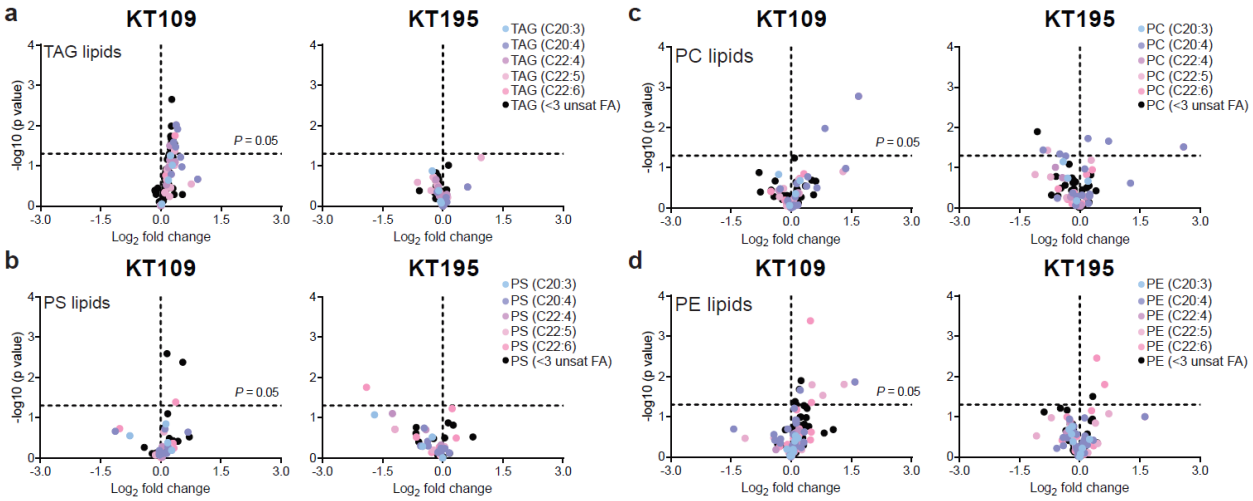

Figure 3.6 Pharmacological disruption recapitulates DAGLβ KO BMDM lipidomic profiles. a) Untargeted lipidomics profiling revealed statistically significant accumulation of PUFA-TAGs in DAGLβ WT BMDMs treated with KT109 but not KT195 (200 nM compounds, 4 h, 37°C; *n*=5 biological samples). b-d) Analysis of additional lipid species including PS, PC, and PE reveal KT109-mediated lipid changes appear to be specific for PUFA-TAGs (*n*=5 biological samples). Dashed lines in volcano plots indicate statistical significance cutoff (horizontal; $P = 0.05$) and direction of fold change in inhibitor/DMSO comparisons (vertical; left quadrant – decreased abundance, right quadrant - increased abundance). Statistical significance was determined using a Holm-Sidak correction following a two-sided binomial test. All data shown are representative of two independent experiments (*n*=2 biologically independent experiments).

To assess the impact of DAGLβ inactivation on bulk TAG levels in BMDMs, we compared the abundance of PUFA- and saturated-TAGs detected in BMDM lipidomes based on ion intensities of MS1 peaks. Unlike PC, PE, and PS lipids, the abundance of PUFA-TAGs represented a minor fraction (~29%) of total TAGs, supporting that disruption of DAGLβ will not likely result in general TAG accumulation as observed for other TAG lipases[17,18] (**Figure 3.7**). In summary, our pharmacology supports our genetic findings of an additional metabolic function for DAGLβ in BMDMs.

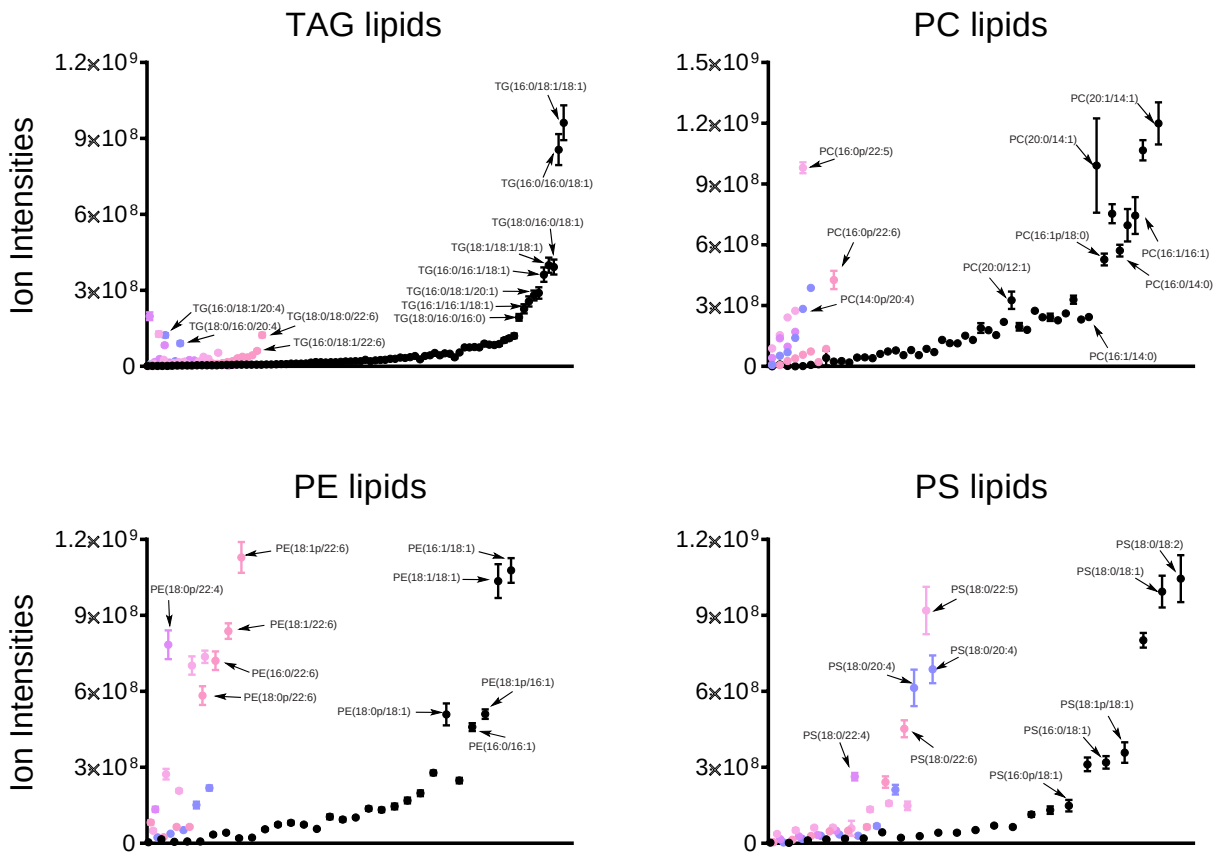

Figure 3.7 PUFA-TAGs are low abundance species compared with saturated counterparts in BMDMs. Untargeted lipidomics profiling of DAGLβ WT BMDM lipid extracts was used to compare lipid species total ion intensities as a function of fatty acyl composition in each respective class. PUFA-TAGs were generally found at lower abundances compared with saturated TAG lipids. In contrast, the differences in abundance of PUFA and saturated phospholipid species appeared to be more evenly distributed (*n*=5 biological samples). All data shown are representative of two independent experiments (*n*=2 biologically independent experiments).

3.4.5 *Biochemical Validation that DAGLβ Exhibits PUFA-Specific TAG Lipase Activity*

We next examined whether DAGLβ could hydrolyze synthetic TAGs in a biochemical substrate assay. These studies were important for establishing TAGs as authentic substrates of DAGLβ given that changes observed in cellular studies could arise from secondary effects due to DAGLβ blockade. We transiently overexpressed mouse DAGLβ in HEK293T cells and measured recombinant DAGLβ activity in membrane fractions by gel-based ABPP with HT-01. We confirmed that treatment with KT109 but not KT195 blocked HT-01 labeling of recombinant DAGLβ overexpressed-HEK293T membrane proteomes (**Figure 3.8a**). We also demonstrated that recombinant DAGLβ showed robust hydrolysis of a fluorogenic lipase substrate compared with non-transfected mock samples and this catalytic activity could be blocked by >80% with KT109 but not KT195 pretreatment (EnzChek™, **Figure 3.8b** and **Figure 3.9**).

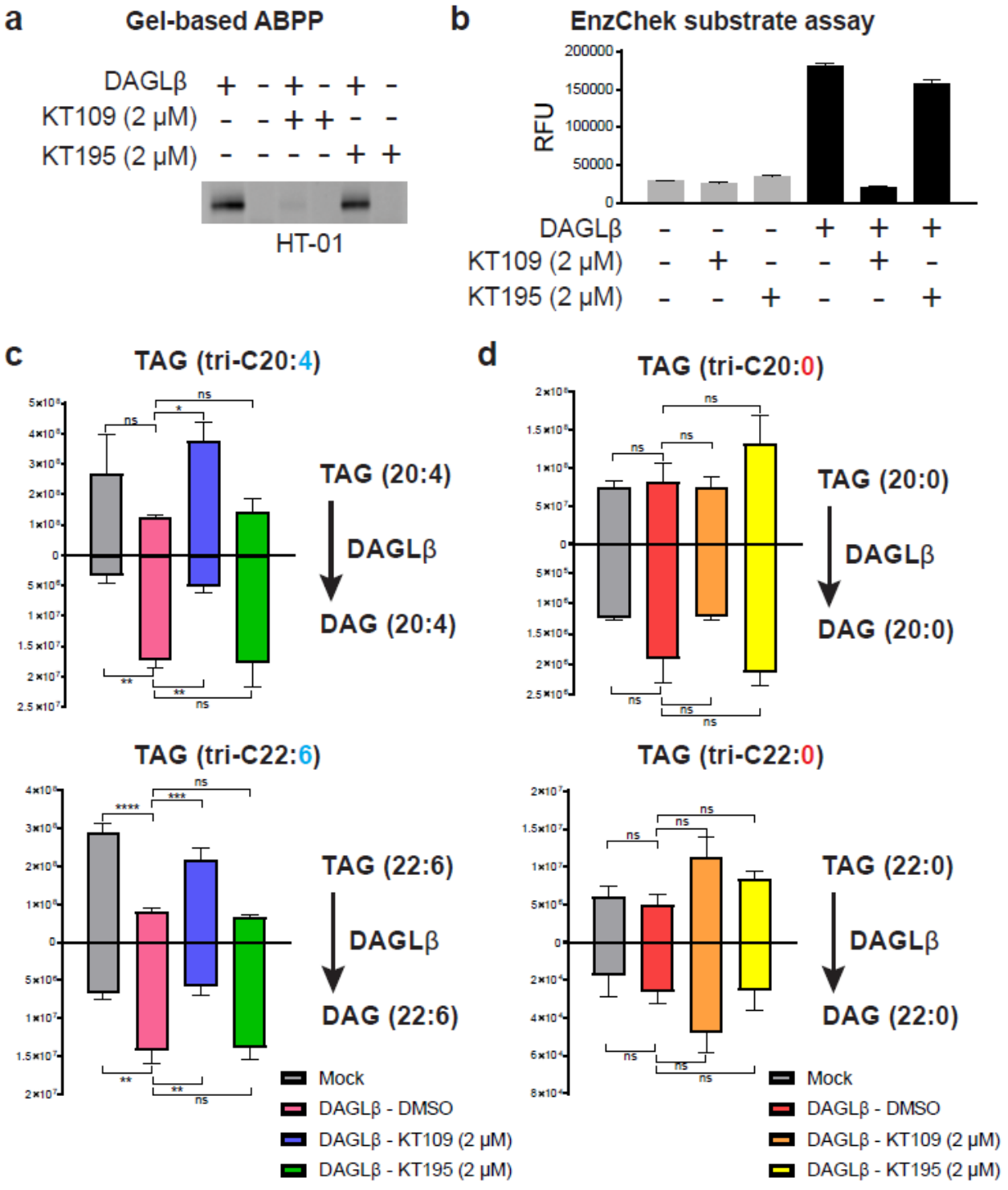

Figure 3.8 Biochemical validation of PUFA-TAGs as authentic DAGLβ substrates. a) Gel-based ABPP analyses confirmed recombinant mouse DAGLβ overexpressed in HEK293T membrane proteomes was active as judged by HT-01 probe labeling (1 μM probe, 30 min, 37°C) that could be blocked *in vitro* by KT109 but not KT195 (2 μM inhibitor, 30 min, 37°C). b) A fluorogenic lipase substrate assay (EnzChek™) was used to confirm recombinant DAGLβ was catalytically active (*n*=4 biological samples). A micelle-based substrate assay was used to

evaluate PUFA- (tri-C20:4 and -C22:6) and matching saturated-TAGs (tri-C20:0 and -C22:0) as substrates for recombinant DAGLβ (*n*=3 biological samples). Recombinant DAGLβ-HEK293T membrane proteomes were incubated with TAG substrates and TAG hydrolysis activity was monitored by targeted LC-MS on a Q-Exactive Plus mass spectrometer configured for parallel reaction monitoring (PRM) of lipid substrate and product abundances. Recombinant DAGLβ efficiently hydrolyzed PUFA-TAGs c) but not saturated TAG counterparts d). Statistical significance was determined using One-Way ANOVA with Holm-Sidak correction; * = $p < 0.05$, ** = $p < 0.01$, *** = $p < 0.001$, **** = $p < 0.0001$. All data shown represent mean ± s.e.m. and are representative of two independent experiments (*n*=2 biologically independent experiments).

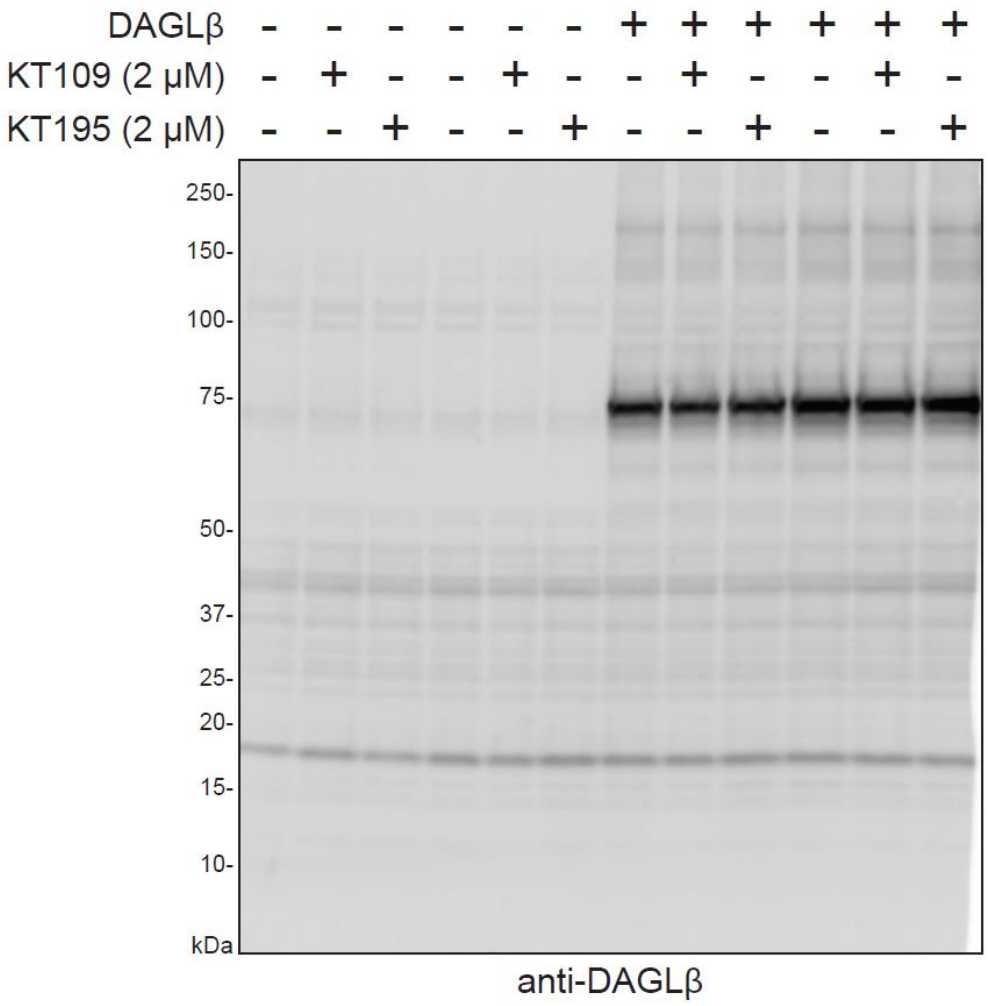

Figure 3.9 Western blot analysis of recombinant DAGLβ expression in HEK293T proteomes. Western blot showed reproducible transient overexpression of recombinant mouse DAGLβ in HEK293T cells (anti-DAGLβ antibody). Treatment of recombinant DAGLβ-HEK293T membrane proteomes with compounds (2 μM of KT109 or KT195, 30 min, 37°C) did not affect expression levels of recombinant DAGLβ protein compared with vehicle controls.

Next, we tested whether recombinant DAGLβ could hydrolyze synthetic TAG substrates and if this lipase showed substrate preference based on fatty acyl composition. We compared saturated and unsaturated TAG pairs to directly test the importance of FA unsaturation on TAG lipase activity of recombinant DAGLβ. Incubation of recombinant DAGLβ membrane proteomes with triarachidonin (C20:4 FA) or tridocosahexaenoin (C22:6 FA) resulted in robust hydrolysis activity that could be blocked with KT109 but not KT195 pretreatment, which supports DAGLβ-specific activity (**Figure 3.8c**). The saturated TAG counterparts (C20:0 and C22:0 FA) were not hydrolyzed by DAGLβ to any appreciable degree (**Figure 3.8d**). In summary, our findings support DAGLβ as a TAG lipase with specificity for lipid species containing PUFAs.

3.5 *Discussion*

Assigning substrate specificity to lipid enzymes *in vivo* is challenging but key to understanding cell metabolism and signaling[19]. Here, we apply chemical proteomics and metabolomics to assign a PUFA-specific triacylglycerol lipase activity for DAGLβ in primary macrophages. Combined with previous reports that DAGLβ can regulate cellular DAG levels[7], our current findings describe DAGLβ as a TAG/DAG lipase that can remodel lipidomes to support the metabolic and signaling demands of macrophages.

We employed untargeted MS-metabolomics and ABPP-SILAC to discover a striking metabolic phenotype in DAGLβ-inactivated primary macrophages that is characterized by accumulation of a minor subset of TAGs that are composed of PUFA chains. Our findings agree with previous studies that showed negligible TAG lipase activity of DAGLβ against mono-unsaturated TAG substrates[3] (**Figure 3.2b**). Instead, we demonstrated using both genetic and pharmacological approaches that DAGLβ blockade results in cellular accumulation of PUFA-TAGs while saturated and low unsaturated counterparts (<3 unsaturation units) remain largely unchanged (**Figure 3.2c** and **Figure 3.6a**). The integration of pharmacological and genetic disruption models was important to provide evidence in support of direct DAGLβ-specific effects on TAG metabolism given that long-term loss of protein could result in network wide compensation. To validate PUFA-TAGs as authentic substrates, we performed biochemical assays to show DAGLβ hydrolyzed PUFA-TAG but not saturated FA counterparts, which further supports its unique specificity for TAG substrates (**Figure 3.8c** and **Figure 3.8d**).

Our analysis of relative lipid abundances showed that the majority of TAG species found in BMDMs were composed of saturated/low unsaturated FAs (<3 unsaturation units) and that PUFA-TAGs represented a low abundance subset. The differences in lipid abundances based on FA composition was not a general phenomenon in BMDMs because PC, PS, and PE showed more equivalent distribution between PUFA- and saturated-lipid species (**Figure 3.7**). Thus,

DAGLβ disruption is not likely to result in general TAG accumulation as observed for adipose triglyceride lipase (ATGL)[20], which can lead to metabolic disorders[21]. The ability of DAGLβ to hydrolyze DAGs and TAGs in macrophages suggests a broader role of this enzyme in neutral lipid metabolism and provides a potential connection between endocannabinoid and bioenergetic pathways. Future studies will include determination of whether DAGLβ is involved in regulation of lipolysis and bulk fatty acid catabolism[22].

In conclusion, our findings illustrate the utility of unbiased global metabolomics to assign unique substrate specificities of enzymes in living systems. DAGLβ has emerged as a promising target for attenuating innate immune activation in animal models of pain and (neuro)inflammation[6,23,24] and our results reveal additional lipid substrates regulated by this enzyme to mediate the metabolic and signaling functions of immune cells.

3.6 *Acknowledgments*

We thank Mark Ross and all members of the Hsu Lab for helpful discussions. This work was supported by the University of Virginia (start-up funds to K.-L.H.) and National Institutes of Health (DA035864 and DA043571 to K.-L.H.; GM801868 to T.B.W.).

Author Contributions

Conceptualization, M.S. and K.-L.H.; Methodology, M.S. and K.-L.H.; Investigation, M.S. and T.B.W.; Validation, M.S., T.B.W., and K.-L.H., Writing – Original Draft, M.S. and K.-L.H.; Writing – Review and Editing, M.S., T.B.W., and K.-L.H.; Funding Acquisition, K.-L.H.; Supervision, K.L.H.

3.7 *References*

1 Gao, Y. *et al.* Loss of Retrograde Endocannabinoid Signaling and Reduced Adult Neurogenesis in Diacylglycerol Lipase Knock-out Mice. *J Neurosci* **30**, 2017-2024, doi:10.1523/JNEUROSCI.5693-09.2010 (2010).

2 Tanimura, A. *et al.* The endocannabinoid 2-arachidonoylglycerol produced by diacylglycerol lipase alpha mediates retrograde suppression of synaptic transmission. *Neuron* **65**, 320-327, doi:10.1016/j.neuron.2010.01.021 (2010).

3 Bisogno, T. *et al.* Cloning of the first sn1-DAG lipases points to the spatial and temporal regulation of endocannabinoid signaling in the brain. *J Cell Biol* **163**, 463-468, doi:10.1083/jcb.200305129 (2003).

4 Long, J. Z. & Cravatt, B. F. The metabolic serine hydrolases and their functions in mammalian physiology and disease. *Chem Rev* **111**, 6022-6063, doi:10.1021/cr200075y (2011).

5 Ogasawara, D. *et al.* Rapid and profound rewiring of brain lipid signaling networks by acute diacylglycerol lipase inhibition. *Proc Natl Acad Sci U S A* **113**, 26-33, doi:10.1073/pnas.1522364112 (2016).

6 Viader, A. *et al.* A chemical proteomic atlas of brain serine hydrolases identifies cell type-specific pathways regulating neuroinflammation. *eLife* **5**, e12345, doi:10.7554/eLife.12345 (2016).

7 Hsu, K. L. *et al.* DAGLbeta inhibition perturbs a lipid network involved in macrophage inflammatory responses. *Nat Chem Biol* **8**, 999-1007, doi:10.1038/nchembio.1105 (2012).

8 Shin, M., Buckner, A., Prince, J., Bullock, T. N. J. & Hsu, K. L. Diacylglycerol Lipase-beta Is Required for TNF-alpha Response but Not CD8(+) T Cell Priming Capacity of Dendritic Cells. *Cell Chem Biol* **26**, 1036-1041 e1033, doi:10.1016/j.chembiol.2019.04.002 (2019).

9 Lee, H. C. & Yokomizo, T. Applications of mass spectrometry-based targeted and non-targeted lipidomics. *Biochem Biophys Res Commun* **504**, 576-581, doi:10.1016/j.bbrc.2018.03.081 (2018).

10 Baggelaar, M. P. *et al.* Highly Selective, Reversible Inhibitor Identified by Comparative Chemoproteomics Modulates Diacylglycerol Lipase Activity in Neurons. *J Am Chem Soc* **137**, 8851-8857, doi:10.1021/jacs.5b04883 (2015).

11 Serbulea, V. *et al.* Macrophage phenotype and bioenergetics are controlled by oxidized phospholipids identified in lean and obese adipose tissue. *Proc Natl Acad Sci U S A* **115**, E6254-E6263, doi:10.1073/pnas.1800544115 (2018).

12 Niphakis, M. J. & Cravatt, B. F. Enzyme Inhibitor Discovery by Activity-Based Protein Profiling. *Annual Review of Biochemistry* **83**, 341-377, doi:doi:10.1146/annurev-biochem-060713-035708 (2014).

13 Folch, J., Lees, M. & Sloane Stanley, G. H. A simple method for the isolation and purification of total lipides from animal tissues. *J Biol Chem* **226**, 497-509 (1957).

14 Taguchi, R., Nishijima, M. & Shimizu, T. in *Methods in Enzymology* Vol. Volume 432 185-211 (Academic Press, 2007).

15 Mann, M. Functional and quantitative proteomics using SILAC. *Nat Rev Mol Cell Biol* **7**, 952-958, (2006).

16 Rostovtsev, V. V., Green, L. G., Fokin, V. V. & Sharpless, K. B. A Stepwise Huisgen Cycloaddition Process: Copper(I)-Catalyzed Regioselective “Ligation” of

Azides and Terminal Alkynes. *Angewandte Chemie International Edition* **41**, 2596-2599, doi:10.1002/1521-3773(20020715)41:14<2596::aid-anie2596>3.0.co;2-4 (2002).

17 Haemmerle, G. *et al.* Defective lipolysis and altered energy metabolism in mice lacking adipose triglyceride lipase. *Science* **312**, 734-737, doi:10.1126/science.1123965 (2006).

18 Inloes, J. M. *et al.* The hereditary spastic paraplegia-related enzyme DDHD2 is a principal brain triglyceride lipase. *Proc Natl Acad Sci U S A* **111**, 14924-14929, doi:10.1073/pnas.1413706111 (2014).

19 Saghatelian, A. *et al.* Assignment of endogenous substrates to enzymes by global metabolite profiling. *Biochemistry* **43**, 14332-14339, doi:10.1021/bi0480335 (2004).

20 Chandak, P. G. *et al.* Efficient phagocytosis requires triacylglycerol hydrolysis by adipose triglyceride lipase. *J Biol Chem* **285**, 20192-20201, doi:10.1074/jbc.M110.107854 (2010).

21 Haemmerle, G. *et al.* ATGL-mediated fat catabolism regulates cardiac mitochondrial function via PPAR-alpha and PGC-1. *Nat Med* **17**, 1076-1085, doi:10.1038/nm.2439 (2011).

22 Zechner, R. *et al.* FAT SIGNALS--lipases and lipolysis in lipid metabolism and signaling. *Cell metabolism* **15**, 279-291, doi:10.1016/j.cmet.2011.12.018 (2012).

23 Shin, M. *et al.* Liposomal Delivery of Diacylglycerol Lipase-Beta Inhibitors to Macrophages Dramatically Enhances Selectivity and Efficacy in Vivo. *Mol Pharm* **15**, 721-728, doi:10.1021/acs.molpharmaceut.7b00657 (2018).

24 Wilkerson, J. L. *et al.* Diacylglycerol lipase beta inhibition reverses nociceptive behaviour in mouse models of inflammatory and neuropathic pain. *Br J Pharmacol* **173**, 1678-1692, doi:10.1111/bph.13469 (2016).

Chapter 4. Elucidating Orthogonal Neuroinflammatory Signaling Pathways Attenuated by Diacylglycerol Lipase Beta Activity in Macrophages

In progress: Timothy B. Ware, Myungsun Shin, Clint Upchurch, Giulia Donvito, Norbert Leitinger, Aron H. Lichtman, Ku-Lung Hsu.

4.1 *Abstract*

Here we apply quantitative chemical proteomics using activity-based protein profiling (ABPP) to identify a signaling relationship between diacylglycerol lipase beta (DAGLβ) and 5'-adenosine monophosphate protein kinase (AMPK) in proinflammatory macrophages. Specifically, in DAGLβ-KO bone marrow-derived macrophages (BMDMs) we observe elevations in AMPK phosphorylation at a canonical activation threonine residue. We demonstrate using DAGLβ-selective inhibitors that the positive regulatory effect on AMPK activation displayed following genetic deletion of DAGLβ is conserved following solely loss of its catalytic activity. Surveying of macrophage metabolic capacity in DAGLβ-disrupted BMDMs using extracellular flux analysis further supports a relationship with AMPK signaling due to its designation as a central energy homeostasis enzyme. Moreover, *in vivo* DAGLβ KO mouse models, which display antinociceptive phenotypes can have this behavior attenuated following AMPK activity perturbation. In summary, our findings strongly implicate AMPK as an orthogonal signaling pathway influenced by DAGLβ activity, offering explanations to idiosyncrasies in signaling effects previously observed in DAGLβ-disrupted models.

4.2 *Introduction*

In response to tissue damage, proinflammatory signals (lipids or cytokines) are released by injured cells and initiate cell-based adaptative and innate immunity mechanisms to protect the host[1]. The activation of these innate immune cells results in a series of immunomodulatory cascades that triggers additional inflammation and the stimulation of nearby nerves, eliciting pain[2]. One of these cascades involves the production of proinflammatory eicosanoid (i.e., prostaglandin) lipids while another cascade centers around the transcription of proinflammatory genes key to cytokine expression[3,4]. Current pharmacological interventions either work at the site of trauma (i.e., non-steroidal anti-inflammatory drugs, NSAIDs) or in the transmission of resulting pain responses (i.e., opioids). However, none of these therapies provide efficacious long-term treatment as the eventual drug tolerance that builds elicits adverse side effects ranging from chronic disease to addiction[5,6]. What is desperately needed is a therapy that displays efficacy in not only thwarting inflammatory signaling, but also relieving pain without consequence over long periods of exposure.

DAGLβ is an enzyme that directly attenuates eicosanoid production through the hydrolysis of diacylglycerol (DAG) lipids upstream of the prostaglandin synthetic pathway[7]. Specifically, DAGLβ exhibits preferential production of arachidonic acid (AA)-esterified MAG pools (i.e., 2-arachidonoyl glycerol, 2-AG) triggering endocannabinoid receptor activation as well as promoting eicosanoid production and therefore proinflammatory signaling[8]. Inhibition of DAGLβ has been found to be efficacious in promoting antinociception sourced through either inflammatory (acute) or neuropathic (chronic) pain models[9,10]. Moreover, long-term DAGLβ inhibitor exposure does not produce characteristic metabolic, behavioral, or addictive side effects[9]. A critical gap in our understanding, however, is how DAGLβ likely attenuates cytokine production as evidence strongly suggests that its role in eicosanoid production does not explain its pain-relieving effects

in chronic pain as NSAIDs, which also target eicosanoid production, are often ineffective in these same chronic models[9,11].

Here, we employed global activity-based protein profiling (ABPP) chemical proteomics to survey orthogonal signaling pathways influenced by genetic disruption of diacylglycerol lipase beta (DAGLβ) in primary macrophages. Our ABPP analysis identified upregulation of 5' adenosine monophosphate-activated protein kinase (AMPK) along with attenuation of several AMPK downstream protein targets. Recapitulation of genetic disruption models with small molecule inhibition of DAGLβ supports direct crosstalk between endocannabinoid biosynthetic and bioenergetic pathways through increases in AMPK phosphorylation and activity. Further support of DAGLβ-mediated AMPK activation was confirmed by demonstrating changes in macrophage glycolytic and oxidative phosphorylation capacity upon DAGLβ inactivation and the ability to reverse antinociception *in vivo* in mice treated with AMPK inhibitors. Collectively, our findings describe a signaling relationship between DAGLβ and AMPK pathways culminating in anti-inflammatory signaling that could be of future therapeutic relevance.

4.3 *Materials and Methods*

Mice. All studies were conducted in 6-12-week-old C57BL/6J, DAGLβ, and DAGLα mice. Mice were housed in the MR6 animal facility (UVa), and Gilmer animal facility (UVa). All studies were carried out under a protocol approved by the ACUC/University of Virginia. All animals were allowed free access to a standard chow diet and water. The animals were housed according to the ACUC policy on social housing of animals. For experiments involving BMDMs, both male and female mice were used in performing described work. Each experiment was controlled by using same-sex littermates.

Bone Marrow Derived Macrophages (BMDMs) differentiation. BMDMs from C57BL/6J or DAGLβ genotype mice were prepared as previously described (see **3.3 *Materials and Methods*** for additional details).

Reagents. Unless otherwise specified, reagents used were purchased from Fisher Scientific. 2-Mercaptoethanol (Sigma-Aldrich) catalog# M6250-250ML. KT109 (synthesized in house), KT195 (Cayman Chemical Company) catalog# 14818. Anti-AMPKα antibody produced in rabbit (Cell Signaling Technology) catalog# 2603S, anti-phospho-AMPKα Thr172 antibody produced in rabbit (Cell Signaling Technology) catalog# 2535S, goat anti-rabbit DyLight 550 (Thermo Fisher Scientific) catalog# 84541. Fetal bovine serum (FBS) and dialyzed FBS were obtained from Omega Scientific. Lipopolysaccharide from *E. coli* (strain O111:B4) was purchased from Sigma-Aldrich (catalog# L2630).

Western Blot Analysis. Cell lysates were separated via centrifugation at 100,000 x g for 45 min at 4°C. Proteins separated by SDS-PAGE (7.5% polyacrylamide, TGX Stain-Free Mini Gel) at 150 V for 55 min. Gel transfers were performed using the Bio-Rad Trans-Blot Turbo RTA Midi Nitrocellulose Transfer Kit with a Bio-Rad Trans-Blot Turbo Transfer System (25V, 10 min). The nitrocellulose blot was then incubated in blocking solution (30 mL, 3% BSA in TBS-T (1.5 M NaCl, 0.25 M Tris pH 7.4 in ddH_2O)) for 1 h at 25°C with gentle shaking. The blot was then transferred

immediately to primary antibody solution (1:1,000 anti-AMPKα or 1:1,000 pAMPKα Thr172) and incubated overnight at 4°C with gentle shaking. The blot was then rinsed 5 times for 5 min in TBS-T, transferred immediately into secondary antibody solution (1:10,000 goat anti-rabbit DyLight 550 in TBS-T), and incubated for 1 h at 25°C with gentle shaking. The blot was then rinsed 5 times for 5 min in TBS-T, transferred into ddH_2O, and imaged by in-blot fluorescence scanning on a ChemiDoc MP Imaging System.

Sample preparation for gel-based competitive activity-based protein profiling (ABPP). Cell pellets were processed using dounce homogenizer. Supernatant was isolated and centrifuged at 100,000 x g for 45 min. Resulting supernatant fraction and resuspended pellet solution were referred as soluble and membrane fraction, respectively. Proteomes (1 mg mL^{-1}) were treated with HT-01 probe at 1 µM final concentration for 30 min at 37°C. The reaction was quenched using SDS-PAGE loading buffer. After separation by SDS-PAGE (10% acrylamide), samples were visualized by in-gel fluorescence scanning using ChemiDoc MP imaging system (Bio-Rad).

Sample preparation for quantitative LC-MS/MS analysis using ATP acyl phosphate probes. Cell lysates used for LC-MS/MS analysis were prepared as previously described (see **2.3 *Materials and Methods*** for additional details).

Sample preparation for quantitative LC-MS/MS analysis using Fluorophosphonate probes. Membrane fraction cell lysates used for LC-MS/MS analysis were prepared as previously described (see **3.3 *Materials and Methods*** for additional details).

Mouse TNFα ELISA screening. DAGLβ WT and KO BMDMs were cultured and differentiated as described above. 100,000 cells/mL were seeded on a 96-well plate in 200 µL of differentiation (L929) media and treated with PBS or 100 ng/mL LPS at 37°C. Supernatant was collected at 1, 2, 4, 6, 16, and 20 h for analysis of TNFα secretion using a mouse TNFα DuoSet ELISA kit (R&D Systems).

Extracellular Flux analysis (Glycolytic Stress Test). Extracellular flux analysis was performed as previously described[12]. In brief, 100,000 cells/mL were seeded into a Seahorse 96-well tissue culture plate (Agilent Technologies). The cells adhered for a minimum of 1 h before treatment. For assessing the glycolytic capacity of the cells, a glycolytic stress test (GST) was performed to measure ECAR, representing the secretion of lactate into the extracellular media. The media used for the GST consisted of unbuffered, glucose-free DMEM; Sigma-Aldrich Cat#: D5030; pH = 7.35 at 37°C; supplemented with 143 mM NaCl and 2 mM glutamine. After three basal ECAR measurements, compounds to modulate glycolysis [20 mM Glucose; 1 µM Oligomycin; 80 mM 2-Deoxyglucose (Sigma-Aldrich)] were injected after every four measurements and ECAR was measured using 12 min measurement periods. Basal glycolysis was calculated by subtracting the average of the post–2-Deoxyglucose measurements from the average of the post-Glucose measurements. Glycolytic capacity was calculated by subtracting the average of the post–2-Deoxyglucose measurements from the average of the post-Oligomycin measurements.

Behavior assessment of animal nociception (mechanical allodynia). Mice were given an injection of 2 µg LPS from Escherichia coli (0111:B4, Sigma-Aldrich), in 20 µL of physiological sterile saline (Hospira Inc., Lake Forest, IL, USA) into the plantar surface of the right hind paw. As previously reported, this is the minimally effective dose of LPS that elicits mechanical allodynia but producing measurable increases in paw thickness[13]. Mice were returned to their home cages after LPS injection for 22 h before all experiments were commenced. Baseline responses to light mechanical touch were assessed using the von Frey test following habituation to the testing environment. In brief, mice were placed atop a wire mesh screen, with spaces 0.5 mm apart, and habituated for approximately 30 min·day^{-1} for 4 days. Mice were unrestrained and were singly placed under an inverted wire mesh basket to allow for unrestricted air flow. The von Frey test utilizes a series of calibrated monofilaments, (2.83–4.31 log stimulus intensity; North Coast Medical, Morgan Hills, CA, USA) applied randomly to the left and right plantar surfaces of the hind

paw for 3s. Lifting, licking, or shaking the paw was considered a response. For all behavioral testing, threshold assessment was performed in a blinded fashion.

4.4 *Results*

4.4.1 *Chemoproteomic Profiling of DAGLβ-Disrupted Systems Reveals Orthogonal Signaling Networks*

We employed a tandem liquid chromatography-mass spectrometry (LC-MS/MS) platform coupled with ABPP for comparing enzyme activities between BMDM cell populations dependent on the presence or absence of DAGLβ. We reasoned that genetic knockout of key immunomodulatory metabolic enzymes in primary macrophages would reveal functional changes in inflammatory signaling that could be captured by chemical proteomics. Bone marrow monocytes were harvested from DAGLβ WT or KO mice and differentiated into BMDMs[12] (see **4.3 *Materials and Methods*** for additional details). For these LC-MS/MS studies, quantitation was achieved by generation of SILAC primary BMDMs as previously described[14].

We treated BMDM proteomes (light – wild-type; heavy – DAGLβ knockout) with the serine hydrolase-directed fluorophosphonate (FP)-alkyne probe[15] to evaluate activity of ~55 detected serine hydrolases using chemical proteomics (**Table 4.1**). Notably, apart from the absence of DAGLβ labeling in the KO BMDM cohort, the only other substantial change in enzyme activity was the downregulation of fatty acid synthase (FASN, **Figure 4.1a**). FASN is a complex homodimer enzyme responsible for the de novo biosynthesis of long-chain fatty acids, but most importantly the formation of palmitate (C16:0), from acetyl-CoA and malonyl-CoA using NADPH[16]. As such, one would expect DAGLβ and FASN to be inversely correlated since both promote either the release or formation of free fatty acids, respectively. However, we observed a potential dependent-based relationship between the two enzymes that becomes more apparent with subsequent investigations into global protein signaling.

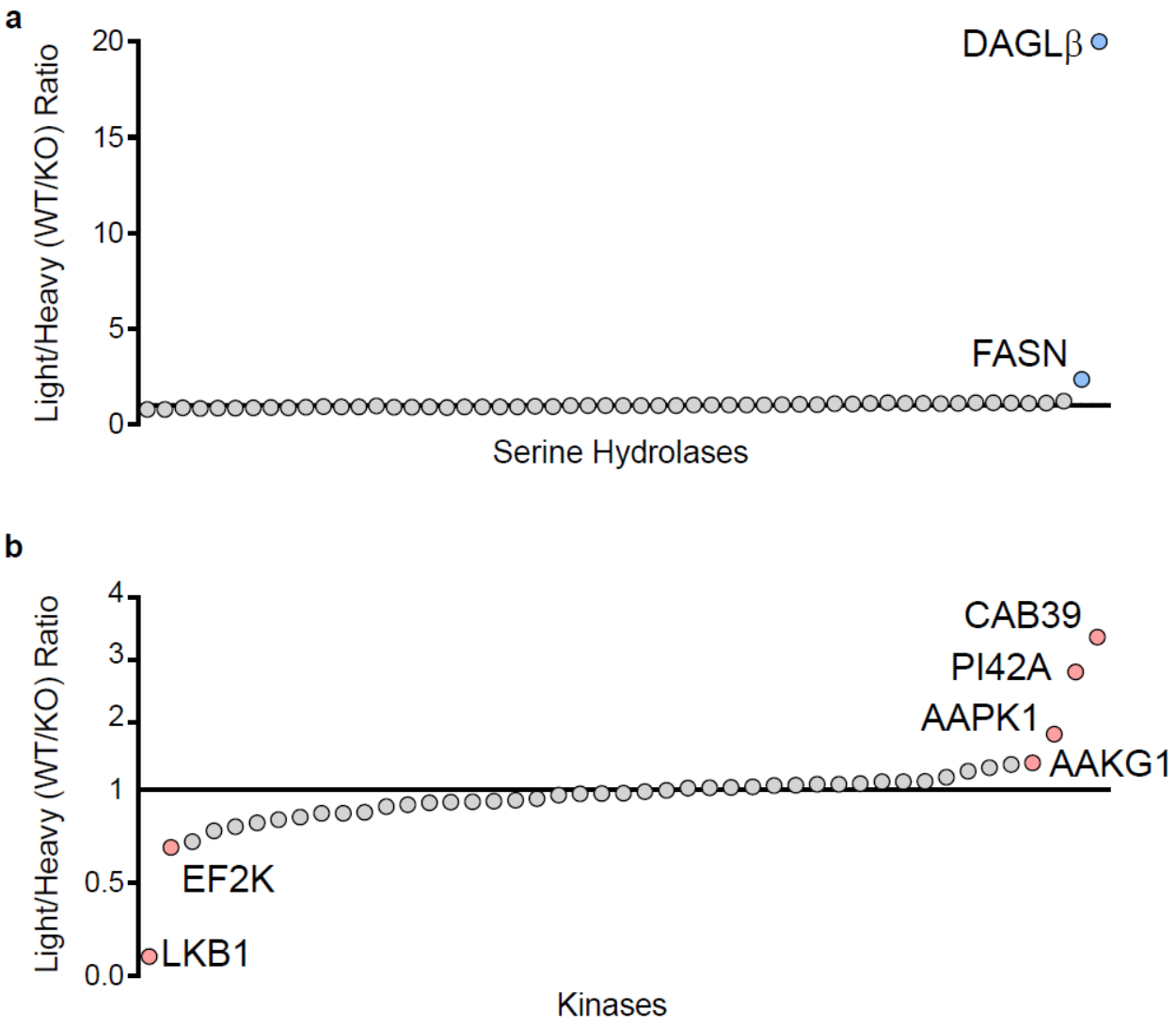

Figure 4.1 Global activity-based profiling of DAGLβ BMDM proteomes in SILAC. a) Chemical proteomics using FP-alkyne probe was performed to map probe-binding sites of serine hydrolase proteins. SILAC light/heavy peptide abundance ratios are calculated from DAGLβ WT (light) and DAGLβ KO (heavy) BMDMs. b) Chemical proteomics using ATP acyl phosphates was performed to map probe-binding sites of kinase proteins. SILAC light/heavy peptide abundance ratios are calculated from DAGLβ KO (light) and DAGLβ WT (heavy) BMDMs. Data shown are representative of two experiments (*n*=2 biologically independent experiments).

In broadening our chemical proteomic investigations into the kinome, we deployed lysine-reactive ATP acyl phosphate probe[17] to profile ~46 kinases (**Table 4.2**) and identified several kinase ATP-binding events (a surrogate for kinase activity)[18] that show DAGLβ expression-dependent regulation (**Figure 4.1b**). Intriguingly, many of the instances involving perturbation of

probe labeling of kinases are centered around 5' adenosine monophosphate-activated protein kinase (AMPK) and specifically, its catalytic α1 (AAPK1) and regulatory γ1 (AAKG1) subunits[19]. Moreover, both an AMPK upstream regulator, liver kinase B1 (LKB1) in complex with calcium-binding protein 39 (CAB39), as well as downstream signaling target, elongation factor-2 kinase (EF2K), were affected by genetic deletion of DAGLβ (**Figure 4.1b**), suggesting disruption of AMPK-related signaling pathways[19,20]. Traditionally AMPK is known to play a critical role in cellular energy homeostasis through sensing and responding to fluctuations in AMP/ATP ratios and as a result, regulates numerous ATP-dependent signaling processes[21]. From our ABPP data we observed fluctuations in probe binding for AAPK1 (SR = 1.9) along with a reported downstream target, elongation factor 2 kinase (EF2K; SR = 0.7) (**Figure 4.1b**). These data support alterations in AMPK activity that combined with the downregulation of FASN may explain the direct relationship it shares with DAGLβ (**Figure 4.1a**). Collectively, our chemical proteomic data strongly implicate an AMPK-centered signaling relationship dependent on DAGLβ expression and catalytic activity.

4.4.2 *Genetic and Pharmacological Inactivation of DAGLβ Activates AMPK*

Our chemical proteomic analyses suggest that DAGLβ expression negatively affects AMPKα1 activity, in that genetic deletion of DAGLβ results in increased AMPK probe labeling. Given that additional downstream signaling targets of AMPK (e.g., FASN and EF2K) were similarly influenced by *Daglb* deletion (**Figure 4.1a** and **Figure 4.1b**), we hypothesized that this relationship between DAGLβ and AMPK also influences AMPK signaling activity. Considering that DAGLβ is a particularly key regulator of inflammatory signaling in macrophages due to its preferential expression amongst the DAGL family[7,14], we proceeded to test our hypothesis using BMDMs in a proinflammatory model.

BMDMs from DAGLβ WT and KO mice were stimulated with lipopolysaccharide (LPS) for 16 h in order to elicit inflammatory signaling processes as reflected in elevated secretions of TNFα cytokine at this time point for both genotypes (**Figure 4.2a** and **Figure 4.2b**). Changes in DAGLβ expression and activity were assessed using western blot analysis and the DAGL-directed activity-based probe (HT-01)[7], respectively. Western blot analysis of these LPS-stimulated BMDMs revealed substantial elevations in threonine 172 (Thr172) phosphorylation (**Figure 4.3a**), which is the canonical activation site for AMPKα catalytic subunit[19], upon genetic knockout of DAGLβ. While total AMPKα expression would be seen to increase following LPS-stimulation (**Figure 4.3a**), phosphorylated Thr172 levels would only increase in systems where DAGLβ was absent. Moreover, these increases in phosphorylated Thr172 levels were sensitive to Dorsomorphin treatment, an AMPK inhibitor[22].

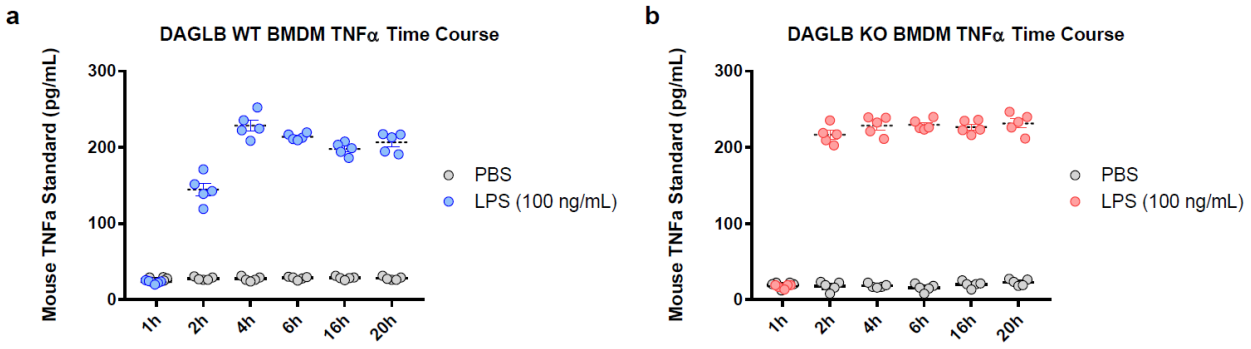

Figure 4.2 Mouse TNFα ELISA time course assayed from LPS-stimulated DAGLβ BMDMs. Assessment of BMDM proinflammatory activation was performed using the R&D Systems mouse TNFα ELISA kit. In brief, BMDMs were cultured in differentiation media (see **4.3 *Materials and Methods*** for additional details) and treated with either phosphate-buffered saline (PBS) or 100 ng/mL LPS over 20 h. Supernatant was then extracted from either a) DAGLβ WT BMDMs or b) DAGLβ KO BMDMs at the reported time points and secreted TNFα measured. All data shown represents mean ± s.e.m.; (*n*=5 biological samples). Data is representative of two experiments (*n*=2 biologically independent experiments).

Next, we tested whether this AMPK signaling effect was solely a consequence of long-term downregulation of DAGLβ activity in the genetic model through employing the DAGLβ-selective inhibitor KT109[7,23]. Again, our western blot analyses reveal total AMPKα expression elevations following LPS-stimulation in DAGLβ WT BMDMs (**Figure 4.3b**). However, interestingly, phosphorylated Thr172 levels would only increase upon KT109 treatment and its resulting DAGLβ inhibition (**Figure 4.3b**). As observed previously (**Figure 4.3a**), these increases in phosphorylated Thr172 levels are Dorsomorphin-sensitive (**Figure 4.3b**) suggesting this signaling event to be specific to AMPK activity.

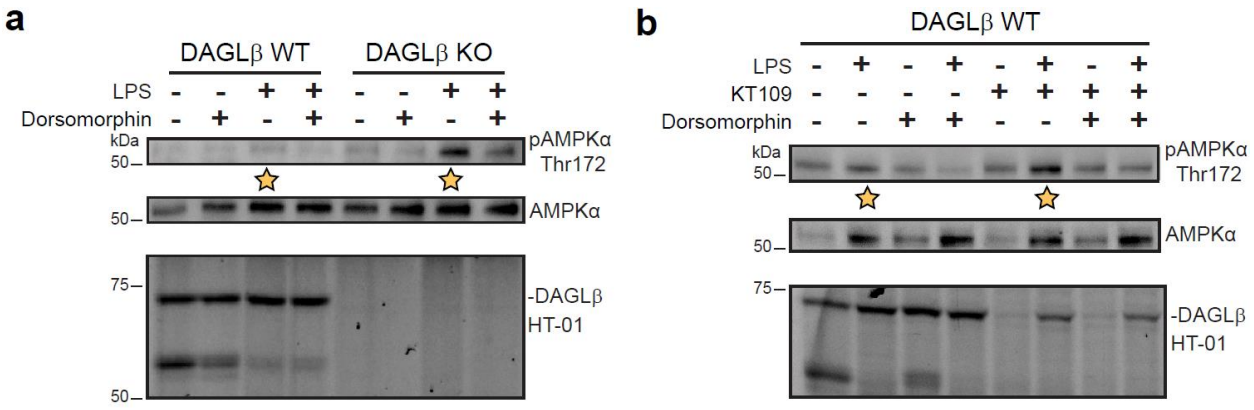

Figure 4.3 DAGLβ disruption positively regulates AMPK phosphorylation in inflammatory signaling. a) DAGLβ WT and KO BMDMs were stimulated with LPS (100 ng/mL, 16 h) and treated *in situ* with Dorsomorphin (10 μM, 4 h). b) DAGLβ WT BMDMs were stimulated with LPS (100 ng/mL, 16 h) and treated *in situ* with KT109 (200 nM, 4 h) and/or Dorsomorphin (10 μM, 4 h). Lysed BMDM membrane proteome was treated with HT-01 probe (1 μM) for 30 mins at 37°C. Soluble fraction of BMDM proteome is used for western blot analysis. Data is representative of three experiments (*n*=3 biologically independent experiments).

In summary, our western blot and small molecule studies support a DAGLβ activity-dependent relationship with AMPK activity in a proinflammatory BMDM system.

4.4.3 *DAGLβ Disruption in Basal Macrophages Promotes Catabolic Bioenergetics*

We next tested if this DAGLβ-AMPK crosstalk influenced cellular energy homeostasis. AMPK activation is initiated by depletion of cellular energy stores (i.e., ATP)[19] and as a result shifts priority from anabolic processes (e.g., fatty acid production, protein biosynthesis, etc.) to catabolic processes (e.g., fatty acid oxidation, glycolysis, etc.)[24]. Specifically, upon activation, AMPK phosphorylates downstream targets acetyl-CoA carboxylase and 6-phosphofructo-2-kianse in order to shut off fatty acid production and promote glycolytic processing, respectively[25,26]. As a result, cells exhibit more aerobic and glycolytic characteristics, becoming more bioenergetic overall. These metabolic homeostasis shifts are even observed in cell systems wherein AMPK has been artificially activated with complex-stimulating compounds[24]. Therefore, we were interested in investigating the physiological ramifications of DAGLβ-mediated AMPK activation on one of its key biological functions, the regulation of cellular energy homeostasis.

Using the Seahorse extracellular flux analyzer system, we could measure extracellular acidification rate (ECAR) due to proton excretion of DAGLβ disrupted BMDMs to interrogate changes in glycolysis[27]. When we measure the glycolytic capacity of basal BMDMs we observe significant elevations in both the stressed and basal ECAR when DAGLβ has been either genetically knocked out ($p < 0.05$) (**Figure 4.4a**). Intriguingly, upon LPS stimulation these metabolic differences exhibited by each respective genotype is lost (**Figure 4.4b**), which is not in agreement with previous observations made where DAGLβ disruption in a proinflammatory state promotes AMPK activity (**Figure 4.3a**). Nonetheless, these metabolic investigations reveal that DAGLβ disruption in BMDMs, at least basally, are more glycolytic in nature, similar to AMPK activated systems[28].

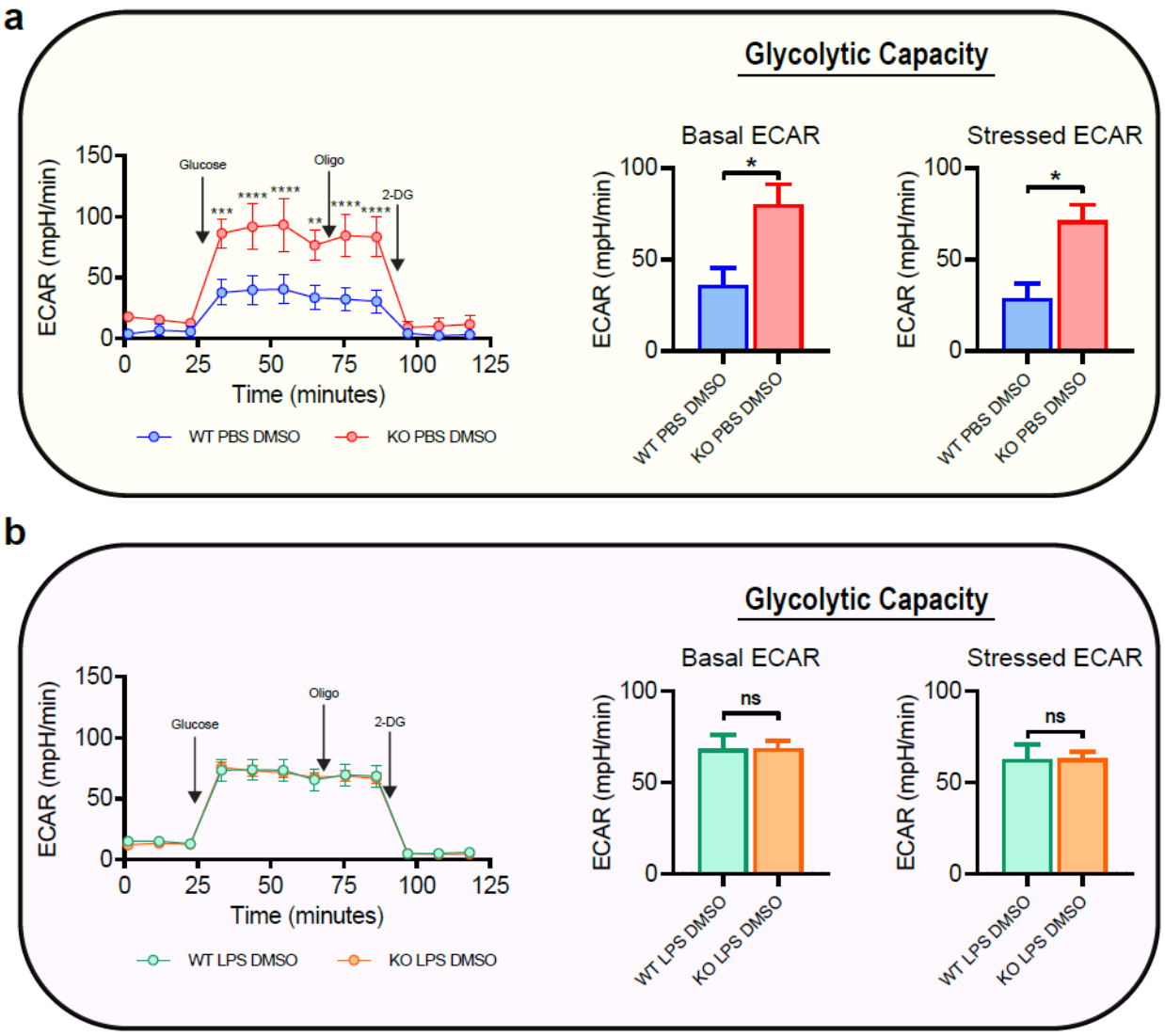

Figure 4.4 Bioenergetics of BMDMs are modulated by DAGLβ disruption. DAGLβ WT and DAGLβ KO BMDMs were analyzed using a Seahorse XF analyzer to interrogate basal and stressed ECAR of cells pretreated with either a) PBS for 16 h or b) 100 ng/mL LPS for 16 h. Extracellular flux analysis experiment proceeded using previously reported conditions (see **4.3 *Materials and Methods*** for additional details). Statistical significance was determined using One-Way ANOVA and Holm-Sidak post-hoc analysis; * = $p < 0.05$, ** = $p < 0.01$, *** = $p < 0.001$, **** = $p < 0.0001$. All data shown represents mean ± s.e.m.; (*n*=2-6 biological samples). All data shown are representative of two experiments (*n*=2 biologically independent experiments).

In summary, our studies involving the interrogation of glycolysis processes within DAGLβ disrupted BMDMs demonstrate close similarities to AMPK activated systems.

4.4.4 *AMPK Activation Contributes to Idiosyncratic Antinociceptive Behavior of DAGLβ KO Mice in an Inflammatory Pain Model*

AMPK activation with AMP analogs (e.g., metformin, AICAR, etc.) is known to be an efficacious therapy for antinociception due to the anti-inflammatory effects of AMPK signaling[29]. Therefore, we set out to investigate whether DAGLβ disruption-mediated AMPK activation could influence nociceptive behavior. DAGLβ WT and DAGLβ KO mice had 2 μg of LPS injected into the intraplantar region of the right hind paw then underwent saline or Dorsomorphin (20 mg kg^{-1}) treatments via intraperitoneal (i.p.) injections daily for five days, followed by a von Frey mechanical allodynia assessment for nociceptive behavior changes (**Figure 4.5a**). Previous reports observe the onset of allodynia following LPS-challenge in the ipsilateral hind paw of LPS-treated DAGLβ WT mice that can be reversed upon KT109 treatment[9]. Intriguingly, DAGLβ KO mice following LPS-challenge do not elicit this same allodynic effect, in fact, they appear to promote antinociception in this inflammatory model[9]. In the present study, we again witness this antiallodynic phenotype in DAGLβ KO mice however, this antinociceptive behavior is reversed upon AMPK inhibition with Dorsomorphin (**Figure 4.5b**).

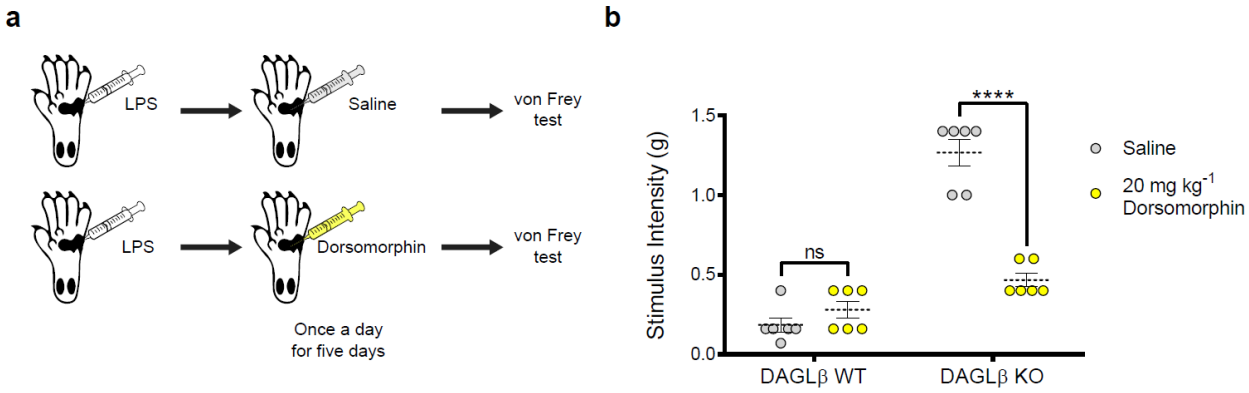

Figure 4.5 DAGLβ-AMPK signaling mediates nociceptive responses in a proinflammatory model. a) Schematic workflow portraying animal nociceptive behavior assessment studies. In brief, DAGLβ WT mice were treated with LPS (2 μg) via intraplantar injection of the right hind paw and then treated with saline or Dorsomorphin (20 mg kg^{-1}) i.p. injections daily for five days. b) Mechanical allodynia via von Frey test was implemented to assess changes in nociceptive behavior as a result of LPS-challenge and Dorsomorphin treatment. Statistical significance was determined using One-Way ANOVA and Holm-Sidak post-hoc analysis; **** = $p < 0.0001$. All data

shown represents mean ± s.e.m.; (*n*=6 mice per condition). All data shown are representative of two experiments (*n*=1 biologically independent experiment).

These nociception behavioral studies suggest that AMPK activation, as a consequence of DAGLβ disruption, influences physiological inflammatory pain sensitization and offers an alternative pathway for leveraging the anti-inflammatory capabilities of AMPK signaling.

4.5 *Discussion*

DAGLs are enzymes that hydrolyze AA-esterified DAGs to biosynthesize 2-AG, an eicosanoid precursor, critical to inflammatory signaling[8]. DAGLβ, in particular, attenuates prostaglandin production in macrophages, cytokine release in dendritic cells, and reverses nociceptive behavior in rodents[7,9,30]. Currently, DAGLβ biological function is ascribed principally to lipid-based signaling however, our findings here describe a complementary kinase-mediated pathway that connects bioenergetics with endocannabinoid biosynthesis as a new mechanism for blockade of inflammation and pain. Here, we apply chemical proteomics, metabolic analysis, and nociceptive behavioral studies, to identify an activity-based relationship between DAGLβ and AMPK in primary macrophages.

We employed ABPP-SILAC with chemical probes that profile serine hydrolases and kinases to identify orthogonal signaling networks perturbed in DAGLβ-disrupted macrophages. Our studies revealed alterations in probe-binding events that were suggestive of alterations in kinase activity. Specifically, we observed upregulation of probe-binding in the catalytic loop of AMPK, but also attenuation of its downstream targets (e.g., EF2K and FASN) (**Figure 4.1a** and **Figure 4.1b**). Western blot analysis of LPS-stimulated macrophages confirmed that alterations in AMPK probe binding resulted in increase in activity as determined by enhanced phosphorylation of T172 in DAGLβ disrupted systems (**Figure 4.3a**). AMPK phosphorylation observed in DAGLβ-KO genetic models were recapitulated using the small molecule inhibitor KT109, which confirms the importance of catalytic activity for DAGLβ-AMPK crosstalk and that the AMPK effects are not due to network wide compensation from long-term DAGLβ blockade in KO systems (**Figure 4.3b**). Altogether, our chemoproteomics and cell biological findings strongly implicate DAGLβ as the initiator of an AMPK-centered signaling cascade, modulating kinase-based pathways.

Since AMPK senses and adjusts cellular energy state, we employed the extracellular flux analyzer to evaluate real-time changes in bioenergetics following DAGLβ disruption. Analysis of

ECAR in DAGLβ KO BMDMs revealed upregulation of glycolysis (**Figure 4.4a**), which is indicative of bioenergetic nature. AMPK activation, in comparison, is characterized by a dynamic shift in metabolic priority from anabolic processes (metabolite biosynthesis) to catabolic processes (i.e., fatty acid oxidation and glycolysis) in order to replenish spent energy stores[21]. Interestingly, glycolytic processes were not elevated in DAGLβ KO BMDMs following LPS stimulation (**Figure 4.4b**) as would be expected based on previous observations (**Figure 4.2a**). However, it is possible that overall toll-like receptor 4 (TLR4) activation following LPS stimulation overrides the metabolic effects generated by AMPK activity as these macrophages begin to polarize towards an M1-state, which is more glycolytic in nature[31]. Collectively, our extracellular flux analysis findings support a DAGLβ-mediated regulation of AMPK activation and signaling *in vivo* due to the shift in metabolic nature of these primary macrophages.

DAGLβ is an efficacious therapeutic target for the alleviation of chronic inflammation and pain[9]. It is suspected that signaling pathways, apart from eicosanoid biosynthesis, contribute to the anti-nociceptive responses of DAGLβ disrupted mammals. DAGLβ KO mouse paws, when stimulated with LPS, demonstrate anti-allodynic effects suggesting uncharacterized regulation of inflammatory pain sensing[9]. However, this idiosyncratic anti-nociception is attenuated following AMPK inhibition with the small molecule Dorsomorphin in this same model (**Figure 4.5b**). Artificial activation of AMPK using AMP analogs and allosteric substrates has been shown to elicit similar anti-inflammatory and pain sensitization effects[32]. Thus, DAGLβ disruption may serve as a promising avenue for leveraging the therapeutic benefits of AMPK activation without dysregulation of additional AMP-sensing systems.

In conclusion, our findings illustrate a putative DAGLβ-dependent orthogonal inflammatory signaling pathway centered around AMPK activation and its downstream signaling effects (**Figure 4.6**). DAGLβ inhibition has demonstrated efficacious reversal of pain signaling and behavior[9] and

our results identify putative signaling pathways which may alter cytokine expression affecting inflammatory signaling over extended periods of time, a hallmark of chronic inflammatory.

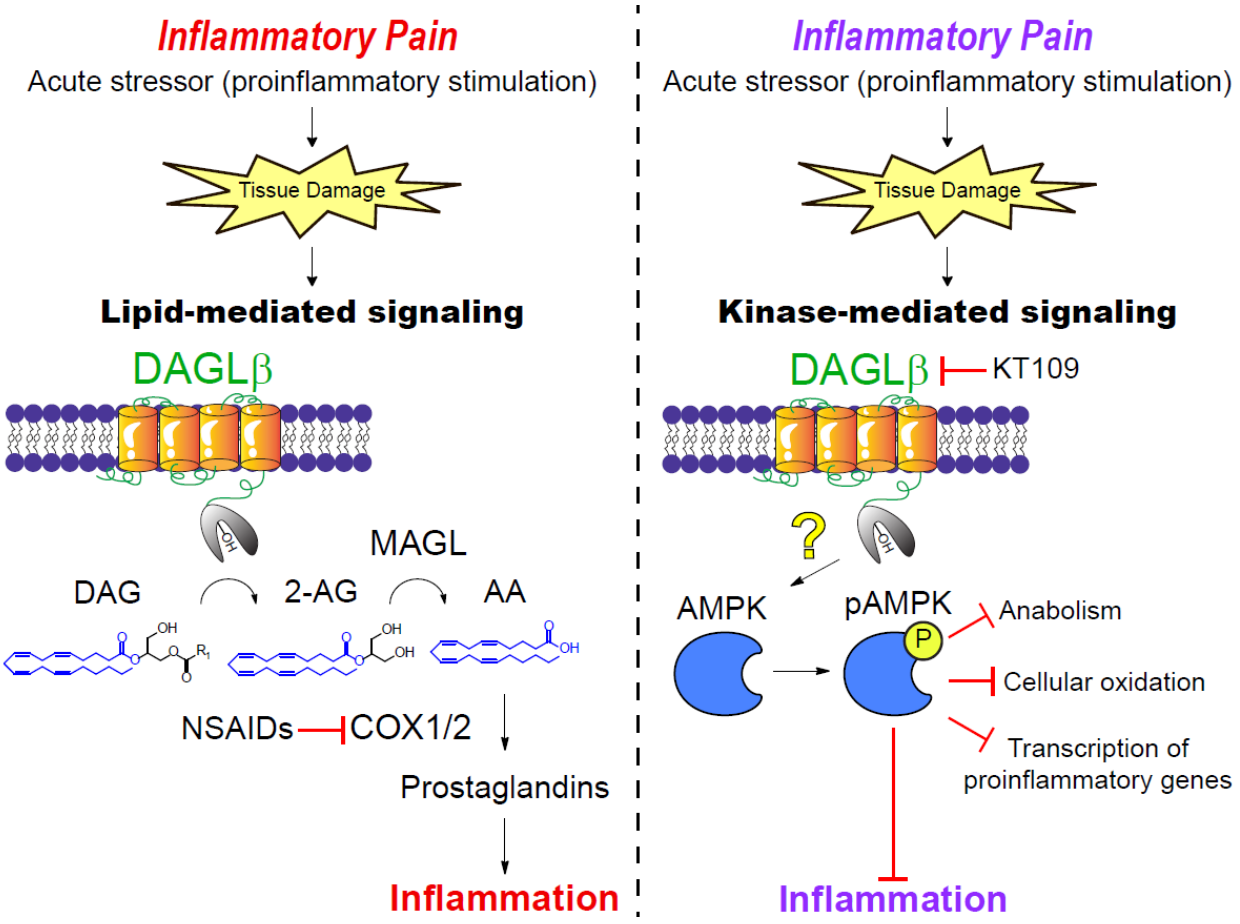

Figure 4.6 Putative Neuroinflammatory Signaling Networks Attenuated by DAGLβ. Pictorial representation of the two mechanism through which DAGLβ regulates inflammatory signaling. The lipid-mediated pathway involves regulation of arachidonic acid-containing DAGs and eventual prostaglandin production. Whereas the kinase-mediated pathway centers around AMPK signaling cascades which become upregulated following DAGLβ disruption.

Uniprot Name	Normalized SILAC Ratio
ESD	0.79
PREP	0.79
APEH	0.87
ACOT6	0.85
PRCP	0.86
DPP7	0.86
SIAE	0.88
PPT2	0.89
ACOT6	0.87
SCPEP1	0.91
ACOT5	0.94
LPL	0.92
AOAH	0.92
ACOT3	0.98
PREP	0.91
PLA2G15	0.91
PGAP1	0.93
SERHL	0.89
ABHD11	0.93
ABHD12	0.93
ABHD13	0.93
ABHD16A	0.93
ABHD10	0.96
APEH	0.95
CTSA	0.99
ABHD12	0.99
LYPLA1	0.99
ACOT1	0.99
NCEH1	1.00
PNPLA7	0.99
LYPLA2	0.99
ACOT5	1.02
ACOT4	1.02
ACOT2	1.02
PNPLA8	1.02
ABHD17B	1.03
ACOT3	1.04
LIPA	1.06
ABHD17B	1.04
PLA2G7	1.10
PAFAH2	1.07
ABHD13	1.11
ABHD11	1.13

PNPLA8	1.11
ACOT4	1.12
PLA2G7	1.09
ABHD16A	1.11
ABHD10	1.14
PGAP1	1.14
PNPLA7	1.12
PNPLA6	1.11
SERHL	1.13
PNPLA6	1.23
FASN	2.35
DAGLB	20.00

Table 4.1 SILAC ratios of enriched serine hydrolase protein IDs detected by LC-MS/MS analysis using the FP-alkyne probe.

Uniprot Name	Peptide Sequence	Normalized SILAC Ratio
STK11	DIKPGNLLLTTNGTLK	0.10
EF2K	YIKYNSNSGFVR	0.69
EF1A1	AAGAGKVTK	0.72
KPCD	KPTMYPEWK	0.78
KCC1A	LVAIKCIAK	0.80
TLK1	YAAVKIHQLNK	0.82
TAOK3	DIKAGNILLTEPGQVK	0.84
BRAF	DLKSNNIFLHEDLTVK	0.85
KCC1D	LFAVKCIPK	0.87
KS6A3	DLKPENILLDEEGHIK	0.87
SGK3	FYAVKVLQK	0.88
KCCG2	TSTQEYAAKIINTK	0.91
IKKB	DLKPENIVLQQGEKR	0.92
KSYK	ADENYYKAQTHGK	0.93
NEK9	DIKTLNIFLTK	0.93
SLK	DLKAGNILFTLDGDIK	0.93
IRAK4	DIKSANILLDK	0.94
MARK1	GNFAKVK	0.94
M3K3	DIKGANILR	0.95
NEK7	ASCLLDGVPVALKK	0.97
PGAM1	AETAAKHGEAQVK	0.98
CDK5	DLKPQNLLINR	0.98
MP2K2	DVKPSNILVNSR	0.98
IRAK3	NQAYAVKLFK	0.99
KSYK	AQTHGKWPVK	1.00
AKT1	GTFGKVILVK	1.01
STK38	DTGHVYAMKILR	1.01
WNK1	IGDLGLATLKR	1.02
ILK	ISMADVKFSFQCPGR	1.03
FER	TPVAIKTCK	1.05
STK10	DLKAGNVLMTLEGDIR	1.05
STK4	DIKAGNILLNTEGHAK	1.07
ROCK1	KLQLELNQER	1.07
BTK	KGSIDVEK	1.08
STK24	DIKAANVLLSEHGEVK	1.11
IRAK3	KHLWYMPEEYIR	1.11
CSK	VSDFGLTKEASSTQDTGK	1.11
E2AK2	DLKPGNIFLVDER	1.18
STRAA	YSIKVLPWLSPEVLQQNLQGYDAK	1.28
PI42C	VKELPTLK	1.34
FES	ADNTPVAVKSCR	1.39

AAKG1	LPVIDPESGNTLYILTHKR	1.41
AAPK1	DLKPENVLLDAHMNAK	1.88
PI42A	ENMPSHFKFK	2.87
CAB39	YISKPENLKLMMNLLR	3.43

Table 4.2 SILAC ratios of enriched kinase probe labeled sites detected by LC-MS/MS analysis using the ATP acyl phosphate probe.

4.6 *Acknowledgments*

We thank Mark Ross and all members of the Hsu Lab for helpful discussions. Operation of the Agilent Seahorse XF analyzer to obtain the data displayed in **Figure 4.3** was performed by Clint Upchurch. Animal nociceptive behavior studies displayed in **Figure 4.5** were conducted at Virginia Commonwealth University in the Lichtman lab by Dr. Giulia Donvito. This work was supported by the University of Virginia (start-up funds to K.-L.H.) and National Institutes of Health (DA035864 and DA043571 to K.-L.H.; DA053107 to T.B.W.).

Author Contributions

Conceptualization, T.B.W., M.S. and K.-L.H.; Methodology, T.B.W., M.S. and K.-L.H.; Investigation, T.B.W. and M.S.; Funding Acquisition, K.-L.H.; Supervision, K.L.H.

4.7 *References*

1 Hamidzadeh, K., Christensen, S. M., Dalby, E., Chandrasekaran, P. & Mosser, D. M. Macrophages and the Recovery from Acute and Chronic Inflammation. *Annu Rev Physiol* **79**, 567-592, doi:10.1146/annurev-physiol-022516-034348 (2017).

2 Bruno, K. *et al.* Targeting toll-like receptor-4 (TLR4)-an emerging therapeutic target for persistent pain states. *Pain* **159**, 1908-1915, doi:10.1097/j.pain.0000000000001306 (2018).

3 Serhan, C. N., Chiang, N. & Van Dyke, T. E. Resolving inflammation: dual anti-inflammatory and pro-resolution lipid mediators. *Nat Rev Immunol* **8**, 349-361, doi:10.1038/nri2294 (2008).

4 Cook, A. D., Christensen, A. D., Tewari, D., McMahon, S. B. & Hamilton, J. A. Immune Cytokines and Their Receptors in Inflammatory Pain. *Trends Immunol* **39**, 240-255, doi:10.1016/j.it.2017.12.003 (2018).

5 Harirforoosh, S., Asghar, W. & Jamali, F. Adverse Effects of Nonsteroidal Antiinflammatory Drugs: An Update of Gastrointestinal, Cardiovascular and Renal Complications. *J Pharm Pharm Sci* **16**, 821-847 (2013).

6 Benyamin, R. *et al.* Opioid Complications and Side Effects. *Pain Physician* **11**, 105-120 (2008).

7 Hsu, K. L. *et al.* DAGLbeta inhibition perturbs a lipid network involved in macrophage inflammatory responses. *Nat Chem Biol* **8**, 999-1007, doi:10.1038/nchembio.1105 (2012).

8 Bisogno, T. *et al.* Cloning of the first sn1-DAG lipases points to the spatial and temporal regulation of endocannabinoid signaling in the brain. *J Cell Biol* **163**, 463-468, doi:10.1083/jcb.200305129 (2003).

9 Wilkerson, J. L. *et al.* Diacylglycerol lipase beta inhibition reverses nociceptive behaviour in mouse models of inflammatory and neuropathic pain. *Br J Pharmacol* **173**, 1678-1692, doi:10.1111/bph.13469 (2016).

10 Wilkerson, J. L. *et al.* The Selective Monoacylglycerol Lipase Inhibitor MJN110 Produces Opioid-Sparing Effects in a Mouse Neuropathic Pain Model. *Journal of Pharmacology and Experimental Therapeutics* **357**, 145-156, doi:10.1124/jpet.115.229971 (2016).

11 Zhao, F. Y., Spanswick, D., Martindale, J. C., Reeve, A. J. & Chessell, I. P. GW406381, a novel COX-2 inhibitor, attenuates spontaneous ectopic discharge in sural nerves of rats following chronic constriction injury. *Pain* **128**, 78-87, doi:10.1016/j.pain.2006.08.032 (2007).

12 Serbulea, V. *et al.* Macrophage phenotype and bioenergetics are controlled by oxidized phospholipids identified in lean and obese adipose tissue. *Proc Natl Acad Sci U S A* **115**, E6254-E6263, doi:10.1073/pnas.1800544115 (2018).

13 Booker, L. *et al.* The fatty acid amide hydrolase (FAAH) inhibitor PF-3845 acts in the nervous system to reverse LPS-induced tactile allodynia in mice. *Br J Pharmacol* **165**, 2485-2496, doi:10.1111/j.1476-5381.2011.01445.x (2012).

14 Shin, M., Ware, T. B. & Hsu, K. L. DAGL-Beta Functions as a PUFA-Specific Triacylglycerol Lipase in Macrophages. *Cell Chem Biol* **27**, 314-321 e315, doi:10.1016/j.chembiol.2020.01.005 (2020).

15 Li, W., Blankman, J. L. & Cravatt, B. F. A functional proteomic strategy to discover inhibitors for uncharacterized hydrolases. *Journal of the American Chemical Society* **129**, 9594-9595, doi:10.1021/ja073650c (2007).
16 Menendez, J. A. & Lupu, R. Fatty acid synthase and the lipogenic phenotype in cancer pathogenesis. *Nat Rev Cancer* **7**, 763-777, doi:10.1038/nrc2222 (2007).
17 Patricelli, M. P. *et al.* Functional interrogation of the kinome using nucleotide acyl phosphates. *Biochemistry* **46**, 350-358, doi:10.1021/bi062142x (2007).
18 Patricelli, M. P. *et al.* In situ kinase profiling reveals functionally relevant properties of native kinases. *Chem Biol* **18**, 699-710, doi:10.1016/j.chembiol.2011.04.011 (2011).
19 Yan, Y., Zhou, X. E., Xu, H. E. & Melcher, K. Structure and Physiological Regulation of AMPK. *Int J Mol Sci* **19**, doi:10.3390/ijms19113534 (2018).
20 McLeod, L. E. & Proud, C. G. ATP depletion increases phosphorylation of elongation factor eEF2 in adult cardiomyocytes independently of inhibition of mTOR signalling. *FEBS Lett* **531**, 448-452 (2002).
21 Hardie, D. G., Ross, F. A. & Hawley, S. A. AMPK: a nutrient and energy sensor that maintains energy homeostasis. *Nat Rev Mol Cell Biol* **13**, 251-262, doi:10.1038/nrm3311 (2012).
22 Yu, P. B. *et al.* Dorsomorphin inhibits BMP signals required for embryogenesis and iron metabolism. *Nat Chem Biol* **4**, 33-41, doi:10.1038/nchembio.2007.54 (2008).
23 Hsu, K. L. *et al.* Discovery and optimization of piperidyl-1,2,3-triazole ureas as potent, selective, and in vivo-active inhibitors of α/ß hydrolase domain containing 6 (ABHD6). *Journal of Medicinal Chemistry* **56**, 8270-8279, doi:10.1021/jm400899c (2013).
24 Herzig, S. & Shaw, R. J. AMPK: guardian of metabolism and mitochondrial homeostasis. *Nat Rev Mol Cell Biol* **19**, 121-135, doi:10.1038/nrm.2017.95 (2018).
25 Carling, D., Zammit, V. A. & Hardie, D. G. A common bicyclic protein kinase cascade inactivates the regulatory enzymes of fatty acid and cholesterol biosynthesis. *FEBS Lett* **223**, 217-222 (1987).
26 Bando, H. *et al.* Phosphorylation of the 6-phosphofructo-2-kinase/fructose 2,6-bisphosphatase/PFKFB3 family of glycolytic regulators in human cancer. *Clin Cancer Res* **11**, 5784-5792, doi:10.1158/1078-0432.CCR-05-0149 (2005).
27 Divakaruni, A. S., Paradyse, A., Ferrick, D. A., Murphy, A. N. & Jastroch, M. Analysis and interpretation of microplate-based oxygen consumption and pH data. *Methods Enzymol* **547**, 309-354, doi:10.1016/B978-0-12-801415-8.00016-3 (2014).
28 Marinangeli, C., Kluza, J., Marchetti, P., Buee, L. & Vingtdeux, V. Study of AMPK-Regulated Metabolic Fluxes in Neurons Using the Seahorse XFe Analyzer. *Methods Mol Biol* **1732**, 289-305, doi:10.1007/978-1-4939-7598-3_19 (2018).
29 Kim, J., Yang, G., Kim, Y., Kim, J. & Ha, J. AMPK activators: mechanisms of action and physiological activities. *Exp Mol Med* **48**, e224, doi:10.1038/emm.2016.16 (2016).
30 Shin, M., Buckner, A., Prince, J., Bullock, T. N. J. & Hsu, K. L. Diacylglycerol Lipase-beta Is Required for TNF-alpha Response but Not CD8(+) T Cell Priming Capacity of Dendritic Cells. *Cell Chem Biol* **26**, 1036-1041 e1033, doi:10.1016/j.chembiol.2019.04.002 (2019).

31 Galvan-Pena, S. & O'Neill, L. A. Metabolic reprograming in macrophage polarization. *Front Immunol* **5**, 420, doi:10.3389/fimmu.2014.00420 (2014).
32 Baeza-Flores, G. D. C. *et al.* Metformin: A Prospective Alternative for the Treatment of Chronic Pain. *Front Pharmacol* **11**, 558474, doi:10.3389/fphar.2020.558474 (2020).

Chapter 5. Conclusions and Future Directions

5.1 *Conclusions and Significance*

The work presented in this dissertation details recent discoveries made concerning the functionality and specificity of DAG metabolizing enzymes. We have employed quantitative metabolomics and protein engineering to acquire insight into the structure-function relationship between DGK superfamily enzymes and DAG substrates. Furthermore, these mass spectrometry technologies used in tandem with DAGLβ genetic models and small molecule inhibitors have revealed its novel functionality as a PUFA-selective TAG lipase in macrophages. Lastly, recent efforts have uncovered a putative connection between DAGLβ activity and AMPK signaling in the regulation of inflammation and animal nociception as a consequence of inflammatory signaling. Since 2016 we have made significant progress towards elucidating the mechanisms controlling DAG-specific signaling effects which in the future may provide a means for researchers to exquisitely attenuate DAG-related signaling effects in human health and disease.

Evolutionary development in mammals has culminated in the constitutive expression of ten DGK isoforms to regulate the phosphorylation of DAG to PA. As such, these enzymes are one of the major pathways through which DAG effector signaling can be shunted, drastically influencing the developmental state of the cell/tissue. While much is currently understood about which DGK isoforms are related to certain disease phenotypes, the specific signals (i.e., lipid molecules) that propagate these effects are lesser known. Since current efforts towards treating dysregulated signaling networks involves small molecule engagement with proteins driving the dysregulation, understanding how these proteins operate is of the upmost importance. However, development of DGK inhibitors has proven challenging due to its sheer diversity in spatiotemporal expression and localization. To complicate matters, these isoforms possess highly conserved catalytic domains with other lipid and protein kinases thereby thwarting conventional drug development attempts as often these regions are selected to obtain drug selectivity and potency.

Early into our investigations we hypothesized that DGK structural diversity would afford it DAG substrate specificity *in vivo* based on interactions between its slightly distinct structural motifs and access to particular DAG pools. The standard from the field used *in vitro* substrate assays to ascertain substate specificity. However, these experiments are limited in both the number of substrates that can be tested as well as how translatable the results are to a native environment. In order to overcome these limitations, we instead employed quantitative LC-MS/MS analysis of native biological systems to investigate the substrate specificity of DGK isoforms. Our work revealed C1 domains as the DAG recognition site of DGK isoforms. While these domains exhibit moderate sequence homology within subtypes (~50-60% identity) they still impart functional specificity against distinct DAG lipids. We ascertained these structure-function relationships through the engineering of first-ever developed C1 chimera DGK proteins, which can serve as a model for future studies assessing functional behavior of other lipid metabolizing proteins.

Apart from investigations into DAG phosphorylation, we were also interested in understanding the role that lipases had in attenuating DAG signaling effects. DAGLs catalyze the hydrolysis of DAG, in a preferential manner, removing *sn*-1 positioned FAs over *sn*-2 positioned FA. This specificity is important as DAGLβ predominately hydrolyses the *sn*-2 arachidonic acid-containing DAGs in liver and immune cells to produce 2-arachidonoylglycerol (2-AG), an endocannabinoid receptor agonist and eicosanoid precursor. It has been demonstrated that pharmacological inhibition of DAGLβ with small molecules produces efficacious anti-inflammatory effects in both acute and chronic models of inflammatory pain by preventing the eventual production of these prostaglandins. However, our current understanding of the endocannabinoid-eicosanoid inflammatory signaling network is unable to explain the antinociceptive behavior we observe in these chronic pain mouse models, suggesting additional immunomodulatory roles for DAGLβ apart from lipid-mediated signaling. In order to reveal these novel relationships, our next

set of investigations centered around identifying these hypothesized orthogonal signaling networks.

We again implemented our metabolomics-based LC-MS/MS platform to profile additional lipid changes in response to DAGLβ disruption through either pharmacological or genetic means in bone marrow derived macrophages (BMDMs). We hypothesized that apart from changes in DAG abundances we would also observe peripheral networks of lipid metabolism being modulated. To accomplish this, we employed untargeted metabolomics-based analyses to measure fluctuations in membrane phospholipid, glycerolipid, sphingolipid, and sterol pools. Interestingly, we discovered that a particular subset of triacylglycerols (TAGs) with polyunsaturated fatty acid (PUFA) (>3 degrees of unsaturation) character accumulated in our DAGLβ-KO BMDMs. Use of DAGLβ-selective inhibitor (KT109) and control (KT195) inhibitors validated our observed lipid metabolism effects as DAGLβ-mediated. Finally, to show that DAGLβ directly acts upon PUFA-TAGs as substrates through a hydrolytic mechanism we developed a biochemical substrate assay in tandem with a LC-MS/MS quantitative readout. We demonstrated that apart from lipids involved in inflammatory signaling (i.e., DAGs, 2-AG, etc.) we discovered a new subset of TAGs modulated by DAGLβ that implicate the enzyme in regulating fatty acid catabolism. Moreover, due to the isomer selectively exhibited by DAGLs for *sn*-1,2 DAGs, these enzymes may function to complement other TAG lipases that exhibit different regioselective preferences, such as ATGL (*sn*-2 selective).

Lastly, using chemical proteomic profiling of DAGLβ BMDMs we uncovered a putative relationship between DAGLβ and AMPK signaling networks. Specifically, we have identified that downregulation of DAGLβ, either genetically or pharmacologically promotes AMPK phosphorylation and hints towards initiating its subsequent signaling effects. In inflammation, AMPK is a well-known upstream regulator of NF-κB proinflammatory cytokine transcription. Artificial activation of AMPK using small molecules (e.g., metformin or AICAR) demonstrates

efficacious downregulation of inflammatory signaling in multiple pain models. Indeed, in our studies we recapitulate this trend wherein idiosyncratic antinociception phenotypes exhibited in DAGLβ-disrupted models can be attenuated by AMPK inhibition. These results offer significant therapeutic implications in the effort of treating chronic pain since current drug therapies (i.e., NSAIDs, opioids) demonstrate adverse side effects following long exposure.

5.2 *Future Directions*

The work presented in this dissertation was the first to identify atypical C1 domains of DGKs as DAG recognition sites. We hypothesized from previous chemical proteomics results a functional role in substrate recognition by C1 domains, as they likely conform around the catalytic regions to form a contiguous active site on DGKs. Our work was limited to investigations involving solely subtype 1 DGK isoforms (α, β, γ). As such, future studies are necessary to ascertain whether C1 domain architecture is similarly crucial to DAG recognition across other DGK superfamily subtypes. Specifically, investigations involving DGKε with its well characterized preference for *sn*-2 arachidonic acid-containing DAGs is a very intriguing option. Much of the literature surrounding this enzyme cites plasma membrane curvature over its own structural uniqueness as a prevailing theory for its observed DAG specificity. A C1 domain chimera protein using DGKε-sourced C1 domains could be generated to test this claim to assess whether the inherent preferences exhibited by DGKε can be transferred to other DGK isoform backbones, which have their own spatiotemporal regulation patterns. Conversely, removing the natural C1 domains of DGKε while preserving its localization to the plasma membrane and therefore access to arachidonic acid-containing DAG pools may reveal a complementary role served by its atypical C1 domains in substrate recognition.

While it can be strongly inferred from annotated DAG synthesis pathways that many of the DGK-accessible DAG pools will be *sn*-1,2 isomers, these studies lack any direct evidence to

suggest their inability to similarly metabolize other regioisomers. To address this concern and identify possible cross reactivity with other DAG isomers, new analytical approaches can be implemented to assess fatty acyl chain position and structure. Use of lipid derivatization methods such as treatment with N,N-dimethylglycine (DMG) to esterify the free hydroxyl group of DAGs has been accomplished in previous studies to improve the ionization efficiency of these lipids by introducing a fixed charge for electrospray ionization. Furthermore, it has been shown that formation of lithiated DMG-DAG adducts for MS analysis can be analyzed via collision induced dissociation to impart *sn* positionality and fatty acyl chain identify of the lipid. Thus, through slight alterations made to the lipid sample preparation and LC-MS/MS analysis workflow, the regioisomer character of DAG metabolism can be quantitatively assessed.

Our characterization of DAGLβ in macrophages revealed its novel functionality as a PUFA-TAG lipase. However, it is not clear whether the closely related DAGLα isoform similarly behaves in this fashion. Interestingly, reported DAGLα KO mouse models exhibit maladaptive metabolic and behavioral phenotypes similar to cannabinoid receptor antagonism effects due to the drastic depletion of brain 2-AG. Furthermore, dysregulation of lipid metabolism in these DAGLα KO models affect neuroinflammatory and neuropsychiatry pathways apart from the expected endocannabinoid-related systems. Future studies could ascertain whether DAGLα similarly hydrolyzes TAGs in the brain and if the loss of this activity contributes to the previously reported behavioral phenotypes displayed by mice. Since DAGLα expression is absent in macrophages, these studies would need to take place in brain tissues, which also express low levels of DAGLβ. However, DAGLβ KO models along with selective small molecules can be used to remove its conflicting influence on the observed lipid metabolism to address these concerns.

Lastly, our studies into the role of DAGLβ in modulating neuroinflammatory pathways has strongly implicated elevated AMPK phosphorylation levels as an orthogonal approach towards inhibiting inflammation-induced pain signaling. While we have demonstrated using genetic

models, pharmacological tools, metabolic assessments, and animal behavioral studies to clarify this relationship, we have yet to explicitly identify a signaling mechanism connecting the two proteins. Traditionally DAG metabolizing enzymes such as DGKs and DAGLs affect protein signaling through depletion of DAG pools, which other effector proteins utilize. AMPK, in this case, lacks canonical DAG recognition regions (i.e., C1 domains), suggesting direct sensitivity to DAG levels as an unlikely theory. However, AMPK is regulated upstream by PKC isoforms through LKB1 complex formation offering a plausible connection wherein elevated DAG pools as a consequence of DAGLβ inhibition, in turn, promotes AMPK activation. Future studies investigating this proposed mechanism could be accomplished by profiling the activity of PKC isoforms and other DAG effector proteins using ABPP proteomic profiling. Understanding the full scope through which DAGLβ regulates neuroinflammation (via lipids and proteins) is critical for the future development of efficacious therapies that would aim to perturb DAGLβ so as to prevent exposure of patients to adverse side effects.

Chapter 6. Publications Resulting from This Work

(‡Co-authors and contributed equally to this work)

Shin M‡, **Ware TB**‡, Lee HC, Hsu KL. Lipid-metabolizing serine hydrolases in the mammalian nervous system. *Biochimica et Biophysica Acta* **1864** (6), 907-921 (2019).

Ware TB‡, Shin M‡, Hsu KL. Metabolomics analysis of lipid metabolizing enzyme activity. *Methods in Enzymology* **626**, 407-428 (2019).

Ware TB, Franks CE, Granade ME, Zhang M, Kim KB, Park KS, Gahlmann A, Harris TE, Hsu KL. Reprogramming fatty acyl specificity of lipid kinases via C1 domain engineering. *Nature Chemical Biology* **16**, 170-178 (2020).

Shin M‡, **Ware TB**‡, Hsu KL. DAGL-Beta Functions as a PUFA-Specific Triacylglycerol Lipase in Macrophages. *Cell Chemical Biology* **27** (3), 314-321 (2020).

Ware TB, Shin M, Upchurch C, Donvito G, Leitinger N, Lichtman AH, Hsu KL. Diacylglycerol lipase beta disruption mediates activated AMPK anti-inflammatory effects. *Manuscript in preparation*.

Additional Publications

Hahm HS‡, Torotich EK‡, Borne AL‡, Brulet JW‡, Libby AH, Yuan K, **Ware TB**, McCloud RL, Ciancone AM, Hsu KL. Global targeting of functional tyrosines using sulfur-triazole exchange chemistry. *Nature Chemical Biology* **16**, 150-159 (2020).

Nass S, Steele F, **Ware TB**, Libby A, Hsu KL, Kinsey S. Monoacylglycerol lipase inhibition via JZL184 attenuates paw inflammation and function deficits in a mouse model of inflammatory arthritis. *Cannabis and Cannabinoid Research*, (2021) *Under review.*

Hussain SS, Tran TM, **Ware TB**, Luse MA, Prevost CT, Ferguson AN, Kashatus JA, Hsu KL, Kashatus DF. RalA and PLD1 promote lipid droplet growth in response to nutrient withdrawal. *Developmental Cell*, (2021) *Under review*.

Ware TB, Hsu KL. Advances in chemical proteomic evaluation of lipid kinases – DAG kinases as a case study. *Current Opinions in Chemical Biology*, (2021) *Under review*.